DE NOVO DESIGNED SAFRANINE ENZYMES

by

GHEEVARGHESE RAJU

A dissertation submitted to the Graduate Faculty in Chemistry in partial fulfillment of the requirements for the degree of Doctor of Philosophy, The City University of New York.

2012

This manuscript has been read and accepted for the Graduate Faculty in Chemistry in satisfaction of the dissertation requirements for the degree of Doctor in Philosophy.

08/28/2012

Date

Prof. Ronald L. Koder

Chair of Examining Committee

08/28/2012

Date

Prof. Maria C. Tamargo

Executive Officer

Prof. Vikas Nanda

Prof. Ruth E. Stark

Prof. Brian Gibney

(Supervisory committee)

THE CITY UNIVERSITY OF NEW YORK

ABSTRACT

DE NOVO DESIGNED SAFRANINE ENZYMES

by

Gheevarghese Raju

Advisor: Professor Ronald L. Koder

De novo designed safranine enzymes are functionally parallel to NAD(P)H: flavinnitroreductases. The non-natural redox cofactor safranine has a very low reduction potential, -290 mV versus flavins -190 mV. A difference of 100 mV provides an additional 2.3 Kcal/mol energy to drive reduction reactions. Also safranine has an intrinsic unstable semiquinone oxidation state providing a doorstep for hydride transfer mechanism. Hence safranine enzymes will perform the electron transfer reaction, which is similar to the natural nitroreductases avoiding all oxygen activating free-radical side reactions. We designed a whole series of safranine binding helical bundles which catalyzes NAD(P)H dependent nitroaromatic reduction. Latest studied saf-X and safX-Loop proteins hold promise towards fully functional artificial enzymes.

A novel synthesis pathway of generating different safranine derivatives was developed. These derivatives differ in their characteristic reduction potentials, fluorescent and visible spectra. This will allow the amendment of reduction reaction towards any particular nitroaromatic substrate. Our goal is to create artificial safranine enzymes, which can be used for cancer prodrug activation, treatment of atherosclerosis, explosive sensing, biofuels as well as green chemical catalysis.

Acknowledgements

It is a pleasure to express my thanks to all the people who made this thesis possible.

My first debt of gratitude must go to my advisor, Prof. Ronald L. Koder. His patience, inspiration and thoughtful guidance helped me to proceed through the doctoral program and complete my dissertation. Prof. Koder, from the depths of my heart I would like to thank you for all your help, encouragement and for being a strong and supportive mentor to me throughout my graduate school career.

I owe special thanks to my dissertation collaborator and committee member, Prof. Vikas Nanda, for his contribution and thoughtful guidance from the beginning to the end of my graduate studies. I would also like to thank Prof. Jose Cerda, project collaborator, for his valuable advice.

I am also very grateful to my dissertation committee members, Prof. Ruth E. Stark, for her time and input over the years, and Prof. Brian R. Gibney for his support and willingness to participate in my final defense committee. Special thanks to Prof. Simon Simms for giving me the opportunity to be part of a great professional community.

Sincere thanks to my friends and lab members, Jeff Chaing, Bernard Everson and Lei Zhang for their help with the project. I would also like to thank Dr. Jessica Norman, Jane Lau and all other lab members for their support and friendship.

I also thank Dr. Fei Xu for her active participation in the project and Dr. Hsin Wang, Dr. Padmanava Pradhan, and Dr. Lijia Yang for their technical support.

Last but not least, I wish to thank my parents, Gheevarghese (Sr.) and Leelamma Raju, my brother Thomas K. Raju and my aunt, Rachael Thomas. They were always supportive, encouraging and their love provided my inspiration and was my driving force. Finally, I owe my deepest gratitude to my wife, Oxana Raju and my little son, Joshua, who were always there cheering me up and stood by me through the good times and bad.

I dedicate my thesis to

Oxana Raju (wife)

Leelamma Raju (mom)

Rachael Thomas (aunt).

Table of Contents

List of Figures

Chapter 1: Introduction and applications.

Chapter 2: Safaranine enzyme – design, expression and binding.

Chapter 3: Manipulating reduction potentials in an artificial safranin cofactor (*p*-Methoxy safranine).

Chapter 4: Novel synthetic route for artificial safranines and spectral studies.

List of Tables

Chapter 3: Manipulating reduction potentials in an artificial safranin cofactor (*p*-Methoxy safranine).

Chapter 4: Novel synthetic route for artificial safranines and spectral studies.

List of Schemes

Chapter 3: Manipulating reduction potentials in an artificial safranin cofactor (*p*-Methoxy safranine).

Chapter 4: Novel synthetic route for artificial safranines and spectral studies.

Chapter-1.

Introduction and applications.

1.1. An overview of artificial enzymes.

Synthetic compounds that facilitate a catalytic chemical reaction are generally called artificial enzymes. Like natural enzymes, they are protein macromolecules containing one or more cofactors, usually organic, inorganic molecules or metals on their active sites. All enzymes bind to a substrate and catalyze reactions with high stereo selectivity and acceleration rate in mild conditions [64].

The processes of molecular recognition and catalysis in enzyme mechanics are contingent on the following factors: proximity effects, reactant destabilization, conformational distortion of reactants, general acid-base catalysis and stabilization of the transition state by lowering the activation energy. In order to harness the functionality of natural enzymes by synthetic means, chemists have attempted to control for these factors by synthesizing small molecules called chemzymes, which mimic the enzyme active sites [45]. On the other hand, bioengineers have used genetic engineering and recombinant technology to create new enzymes with modified activities and specificities [51-53]. An advance in the chemical synthesis has led to peptide synthesis and novel molecular assemblies of bioorganic molecules. Sophisticated computational techniques have made it relatively easy to design and tailor the desired characteristics into fine protein-cofactor bundles [64]. With these technologies in hand, there has been a great effort to design and

control complex and precise molecular recognition and catalysis in the creation of artificial enzymes for scientific, medical and commercial purposes [63-65].

The efforts of synthetic chemistry in creating chemzymes to mimic the active site of the enzymes have met with some success [45-48]. For substrate binding, chemzymes have a binding cavity constructed by water-soluble ring shaped oligomers such as cyclodextrin, calixarene or crown ether. Through selective organic synthesis functional groups are anchored to the host molecule; these functional groups can execute the enzymatic reaction while the host molecule specifically binds the substrates. There are numerous reports of chemzymes being used as artificial glycosidases, oxidases, epoxidases and esterases [46,47]. They also catalyze cyclo-additions, conjugate additions and self-replication processes. Nevertheless, very few chemzymes have been reported that can perform Michaelis-Menten kinetics in aqueous medium, neutral pH or ambient temperature. Even successful ones are suffering from poor reaction rate, blunt functionalization or weak binding properties [45,46]. Moreover, unlike natural enzymes, artificial counterparts have acute toxicity making them unfit for clinical applications and environmentally hazardous.

The limited success and inherent toxicity of chemzymes highlights the advantages of recombinant DNA technology and de novo protein design [49,50]. Through strategic manipulation of genes, bioengineers are able to add new properties and fine-tune structure-function relationships in the construction of novel proteins. Many groups have worked on novel antibody therapeutics exploring this technology. There were several reports in which entirely human antibodies were created *in vivo* or *in vitro*, made by selection from large repertories [51]. Interesting developments have been made in the

area of catalytic antibodies. From a combinatorial antibody Fab library using the enzyme complementation of an auxotrophic *E.coli* strain, careful selection in candidates of catalysts was made. The function of these catalysts was improved by the design and choice of transition analogue. An effective Fab, isolated by the above method, showed an estimated catalytic rate enhancement of 10^8 compared to its natural *E.coli* enzyme counterpart of 10^{16} – fold [86]. However most catalytic Fabs are modest and none of them have reached the catalytic rate level effectiveness of a natural enzyme.

New initiatives in artificial protein engineering were based on direct mimicking using small peptides or amino acids. Chemist synthesized a scaffold of histidine residues, which mimics certain metalloproteins and enzymes such as hemocyanin, tyrosinase and catechol oxidase that has type-3 copper binding sites [87].

Recently, scientists have coordinated a semi random approach to determine the minimal requirements of four helix fashioned protein folding. De novo proteins based on polar and non-polar binary code have become the keystone in protein design [16, 65]. Computer algorithms have been generated to define the hydrophobic core packing requirements [64]. Researchers have found success in computationally grafting the metal binding cavity to redox-enzymes for creating novel enzymes [52,53,56,60]. Artificial catalytic electron transfer enzymes have been made, containing a heme cofactor ligated to histidine in four alpha helix strands, designed with a composite approach of binary patterning and computational active site design [38,64]. These successes proved that complex topologies are not required for enzyme catalysis [63]. In this theses work, our approach used a hybrid of computational and binary patterning for designing artificial proteins [13-22,56-60]. A novel synthesis generated a variety of artificial cofactors

differing in photophysical and electrochemical properties. Therefore, safranine enzymes hold great potential in catalytic electron transfer reactions.

1.2. Flavin-dependent oxidoreductases and their flavin chemistry.

Many catalytic enzymes, like redox metalloenzymes, undergo one-electron catalystic reactions. Other enzymes, like nicotinamide-nucleotides transferases, are involved in two-electron processes in various biological systems [89]. Flavoenzymes are unique in the fact that they can participate in both one-electron and two-electron reactions. In the reductive half-reaction a substrate or an electron donor is oxidized with simultaneous reduction of flavin, and in oxidative catalytic half-reactions, reduced flavin is oxidized by a substrate or an electron donor [8].

In general, flavoenzymes are classified into five categories based on the substrates involved in the types of half-reactions [75,76]. In transhydrogenases, two-electron equivalents are transferred with hydrogen ions from one substrate to the other. Dehydrogenase-oxidases transfer two-electrons to flavin cofactor from an organic substrate, where an oxidizing substrate which is a molecular oxygen is reduced to hydrogen peroxide. . Dehydrogenase-monoxygenases are the group in which a reduced pyridine nucleotide is involved in reducing a flavin while also using O_2 in an oxidation reaction where one oxygen atom is inserted into a cosubstrate while the other forms a molecule of water. Dehydrogenase-electron transferases are the flavoenzymes that undergo two-electron transfer from a reduced substrate and then are reoxidized in successive single electron transfers to acceptors. It is possible to further subdivide this class to identify the flavoenzymes, which undergo a reverse mechanism. In one type of

electron transferases, the flavin receives two electrons, one at a time, and then transmits them in the two-electron reduction step. While in the other type, flavin is reduced and reoxidized in one-electron steps [76].

Over the last decades scientists have used flavoenzymes to catalyze many reactions. Alcohol oxidation, amine oxidation, hydroxylation, Bayer-Villiger oxidation, sulfoxidation, Epoxidation, halogenation and Thiol oxidation are few of them [81-85].

Flavin reductases that are well known for catalytic reduction in the biological world are the motivation behind the design and synthesis of the artificial safranine enzymes. During catalytic reduction the flavin cofactor [8] undergoes destabilization by accepting redox equivalents from a reducing substrate and further transfers those equivalents to an oxidized acceptor [39]. Flavin reductases exhibit both one electron and two-electron transfer in reductions.

In the study of *Enterobacter cloacae* NAD(P)H:nitroreductase, two electron equivalents are transferred along with a hydrogen ion ($^1H^+$) via a ping-pong mechanism (Fig. 1.1) [36]. The overall mechanism includes the formation of a charge-transfer complex followed by a partially rate-limiting step of one electron and proton transfer [40].

Nitroreductases contain either flavin mononucleotide (FMN) or flavin adienine dinucleotide (FAD) as a cofactor [82]. All flavoenzymes explained above function by achieving redox states of a highly conjugated isoalloxazine moiety in the flavin molecule [77]. Depending on the different protonation states, there could be an oxidized, flavin semiquinone radical or hydroquinone intermediate [8,39]. In some mono and dioxygenase enzymes, a highly reactive flavin hydroperoxide intermediate could form

[78,79]. In catalytic reactions, flavin chemistry is regulated by specific interactions between the cofactor and the apoenzyme, adjusting the pKa's and reduction potentials of the flavin intermediates [88].

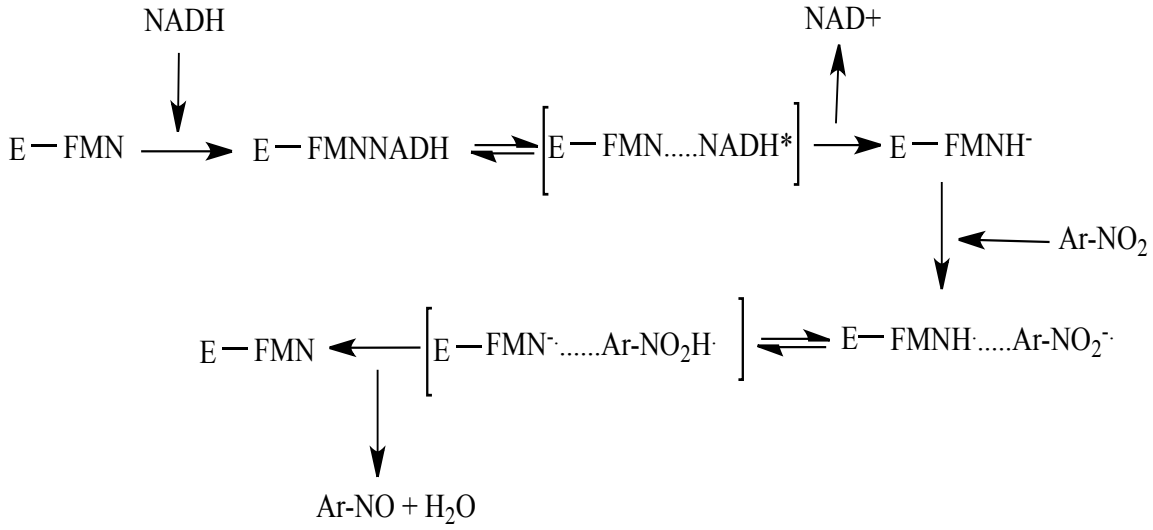

Figure 1.1. Ping-pong mechanism includes the formation of charge-transfer complex followed by a partly rate-limiting step of one electron and proton transfer. (E = Enzyme, FMN = Flavin mononucleotide, A = Substrate getting reduced)

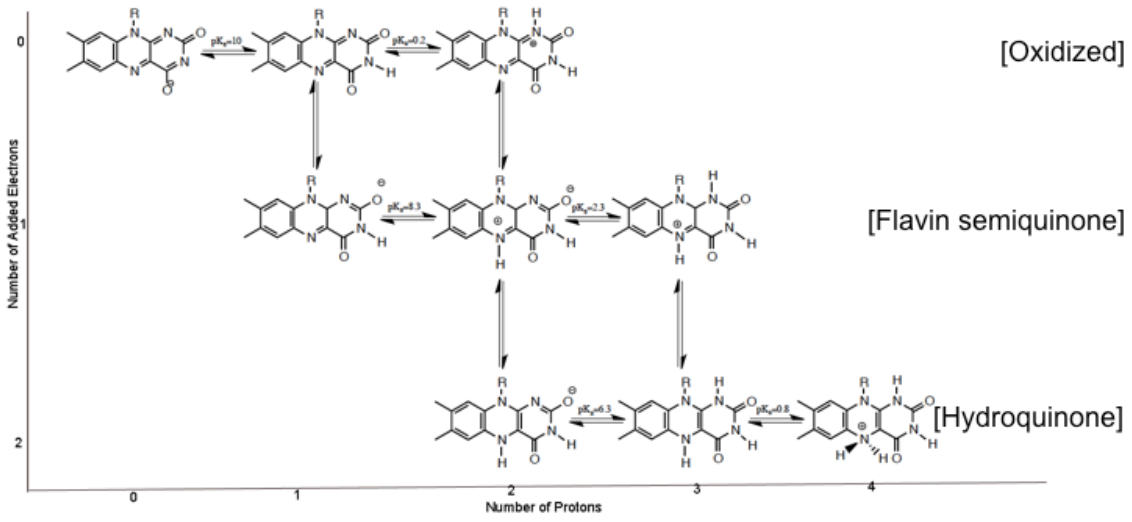

Figure 1.2. The three oxidation states of flavin and the normally accessible conjugate acids and bases at each oxidation level. [Adapted from dissertation of Ronald Koder- A Biochemical and biophysical Investigation of *Enterobacter Cloacae* nitroreductase.]

1.3. Safranine enzyme and safranine chemistry.

Safranine enzymes are synthetic analogues of flavin reductases expected to perform redox reactions in which two electron equivalents are transferred along with a hydrogen ion ($^1H^+$) via ping-pong mechanism [36]. To design saf-proteins, our collaborator Prof.Vikas Nanda and his colleagues used a ProCAD algorithm to select the consensus residues of the binding cavity. Then, keystone residues were fit to the α-helices, simply assembled using binary patterning [13-22,63-65]. Different iterations of saf-proteins were made and analyzed for structural and binding properties. Binding results of the latest Saf-X and SafX-Loop proteins show that they are potential candidates for a fully functional artificial enzyme. We generated derivatives of safranine, a flavin-like cofactor that has a more negative reduction potential [25,37]. Safranine itself has a much lower reduction potential than flavin, (-290 mV versus flavins -190 mV) which could drive the reduction with an additional 2.3 Kcal/mol energy [99]. Also, it has an intrinsic unstable semiquinone oxidation state, which ensures that all free radical reactions are avoided and selects (two electron together with one proton) hydride transfer mechanism [100]. We created a novel synthesis to modify the safranine by altering the functional groups of phenyl ring on N(10) position, which resulted in cofactors with range of reduction potentials [24,90]. This enables tuning of the safranine cofactors, which differ in photophysical and electrochemical properties. This synthesis also enables the incorporation of isotopically labeled nitrogen at the N(5) position in the phenazine ring of the safranine analogues. The isotopic chemical shift of the cofactor translates its chemical reactivity. This approach will aid in enzyme design by removing the necessity of remodeling the enzyme to “tune” the cofactor reactivity for the desired task.

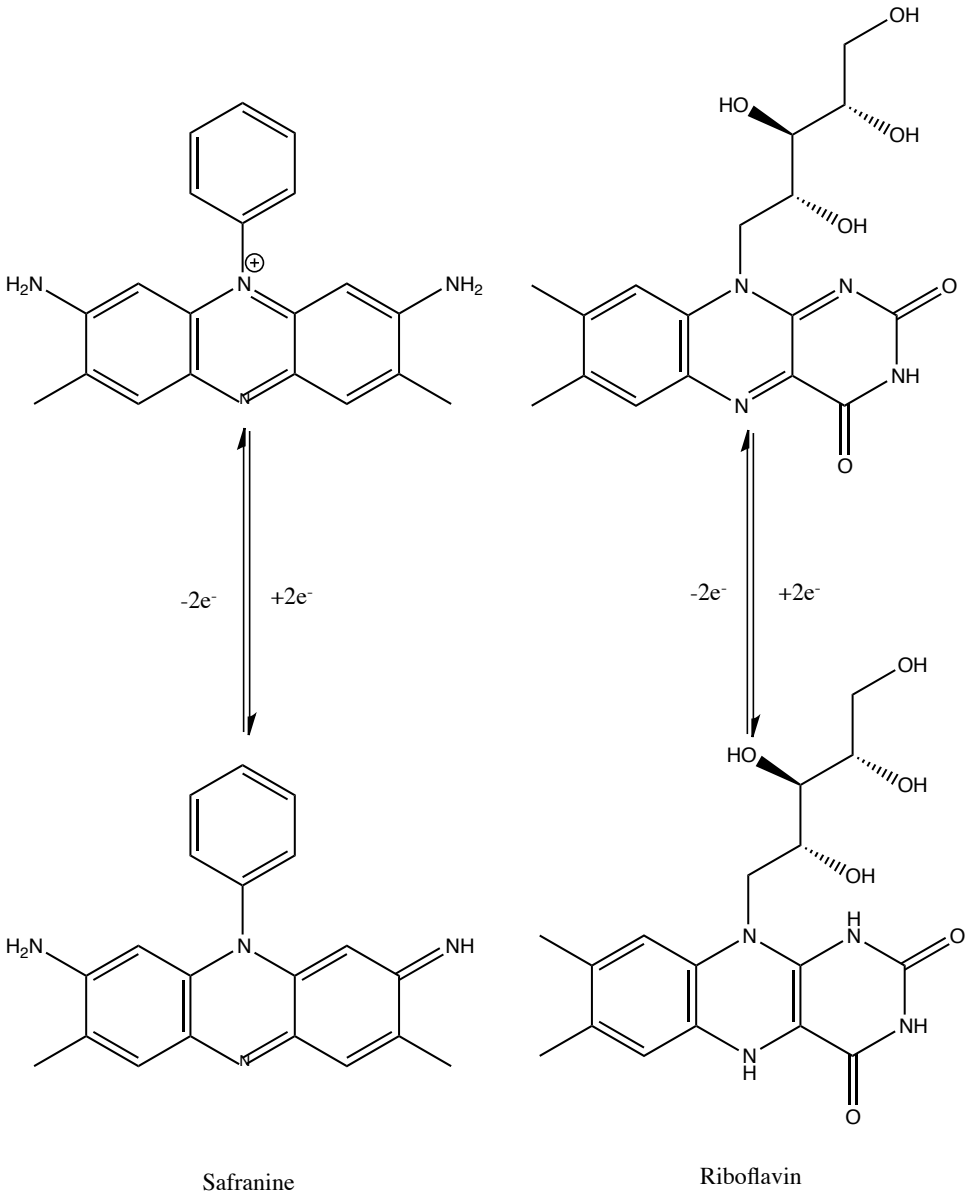

Safranine Riboflavin

Figure 1.3. The two-electron reduction of safranine O and riboflavin.

1.4. Safranine enzymes for cancer prodrug activation.

In the cancer treatment, especially in the metastatic stage, chemotherapy remains the key treatment. The administration of cytotoxic drugs intravenously or orally is the most common method. Most of the drugs used in chemotherapy are less selective on tumor cells than healthy normal cells. Enzyme Prodrug Therapy is adapted as an alternative to chemotherapy, utilizing less toxic drugs to destroy the tumor and minimized the damage to healthy cells. Antibody-Directed Enzyme Prodrug Therapy [ADEPT] uses the monospecific antibody enzyme bundle that can specifically bind to the tumor cells [91]. The prodrug administered orally or intravenously is activated by the enzymes in the cancer cells. Virus Directed Enzymes Prodrug Therapy [VDEPT] or Gene-Directed Enzyme Prodrug Therapy [GDEPT] is the latest development in this area of cancer therapy research, and is a method that tumor directed virus with modified DNA (DNA enables the expression of enzyme which reduce the prodrug), is introduced into the tumor where the enzyme is directly expressed in the cancer cell [92].

E.coli nitroreductase (*E.coli* NR) and the nitroaromatic drug 5-aziridinyl2,4-dinitrobenzamide (CB1954) enzyme-prodrug is one of the most efficient combinations in the clinical trials [66,67]. A catalytic reaction of the four-electron reduction step used by the two NADH molecules driven by a flavin mononucleotide cofactor in *E.coli* NR reduces CB1954. An aryl hydroxylamine reduction product from a *p*-nitro group in CB1954 forms a covalent adduct with guanine bases of the target DNA. This opens up an aziridine moiety in the drug molecule and then causing apoptosis by reacting with the opposing strand of the same DNA [94]. The *E.coli* NR/CB1954 combination is efficient

in poorly vascularized hypoxic solid type tumors treatment [93]. The nitroreduction of *E.coli* NR operates by a ping-pong bi-bi kinetic mechanism [36]. In healthy normal oxygen-rich cells, the enzyme regenerates itself from a reaction between the two-electron reduced enzyme intermediate and oxygen. Thus, the specificity of the prodrug is heightened only by reduction in the oxygen deficient tumor cells where the *E.coli* NR can execute a full four electron nitroreduction. This approach minimizes the general cytotoxicity problem of chemotherapy. The main disadvantage of this enzyme-prodrug method is the generation of hydrogen peroxide, a toxic byproduct, in the healthier oxygen rich cells as the result of the oxidation of *E.coli* NR [95].

E.coli NR follows an oxygen insensitive pathway rather than an oxygen sensitive pathway, which gives it an upper hand over other naturally occurring nitroreductases [68]. The one-electron reduction in an oxygen sensitive pathway can create nitroaryl radicals, which react promptly with oxygen to generate oxygen chain reactions or superoxides, causing further damage [95]. Also *E.coli* NR/CB1954 initiates apoptosis in all stages of the cell cycle. In addition to all these advantages, this *E.coli* NR activated hyrdoxylaromatic prodrug has a bystander effect, which could diffuse through cells [93]. This would help to extend the damage of the tumor cells even though the tumor is not properly vascularized. All current gene directed or antibody paired enzyme prodrug activations need some level of vascularization in the tumor.

CB1954 reactions with other human enzymes will negate all the benefit of this enzyme-prodrug treatment. An enzyme called DT diaphorase can also achieve oxygen insensitive nitroreduction and trigger the full activation of the prodrug [68]. CB1954 can also be fully or partially activated by other enzymes, including cytochrome P_{450} reductase,

succinate dehydrogenase and glutathione reductase, causing non-specific cytotoxicity [96].

To solve this problem, chemists have redesigned the CB1954 by modifying aryl nitro groups using the Hammet effect [97]. These revised prodrugs show much improvement in preclinical models, particularly in their bystander effect and their cytotoxic activity over the tumor cells [97]. So far, no progress has been made on the lowering nonspecific prodrug activity. An alternative effort is to mutate the nitroreductase enzyme so that it could drive the reduction reaction thermodynamically effective [36]. This could possibly lower the reactivity of the prodrug. Several groups working on this have reported many downsides to this problem [36,100]. The broad substrate specificity of the nitroreductases is a challenge. Any mutation leads to the alteration of the reaction site causing either a structural collapse or a disruption in the flavin chemistry of the enzyme. Flavin chemistry itself is very poorly understood. In only two percent of nitroreductase enzymes, can flavin destabilize the semiquinone oxidation state that drives the oxygen-insensitive two-electron reduction. Any small mutation or structural change to the flavin binding site can lead to an increased stability of the semiquinone state and initiates a toxic superoxide generating catalytic reaction chain.

Safranine binding enzymes are good alternatives in that situation. They are artificial enzymes with non-natural cofactors. These enzymes do not interact with other metabolic functions and their constituents can be excreted through major metabolic waste-discarding routes in the body. Artificial nitroreductases could be a viable alternative in both ADEPT and VDEPT/GDEPT prodrug methods. The reduction chemistry of safranine is far better than the flavins in natural nitroreductases. Moreover, in artificial

enzyme design, we can tune both the cofactor and the enzyme for reduction potential and substrate specificity. A lower reduction potential in the safranine derivative can drive the activation of the prodrug much faster. This would permit us to redesign less potent prodrugs for chemotherapy. Safranine has a very low reduction potential so that it could drive a reduction reaction 100mV or 2.3 Kcal/mol stronger compared to flavin [99]. Synthesizing new derivatives of safranine, with various reduction potentials, could further improve the energetics in the reduction chemistry. Using artificial safranin enzymes, there would be no toxic byproducts during the reduction activation of the prodrug. Safranine itself posseses an intrinsic unstable semiquinone oxidation state ensuring that it takes an oxygen-sensitive pathway thus avoiding all other free radical formation.

Many CB1954 variants have been synthesized [97, 98]. These variants of prodrugs have different two-electron reduction potentials. To reduce the unwanted reactions with intrinsic human enzymes, the prodrug has been redesigned with bulky substituents or is made to be highly charged. Once the enzymatic activity is optimized, the prodrug that is least reactive to intrinsic human enzymes can be selected and coupled with the optimized safranine enzymes. The efficiency of these prodrug-artificial enzyme pairs can be studied in an *in vitro* tumor cell culture assay. The successful candidates would then be selected for clinical testing. With their power of reduction driving force and engineering flexibility for specificity, safranine enzymes could be a way to tackle complications of chemotherapy.

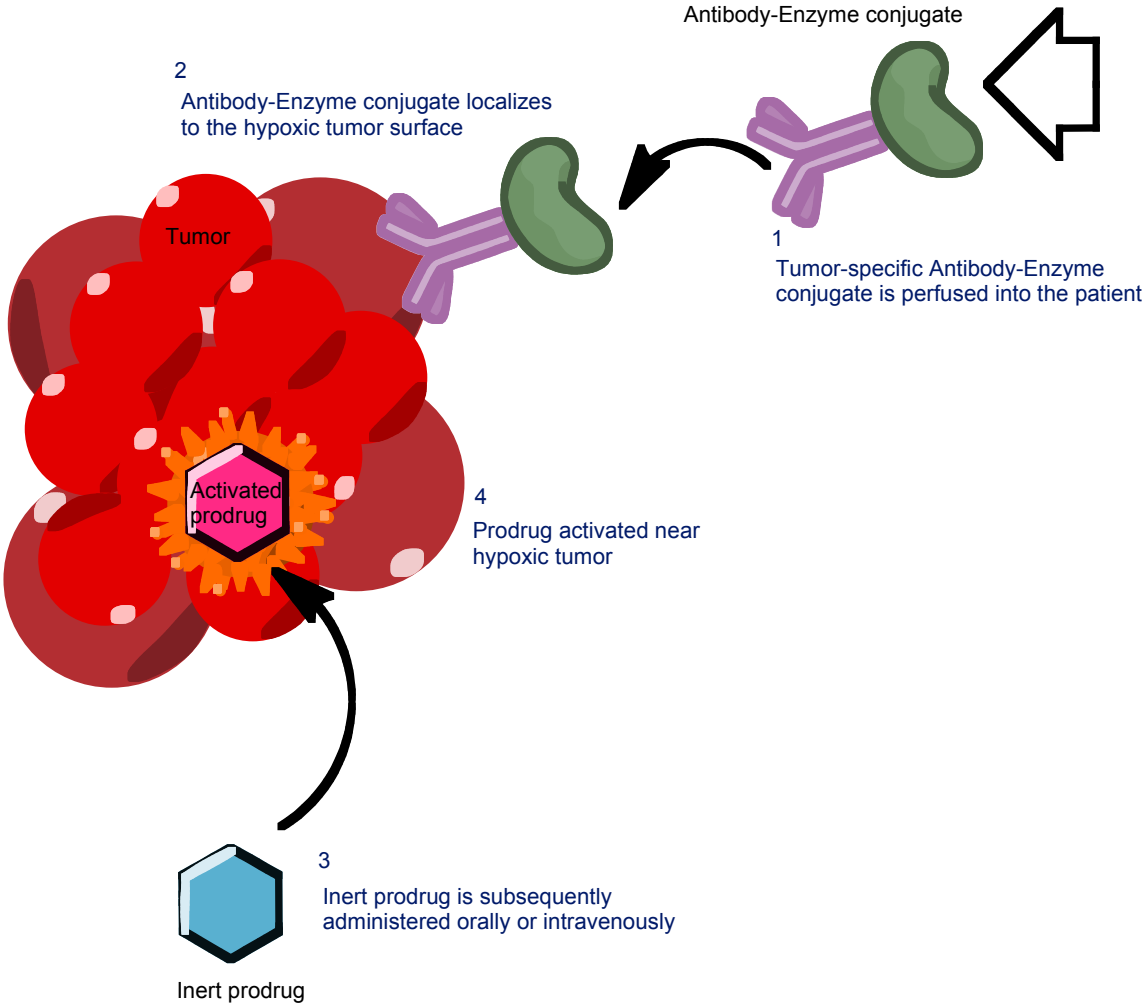

Figure 1.4. Antibody-Directed Enzyme Prodrug Therapy [ADEPT] uses the monospecific antibodies-enzyme bundle that can specifically bind to the tumor cells.

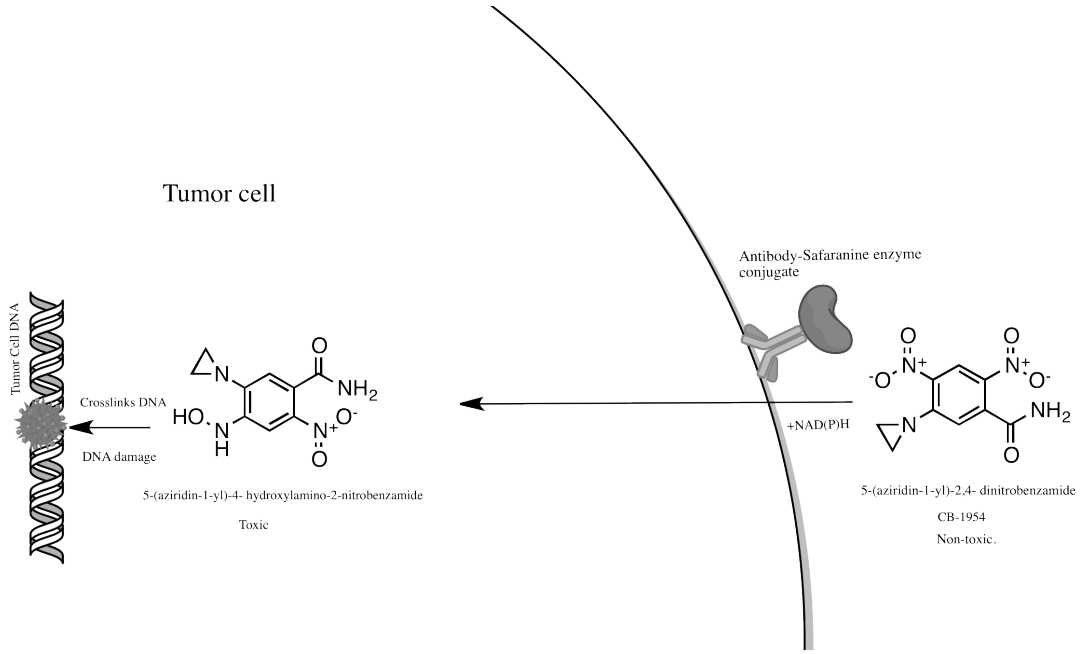

Figure 1.5. Antibody Directed Enzymes Prodrug Therapy [ADEPT] with safranine enzyme. Illustration of safranine enzyme activating cancer drug-CB1954

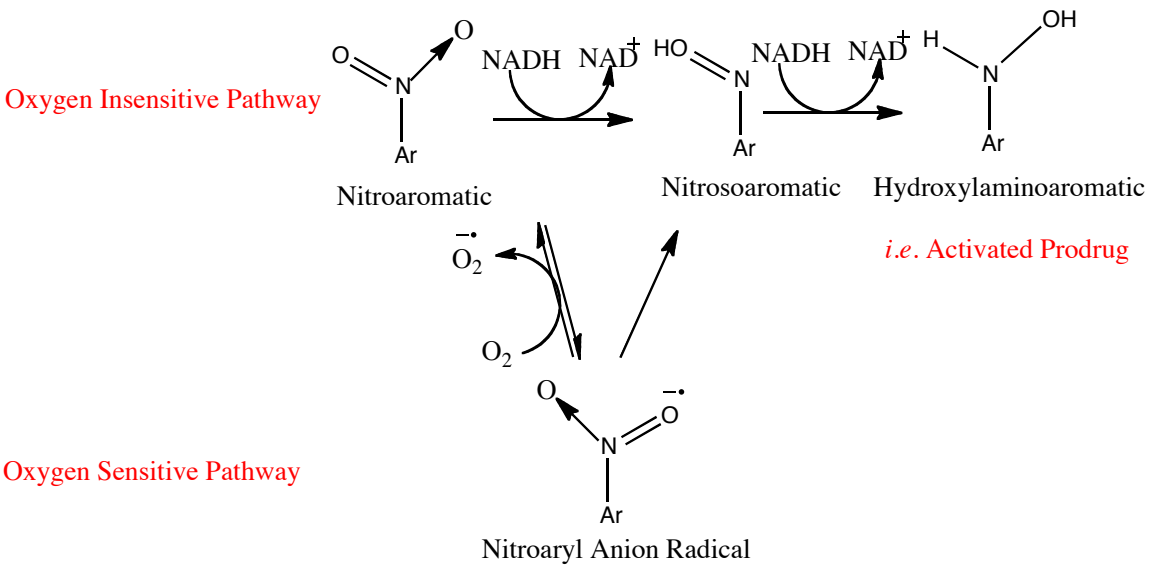

Figure 1.6. Oxygen sensitive and insensitive nitroreduction pathways.

1.5. Oxysterol reductive safranine enzymes (ORSE), a promising solution for atherosclerosis.

Atherosclerosis can be asymptomatic during early stages. Most commonly it is symptomatic when it hampers the coronary and cerebral circulation being the underlying cause of CVD, PAOD or stroke. If the symptom is just angina pectoris (chest pain) it can be treated non-pharmaceutically with regular exercise, dietary regulation and quitting smoking. In severe cases, surgical intervention such as angioplasty (expansion of the narrowed arteries) and bypass surgeries are performed. Statins are a group of widely prescribed medicine (can be prescribed before or after surgery), which competitively inhibit HMG-CoA reductase, the precursor enzyme in the HMG-CoA reductase pathway responsible for cholesterol levels [1-5]. This forces the liver cells to produce more LDL receptors, which clear a large amount of low density lipoprotein (cause risk of atherosclerosis) from the plasma. Statins have two major side effects: liver enzyme disorder and skeletal muscle damage that may result in kidney failure. Current clinical studies show that a combination of medical treatments, including statins, niacins and other cholesterol absorption or inhibiting agents like Ezetimibe, is more successful [5]. However, all current medical treatments are criticized for their cost, undesired side effects, prolonged period of use and patented control.

7-ketocholesterol together with its hydroxyl derivative, 7-hydroxycolesterol, are the most abundant oxidation products found in human atheromatic plaques [6, 7]. In addition, plaques contain other oxidative products of triglyceride, phospholipid and proteins. There are studies showing that 7-ketocholesterol competitively inhibits cholesteryl 7-α-

hydroxylase, the rate-limiting enzyme in the bile acid synthesis [6,7]. The intravenous administration of excess 7-ketocholesterol to rats resulted in reduced biosynthesis of bile acid, proving the complexity of devising a treatment by natural enzymes [6]. Drug mediated inhibition of HMG-CoA can remove excess 7-ketocholesterol from the blood in the liver, but it leads to unexpected side effects and chemotoxicity. Moreover, surgery is the only option for removal of complicated lesions. A potential solution is to use a catalytic enzyme *in vivo*, which will specifically bind 7-ketocholesterol and reduce it to its hydroxy-derivative, a precursor of bile acid biosynthesis. None of the natural enzymes such like oxysterol binding protein (OSBP) are capable of such processes.

The artificial oxysterol reductive safranine enzyme (ORSE) is designed to specifically bind 7-ketocholesterol in the bloodstream and reduce it to 7-α-hydroxycholesterol. 7-α-hydroxycholesterol is removed by a bile acid synthesis pathway upregulated by LXR (liver X receptor). The effective removal of oxysterols from the blood leads to the diffusion of plaques and the clearing of arteries via eradicating lesions. This is a promising solution for atherosclerosis. Oxysterol reductive safranine enzymes (ORSE) could be highly specific, stable and reversible in binding. Hence, they will be more effective and have no cytotoxicity, and their constituents can be excreted through the major metabolic waste-discarding routes in the body.

Oxysterol binding proteins (OSBP) have been known as sterol sensors that regulate sphingomyelin synthesis and the activity of extracellular signal-regulated kinases (ERK) [9-12]. There are nine oxysterol binding proteins (OSBP)-related (ORP) structures in the Protein Database. Five of them are yeast ORP-Osh4 bound to different sterols such as ergosterol, cholesterol and 7-, 20-, 25-hydroxycholesterol. In all the structures, the sterols

bind to Osh4 in the central tunnel of a 19 strand β-barrel (residues 115-293). The remarkable aspect of this binding is that oxysterol recognition by Osh4 is mostly through water-mediated interactions [41-44]. The 434 amino acid long protein contains a lid (residues 1-29) that covers the tunnel opening. Sterol ligands stabilize the closed conformation of the lid via direct Van der Waals interactions with Trp 10, Phe13, and the conserved residues, Leu 24 and Leu 27. A conformational change is generated by the loss of ligand-lid interaction and the lid moves away to free the ligand [41]. The lid at the tunnel opening is conserved in all ORPs [43].

OSBP is an 809 amino acid protein, containing an N-terminal glycine-alanine rich region, a PH (Pleckstrin homology**)** domain, a leucine zipper, endoplasmic reticulum (ER) protein binding region and sterol binding region (residues 408-459). Alignment of OSBP with Osh4 shows that $OSBP_{408-459}$ perfectly overlaps the lid region of Osh4. Mutational studies show the presence and importance of a Cholesterol Recognition/interaction Amino acid Consensus motif (CRAC): $(L/V)X_{(1-5)}YX_{(1-5)}(R/K)$ in these 51 residues. Once docked to the membrane, sterol binding domain extracts the sterol and moves it into the β-barrel region [42].

To achieve oxysterol binding we need to modify the safranine binding protein (SBP) interhelical loop. The Osh4 1α-oxysterol binding loop from the 1α domain of Osh4-Oxy sterol binding protein (Osh4-OSBP) is modified to fit to the interhelical loop of SBP. A comparison of the structures of the Osh4-OSBP loop and interhelical loop of the four α - helix bundle SBP, showed that to fuse these domains we need to mutate and modify the torsion angles of the end terminal residues of Osh4-OSBP loop. Methionine 1, aspartic acid 2 and Leucine 36 are mutated by preserving all other residues and their

conformations in Osh4-OSBP loop. Using a Ramachandran plot in Swiss PDB viewer, the torsion angles of those mutated residues are adjusted in such a way that the two domains are compatible to fit each other.

In brief, first we could construct a combinatorial library of randomly mutating interhelical loops on safranine binding enzyme (SRE). Using codon cassette mutagenesis, we could incorporate a mutagenic primer into the parental plasmid to get the mutated plasmid [29-32]. Digestion, transformation, cell growth, lysis and enzyme activity study of all the variants could be done on a microtiter plate. The Steady-state fluorescence emission spectral change during the reduction of 7-ketosterol can be monitored on the microtiter plate instantaneously by a fluorescence microplate reader [26-28, 33-35].

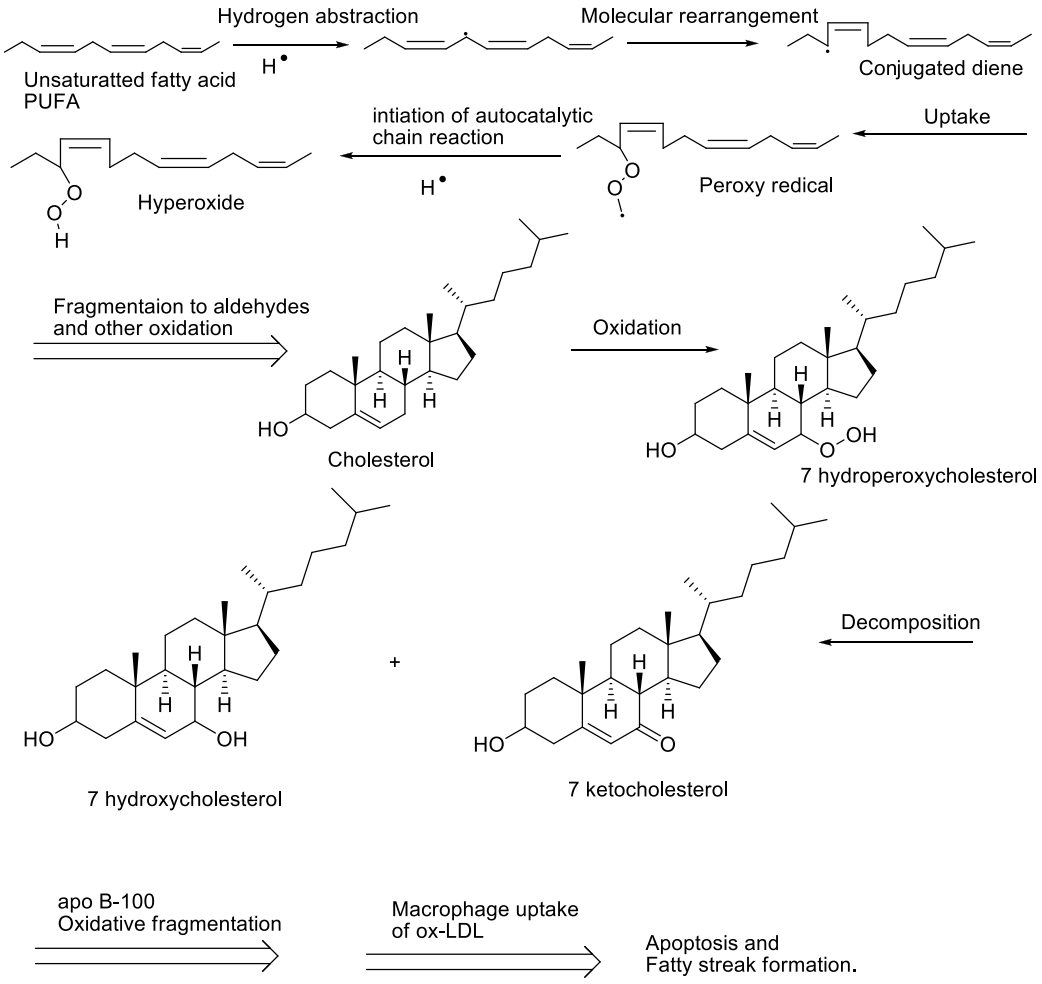

Figure 1.7. Chemistry behind the atherosclerosis.

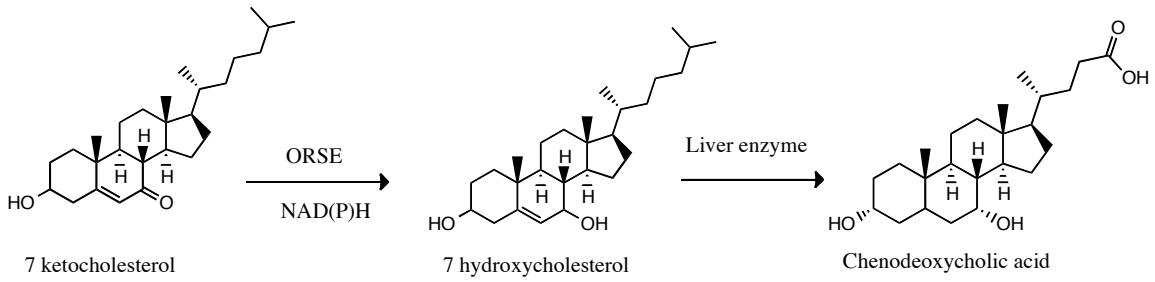

Figure 1.8. Proposed catalytic chemistry of ORSE

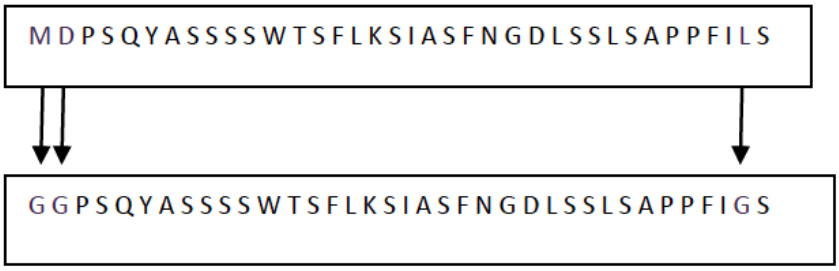

Figure 1.9. Above Osh4-OSBP loop sequence and below methionine 1, aspartic acid 2 and leucine 36 are mutated to glycine.

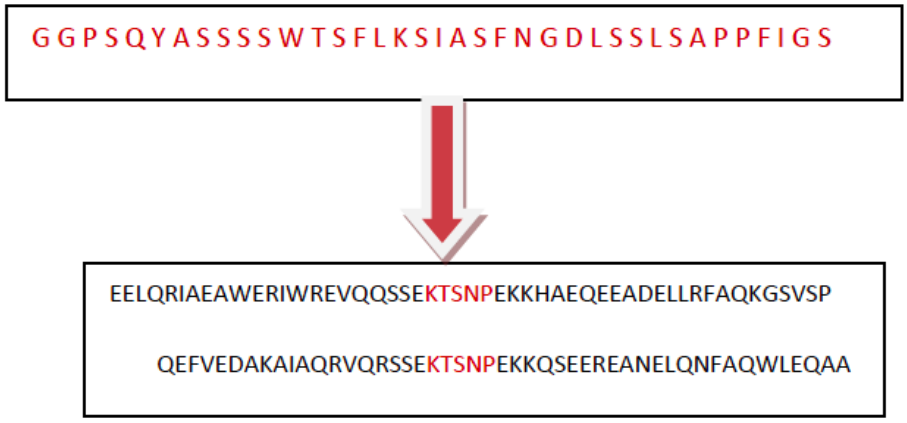

Figure 1.10. Above the mutated Osh4-OSBP loop sequence and below the SBP sequence, the interhelical loops are highlighted. The arrow indicates interhelical loops of SBP that are replaced by mutated Osh4-OSBP loop.

1.6. Safranine enzymes in explosive detecting as a biosensor.

Nitroreductase activity on explosives like hexahydro-1,3,5-trinitro-1,3,5-triazine (RDX) , octahydro-1,3,5,7-tetranitro-1,3,5,7-tetrazocine (HMX), 2,4-dinitrotoluene (DNT), 2,4,6-trinitrotoluene (TNT) and glycerol trinitrate (GTN) are well established [69-73]. Inexpensive efficient detection of these nitroaromatic compounds has been made possible by the development of nitroreductase biosensors. There are several sophisticated instruments like HPLC or MS that are sufficient to detect even traces of such nitroaromatics. But these instruments are limited in their range of utility since leakages of explosive chemicals often happens in remote areas or in situations where immediate sample detection has to be done on site. Environmental contamination by nitroaromatic compounds is considered serious, and rapid detection and counter actions are crucial to prevent further damage. Enzymatic biosensors are developed as an expedient, portable and accurate detection system [72].

Environmental contamination due to these nitrocompounds comes from an industrial production facilities or their waste disposal. It also occurs in deployment and other military activities. Explosives are often piled up in storage, manufacturing and decommissioning facilities, and many of them, like TNT, are used as intermediates in dye and photographic industries. TNT was listed by the various environmental protection agencies as a major contaminant to the soil and ground water because of its heavy usage by the military in the past [101]. It has been shown that the metabolites of TNT are carcinogenic for many organisms including humans [101]. Bioremediation is an excellent tool to remove such contaminants [71,105]. Nirtroreductases are expressed in

microorganisms have been successfully investigated for the degradation of various nitrocompounds. *Klebsiella* sp., *Pseudomonas pseudoalcaligenes* JS52 and *Pseudomonas putida* JLR1 are some of the microorganisms where the nitroreductases have been cloned and studied [102-104]. Phytoremediation is another conceivable technology because there are no difficulties in implementation, and it is eco-friendly and maintenance free [101,105]. Transgenic plants have been made using genetic modification by transplanting a bacterial or mammalian gene to express an enzyme. *Nicotiana tabacum* (Tobacco plants) infused with *nsf*1 nitroreductase gene from *Enterobacter cloacae*, *E.coli* nitroreductase gene expressed in *Arabidopsis thaliana* (Thale cress plant) and *pnrA* nitroreductase gene of *Pseudomonas putida* JLR1 expressed in *Populus tremuloides* (Aspen trees) are some of the transgenic plants being investigated [101,106,107].

Nitroreductases that reduce the nitroaromatic or nitroheterocyclic derivatives via type I oxygen-insensitive or type II oxygen-sensitive reductions are suitable for the design of explosive-detecting biosensors [36, 108]. These sensors are metal electrodes, often gold, where nitroreductases are attached through thiol linkages [72]. Enzymes expressed with a terminal cysteine tag can also form a self-assembled monolayer at the electrode surface. These enzymes will selectively bind to the substrate in its vicinity and catalyze chemical modification. The quantity of explosives can be easily determined by the electron flow from the electrode. In laboratory conditions, NADH is the electron mediator, which shuttles the electron from electrode to enzyme [72]. In the field, the more stable synthetic mediator, ferrocene dicarboxylic acid, can be used. Naal *et al.* reported that they constructed a fusion type biosensor with a maltose binding protein [MBP] and a nitroreductase [NR] [73]. They claim that this fusion helps the electron-transfer kinetics

of the immobilized enzyme [73]. The MBP-NR fusion was immobilized to an electrode which was modified with an electropolymerised film of *N*-(3-pyrrol-1-ylpropyl)-4,4'-bipyridine [PPB]. The MBP domain shows a high and specific affinity towards these films with the immobilized NR retaining all the enzymatic activity. This fusion biosensor exhibited a high activity towards the electrocatalytic reduction of TNT and DNT, up to 50 μM in solution at a potential of -0.35V versus Ag/AgCl [73].

Bryant *et al.* studied the oxygen-insensitive type I nitroreductase from the *Enterobacter cloacae* strain 96-3 which shows a broad substrate specificity towards TNT, 4-nitroacetophenone, 4-nitrobenzene methyl sulfonate and 4-nitrophenol [108]. Koder *et al.* studied exclusively the mechanism of nitroreductase from *Enterobacter cloacae* and found that the most oxidizing substrate is DNT with an efficiency of $k_{(cat)}/K_M$ value 1 order of the magnitude, which is higher than FMN, FAD, *p*-nitrobenzoate or riboflavin [36]. Some of the early studies of nitroreductases, reported that the reduction of nitramine happens only in anaerobic conditions through a stable nitroso intermediate [69]. The nitramine explosives they examined are RDX and HMX. Their report lacked specific evaluation of a particular enzyme activity. All studies were done in mixed bacterial cultures. Later, Binks *et al.* and Coleman *et al.* found that RDX biodegradation is possible in an aerobic environment without producing nitroso intermediates [109,110]. Kitts *et al.* showed that an enteric bacterium *Morganella morganii* strain B2 was efficient in reducing the nitro groups of both RDX and TNT [111]. Efforts of the same group illustrate that these bacteria exhibit type I oxygen-insensitive nitroreductase activity for the reduction of nitro groups on both nitramines and nitroaromatic explosives [69].

Safranine enzymes are currently the best alternative for the natural nitroreductases used in biosensors. They have artificial phenosafranine derivative cofactors varying in reduction potential, allowing the design of a single sensor with an array of safranine enzymes that detect and biodegrade both nitramines and nitroaromatic explosives. Each enzyme can be incorporated with different cofactor, enabling one sensor with a range of functionality. Also, designing protein candidates with complementary binding pockets could broaden the substrate specificity. Such biosensors would be decisive in cases where there is no prior knowledge of the explosives that are leaked or deployed. Since all phenosafranine derivatives possess a visible-range spectral shift on reduction, detection and degradation could be easily spotted on such a multi-function sensor. The advantages of these biosensors would be their effectiveness in detection and low fabrication cost.

Most nitroreductases loose their electrocatalytic efficiency when attached to an electrode [73]. This may be due to their lack of structural stability on a metal platform. To circumvent these problems scientists have designed immobilized fusion proteins. In general, artificial enzymes are designed to be simple and have great structural stability, maintaining their configuration regardless of their proximity to metal or polymer surfaces. As such the electron transfer kinetics of our artificial safranine enzymes on a metal surfaces can be regulated to be the same as in the solution. It should also be feasible to incorporate safarine enzymes into transgenic plants for phytoremediation or with into microorganisms for bioremediation.

Phenosafranine has an intrinsic highly stable semiquinone property. It is expected that the enzyme could undergo a type I oxygen-insensitive activity no matter what type of substrate it binds to. Such mechanisms generally do not need any mediators or do not

produce any intermediate products. Given these characteristics, an artificial safranine enzyme based biosensor would be less complicated to design and easy to use. Since all safranine analogues differ in their photophysical properties and do not fluoresce in the reduced state, they can be separately monitored either in the mixed solutions of two species, or in the mixed complexes of the two cofactors with one or more proteins. This makes them an ideal candidate for biochemical sensor arrays. In general, safranine enzymes are superior to all other natural nitroreductases in stability, efficiency, accuracy and production cost for their role in explosive-detection biosensors.

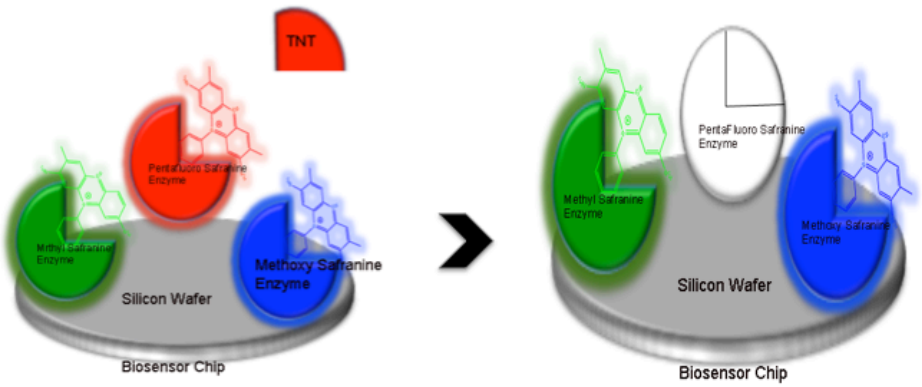

Figure 1.11. Pictorial representation of a TNT-specific safranine-enzyme in a safranine-enzyme array biosensor detecting the TNT molecule. Safarnine enzymes differ in photophysical roperties upon substrate binding and in reduced state. In above illustration unbound safranine enzyme is spectrally different from TNT bound safranine enzyme (colorless).

1.7. Safranine enzymes for biocatalytic green chemistry.

Biocatalytic organic synthesis using enzymes is widely accredited and practiced more and more in chemical synthetic fields, simply because it is as robust as other methods, ecofriendly, cost efficient and stereospecific [80,84]. Flavoenzymes play a key role in many biological enzymatic reactions. They catalyze regio- and enantiospecific reactions. To achieve such enantiopure compounds through the chemical synthesis route is either difficult or has a high production cost. A variety of chemicals can be synthesized through flavoenzyme dependent biocatalytic methods [80]. In biotechnology, falvin-enzymes are admired for their catalytic efficiency and have strong advantages over the conventional chemical route in their renewability, fewer byproducts and mild reaction conditions [62,74,84]. Flavooxidases and monooxygeneses have gained specific interest for use in oxyfunctionalization. More and more chemical, pharmaceutical and food industries are adopting flavooxidoreductases in developing new applications [80,84].

One reason for the widespread interest in developing artificial enzymes is that they are potentially more economical than natural ones. Another is that their proteins are expressed from *E. coli* in laboratory conditions, making them more environmentally friendly as well. However, the main advantage may be that artificial enzymes can optimize for reduction potentials, substrate or ligand affinity, hydrophobicity, chemical reactivity, and photophysical properties. Thus, single enzyme can be modified and used for different types of reactions. Safranine enzymes are designed for performing reduction catalysis. Moreover, the artificial flavin-like safranine cofactors are structurally and energetically tuned for their reduction potentials. The more negative reduction potential of these compounds, the more driving force for catalytic reactions. Thus, safranine

enzymes are a better option than natural flavin-enzymes in biocatalytical reactions. Also, all these properties make them sufficient to be used as catalysts in enzymatic biofuel cells [112,113].

1.8. Bibliography.

1. Ishwarlal Jialal, Sridevi Devaraj. *Clinical Chemistry,* **1996**, 42, (4), 498-506.

2. Shobini Jayaraman, Donald L. Gantz, Olga Gursky. *Biochemistry,* **2007**, 46, 5790-5797.

3. Ira Tabas. *Arterioscler. Thromb. Vasc. Biol.* ,**2005**, 25, 2255-2264.

4. Martin R. Bennett. *Arterioscler. Thromb. Vasc. Biol.,* **2002**, 22, 713-714.

5. Charis Costopoulos,Tze Vun Liew, Martin Bennett. *Biochemical Pharmacology,* **2008**, 75, 1251-1261.

6. Malcolm A. Lyons, Andrew J. Brown. *The International Journal of Biochemistry & Cell Biology,* **1999**, 31, 369-375.

7. Alfonso Valenzuela, Julio Sanhueza, Susana *Nieto. Bio. Res.,* **2003**, 36, 291-302.

8. V. Massey. *Biochemical Society Transactions,* **2000**, 28, (4), 283-296.

9. Daoguang Yan, Markku Lehto, Laura Rasilainen, Jari Metso, Christian Ehnholm, Seppo Yla-Herttuala, Matti Jauhiainen, Vesa M. Olkkonen. *Arterioscler. Thromb. Vasc. Biol.,* **2007**, 27, 1108-1114.

10. Yoshichika Kawai, Akiko Saito, Noriyuki Shibata, Makio Kobayashi, Satoshi Yamada, Toshihiko Osawa, Koji Uchida. *The Journal of Biological Chemistry,* **2003**, 278, (23), 21040-21049.

11. Young Jun Im, Sumana Raychaudhuri, William A. Prinz, James H. Hurley. *Nature,* **2005**, 437, 154-158.

12. Wenling Chen, Guoxen Chen, Daphne L. Head, David J. Mangelsdorf, David W. Russell. *Cell Metabolism,* **2007,** 5, 73-79.

13. Stephen Betz, Robert Fairman, Karyn O'Neil, James Lear, Wililiam Degrado. *Phil. Trans. R. Soc. Lond. B* , **1995**, 348, 81-88.

14. Ronald L. Koder, P. Leslie Dutton. *Dalton Trans.,* **2006**, 3045-3051.

15. Yinan Wei, Tun Liu, Stephen L. Sazinsky, David A. Moffet, Istvan Pelczer, Michael H. Hecht. *Protein Science,* **2003**, 12, 92-102.

16. Satwik Kamtekar, Jarad M. Schiffer, Huayu Xiong, Jennifer M. Babik, Michael H. Hecht. *Science,* **1993**, 262, (5140), 1680-1685.

17. J. A. Silverman, R. Balakrishnan, P. B. Harbury. *PNAS,* **2001**, 98, (6), 3092-3097.

18. G. V. Semisotnov, N. A. Rodionova, O. I. Razgulyaev, V. N. Uversky, A. F. Gripas, R. I. Gilmanshin. *Biopolymers,* **1991**, 31, 119-128.

19. Beth Allyn Krizek, Barbara T. Amann, Valda J. Kilfoil, Denise L. Merkle, Jeremy M. Berg. *J. Am. Chem. Soc.,* **1991**, 113, 4518-4523.

20. Amit R. Reddi, Tabitha R. Guzman, Robert M. Breece, David L. Tierney, Brian R. Gibney. *J. Am. Chem. Soc.,* **2007**, 129, 12815-12827.

21. Shiluan Yi, Brian L. Boys, Anne Brickenden, Lars Konermann, Wing-Yiu Choy. *Biochemistry,* **2007**, 10, 1021-1031.

22. Byoung-Chul Lee, Tammy K. Chu, Ken A. Dill, Ronald N. Zuckermann. *J. Am. Chem. Soc.,* **2008**, 2117-2125.

23. Brian. R. Gibney, Francesc Rabanal, Jack J. Skalicky, A. Joshua Wand, P. Leslie Dutton. *J. Am. Chem. Soc.,* **1999**, 121, 4952-4960.

24. H.B. Goodbrand, Nan-Xing Hu. Journal of Organic Chemistry **1999**, 64, 670-674.

25. K. M. Kadish, B. Boisselier-Cocolios, B. Simonet, D. Chang, H. Ledon, D. Cocolios. *Inorg. Chem.,* **1985**, 24, 2148-2156.

26. Takahiro Nakaminami, Susumu Kuwabata, Hiroshi Yoneyama. *Anal. Chem.,* **1997**, 69, 2367-2372.

27. Tokuji Ikeda, Shinji Ando, Mitsugi Senda. *Bull. Chem. Soc. Jpn.,* **1981**, 54, 2189-2193.

28. Kazuhiro Hojo, Hideki Hakamata, Ayumi Ito, Akira Kotani, Chisaki Furukawa, Yu-Ya Hosokawa, Fumiyo Kusu. *Journal of Chromatography A.,* **2007**, 1166, 135-141.

29. Deena M. Kegler-Ebo, Catherine M. Docktor and Daniel DiMaio. *Nucleic Acids Research.,* **1994**, 22, (9), 1593-1599.

30. Deena M. Kegler-Ebo, Glenda W. Polack, Daniel DiMaio. *Methods in Molecular Biology.,* **1996**, 57, 297-310.

31. P Straub, M Lloyd, EF Johnson and B Kemper. *J. Biol. Chem.,* **1993**, 268, (29), 21997-22003.

32. JF Reidhaar-Olson and RT Sauer. *Science.,* **1988**, 241, (4861), 53-57.

33. Lesley Davenport, Jay R. Knutson, Ludwig Brand . *Biochemistry,* **1986**, 25, 1186-1195.

34. Daniel Wustner. *Chemistry and Physics of Lipids.,* **2007**, 146, 1-25.

35. Soumi Mukherjee, Amitabha Chattopadhyay. Chemistry and Physics of Lipids. **2005**, 134, 79-84.

36. Koder R.L, Miller A.F. *Biochimica et biophysica acta.,* **1998**, 1387, 395-405.

37. Noah N. Niufar, Fiona L. Haycock, Jodi L. Wesemann, Jason A. MacStay, Victor L. Heasley, Peter Kovacic. *Rev. Soc. Quim. Mex.,* 2002, 46, (4), 307-312.

38. R. Blake Hill, Daniel P. Raleigh, Angela Lombardi, William F. Degrado. *Acc. Chem. Ress.,* **2000**, 33, (11), 745-754.

39. Benfang Lei, Shiao-Chun Tu. *Biochemistry.* **1998**, 37, (41), 14623-14629

40. Henrikas Nivinskas, Sigita Staskeviciene, Jonas Sarlauskas, Ronald L. Koder, Anne-Frances Miller, Narimantas Cenas. *Archives of Biochemistry and Biophysics.,* **2002**, 403, 249-258.

41. Young Jun Im, Sumana Raychaudhuri, William A. Prinz, james H. Hurley. *Nature.* **2005**, 437 (7055), 154-158.

42. Ping-Yuan Wang, Jian Weng, Sungsoo Lee, Richard G. W. Anderson. *The Journel of Biological Chemistry.* **2008**, 283, (12), 8034-8045.

43. Monika Suchanek, Riikka Hynynen, Gred Wohlfahrt, Markku Lehto, Marie Johansson, Hannu Saarinen, Anna Radzikowska, Christoph Thiele, Vesa M. Olkkonen. *Biochem. J.* **2007**, 405, 473-480.

44. Marta Murcia, Jose D. Faraldo-Gomez, Frederick R. Maxfield, Benoit Roux. *Journel of Lipid Research.* **2006**, 47, 2614-2630.

45. Jeannette Bjerre, Cyril Rousseau, Lavinia Marinescu, Mikael Bols. *Appl Microbiol Biotechnol.* **2008**, 81, 1–11.

46. R. Breslow, *Artificial Enzymes.* **2005**, WILEY-VCH Verlag GmbH & Co. KGaA, Weinheim .

47. Yukito Murakami, Jun-ichi Kikuchi, Yoshio Hisaeda, and Osamu Hayashida, *Chem. Rev.,* **1996**, 96, 721-758.

48. Xin Huang, Xiaoman Liu, Quan Luo, Junqiu Liu and Jiacong Shen. *Chem. Soc. Rev*., **2011**, 40, 1171–1184.

49. Johannes Steinreiber, Thomas R. Ward. *Coordination Chemistry Reviews*. **2008**. 252 , 751–766.

50. Pedro C. Marijuhn. *BioSystems* .**1995**. 35,167-170.

51. Grifftiths, A. D. *et al. EMBO J*. **1994**. 13, 3245-3260.

52. Fazgerald, M. M., Churchill, M. J.,McRee, D. E. and Goodin, D. B. *Biochemistry*. **1994**. 33, 3807-3818.

53. Robertson, D. E. et al. *Nature*. **1994.** 368, 425-432.

56. Ilan Samish, Christopher M. MacDermaid, Jose Manuel Perez-Aguilar, and Jeffery G. Saven. *Annu. Rev. Phys. Chem.* **2011**.62:129-149.

57. C.A. Floudas, H.K. Fung, S.R. McAllister, M. Mönnigmann, R. Rajgaria. *Chemical Engineering Science.* **2006.** 61, 966 – 988.

58. Almer M. Van der Sloot, Christina Kiel1, Luis Serrano and Francois Stricher. *Protein Engineering, Design & Selection.* **2009**. 22 .9. 537–542.

59. Navin Pokala and Tracy M. Handel. *Journal of Structural Biology.* **2001**.134, 269–281.

60. Shaun M Lippow, and Bruce Tidor. *Current Opinion in Biotechnology.* **2007**, 18,1–7.

62. Kouji Takeda , Junichi Sato, Kazuyuki Goto, Takanori Fujita, Toshihiro Watanabe, Mitsuru Abo, Etsuro Yoshimura, Junichi Nakagawa, Akira Abe, Shinji Kawasaki, Youichi Niimura*. Biometals*. **2010**. 23:727–737.

63. Koder R.L.,Anderson, R., Soloman, L.A., Reddy, K.S., Moser, C.M., Dutton, P.L. *Nature.* **2009**. 458:305-309.

64. Nanda, V. and Koder, R.L. *Nature Chemistry.* **2010**. 2, 15-24.

65. West MW and Hecht MH. *Protein Science*. **1995**. 4, 2032-2039.

66. G.A. Prosser, J.N. Copp, S.P. Syddall, E.M. Williams, J.B. Smaill,W.R. Wilson, A.V. Patterson, D.F. Ackerley. *Biochemical Pharmacology.* 2010.79, 678–687.

67. Richard J Knox, Philip J Burke, Shiuan Chen, David J Kerr. *Current Pharmaceutical Design*. **2003**. 9, 2091-2104.

68. Koder, R.L., Haynes, C.H. Rodgers, M.A. and Miller, A. -F. *Biochemistry.* **2002**. 41, 14197-14205.

69. Christopher Kitts, Chad E. Green, Rebecca A. Otley, Marc A. Alvarez, and Pat J. Unkefer. *Canadian Journal of Microbiology*. **2000**.46, 278-282.

70. Iuri Marques de Oliveira1, Diego Bonatto and João Antonio Pêgas Henriques. *Current Research, Technology and Education Topics in Applied Microbiology and Microbial Biotechnology*. **2010**. 1008-1019.

71. Anke, H., Kuhn, A. & Weber, R. W. S. *Mycological Progress*. **2003.** 2, 219-225.

72. Richard G. Smith , Natasha D'Souza and Stephen Nicklin. *Analyst*. **2008**. 133, 571-584.

73. Naal Z, Park JH, Bernhard S, Shapleigh JP, Batt CA, Abruña HD. *Anal Chem*.**2002**. 74,140-8.

74. Mariëlle J. H. Moonen, Marco W. Fraaije, Ivonne M. C. M. Rietjens, Colja Laane, Willem J. H. van Berkel. *Advanced Synthesis & Catalysis*. **2002**. 344, 1023-1035.

75. P. Hemmerich, V. Massey and H. Fenner. *FEBS Lett*. **1977**. 84, 5–21.

76. International Union of Biochemistry, *Nomenclature of Electron-Transfer Proteins in Enzyme Nomenclature, Recommendations* 1984, Academic Press, Orlando, FL.

77. Vivi Joosten, Willem JH van Berkel. *Current Opinion in Chemical Biology*. **2007**. 11, 195-202.

78. Retsu Miura. *The Chemical Record.* **2001**. 1, 183-194.

79. P. Hemmerich, G. Nagelschneider and C. Veeger. *FEBS Lett*. **1970**. 8, 69–83.

80. A Schmid, JS Dordick, B Hauer, A Kiener, M Wubbolts. *Nature*. **2001**. 409, 258-266.

81. Marco W. Fraaije, Willem. J.H van Berkel. *Biocatalysis in the Pharmaceutical and Biotechnology Industries.* **2006**. CRC Press.

82. Giovanni Gadda, Kevin Francis. *Archives of Biochemistry and Biophysics*. **2010**. 493, 53-61.

83. Tathagata Mukherjee, Yang Zhang, Sameh Abdelwahed, Steven E. Ealick and Tadhg P. Begley. *J. Am. Chem. Soc.* **2010**. 132, 5550–5551.

84. Chaiyen P. *Arch Biochem Biophys*. **2010.** 493, 62-70.

85. Roberto Orru, Hanna M. Dudek, Christian Martinoli, Daniel E. Torres Pazmino, Antoine Royant, Martin Weik, Marco W. Fraaije, and Andrea Mattevi. *The Journal of Biological Chemistry.* **2011**. 286, 29284–29291.

86. Carlos F. Barbas III, Angray S. Kang, Richard A. Lerner and Stephen J. Benkovic. Biochemistry. 1991. 88, 7978-7982.

87. Lewis, E. A. and Tolman, W. B. *Chemical Reviews.* **2004**. 104, 1047-1076.

88. Cerda, J.F., Koder, R.L., Lichtenstein, B.R., Moser, C.M., Miller, A.-F., Dutton, P.L. *Org. & Biomol. Chem.* **2008**. 6, 2204-2212.

89. Kornberg, A and Pricer, W.E. *J. Biol. Chem.* **1951.** 2, 535–541.

90. Raju, G., Capo, J., Lichtenstein, B.R., Cerda, J.F., Koder, R.L. *Tetrahedron Letters.* **2012**. 53, 1201–1203.

91. Chester, K., Pedley, B., Tolner, B., Violet, J., Mayer, A., Sharma, S., Boxer, G., Green, A., Nagl, S., Begent, R. *Tumor Biology*. **2004**. 25, 91-98.

92. Xu, G., McLeod, H.L. *Clinical Cancer Research*. **2001**. 7, 3314-3324.

93. Bridgewater, J.A., Knox, R.J., Pitts, J. D., Collins, M.K., Springer, C.J. *Human Gene Therapy*. **1997**. 8, 709-717.

94. Siim, B.G., Denny, W.A., Wilson, W.R. *Oncology Research*. **1997**. 9, 357-369.

95. Sawyer, D.T. *Oxygen Chemistry*. ed. **1991**.Oxford University Press: New York.

96. Knox, R.J., Boland, M.P., Friedlos, F., Coles, B., Southan, C., Roberts, J.J. *Biochemical Pharmacology*. **1998**. 37, 4671-4677.

97. Frieldos, F., Denny, W.A., Palmer, B.D., Springer, C.J. *Journal of Medicinal Chemistry*. **1997**. 40, 1270-1275.

98. Bailey, S.M., Knox, R.J., Hobbs, S.M., Jenkins, T.C., Mauger, A.B., Melton, R. G., Burke, P.J., Connors, T.A., Hart, I. R. *Gene Ther*. **1996**. 3, 1143-50.

99. Clarke, W.M. *Oxidation Reduction Potentials of Organic Systems*. ed. **1960**. The Williams and Wilkins Co., Baltimore.

100. Nivinskas, H., Koder, R.L., Anusevicius, Z., Sarlauskas, J., Miller, A.-F. Cenas, N. *Arch. Biochem. Biophys.* 2001. 385, 170-178.

101. Hannink N, Rosser S, French C, Basran A, Murray J, Nicklin S, Bruce N. *Nat Biotechnol*. **2001**. 19, 1168-1172.

102. Perez-Reinado E, Blasco R, Castillo F, Moreno-Vivi.n C, Rold.n RD. *Appl Environ Microbiol*. **2005**. 71, 7643–7649.

103. Nokhbeh MR, Boroumandi S, Pokorny N, Koziarz P, Paterson ES, Lambert IB. *Mut Res.* **2002**. 508, 59–70.

104. Takeda K, Lizuka M, Watanabe T, Nakagawa J, Kawasaki S and Nimura Y. *FEBS Lett.* **2006**. 274,1318–1327.

105. Van Aken B. *Curr Opin Biotechnol*. **2009**. 20, 231-236.

106. Van Dillewijn P, Couselo JL, Corredoira E, Delgado A, Wittich RM, Ballester A, Ramos JL. *Environ Sci Technol*. **2008**. 42, 7405-7410.

107. Kurumata M, Takahashi M, Sakamotoa A, Ramos JL, Nepovim A, Vanek T, Hirata T. *Morikawa H.Z Naturforsch C*. **2005**. 60, 272-278.

108. Bryant, C., Deluca, M. *J. Biol. Chem*. **1991**. 266, 4119-4125.

109. Binks, P., Nicklin, S., and Bruce, N.C. *Appl. Environ. Microbiol*. **1995**. 61, 1318-1322.

110. Coleman, N.V., Nelson, D.R., and Duxbury, T. *Soil Biol. Biochem*. **1998**. 30, 1159-67.

111. Kitts, C.L., Cunningham, D.P., and Unkefer, P.J. *Appl. Environ. Microbiol*. **1994**. 60, 4608-4611.

112. Sokic-Lazic, Daria; Shelley D. Minteer. *Electrochemical Solid-State Letters*. **2009**. 12, 26-28.

113. Moehlenbrock, Michael J.; Shelley D. Minteer. *Chemical Society Reviews.* **2008**. 37, 1188-1196.

Chapter 2.

Safaranine enzyme – design, expression and binding.

2.1. Summary.

We are constructing a series of de novo designed protein-cofactor bundles to do electron transfer reactions similar to those done by natural flavoenzymes. These safranine enzymes with safranines as the cofactors will serve as improved NADH acceptor. Our modified safranine derivatives will play the role of the oxygen-insensitive flavin cofactors in natural flavoenzymes, allowing for catalytic activity to be tuned toward particular nitroaromatic substrates by selection of the appropriate derivative. These novel protein-cofactor bundles are intended for use in cancer prodrug activation, treatment of atherosclerosis, explosive sensing, biofuel cells and green chemical catalysis.

2.2. Introduction.

Protein design has expanded its boundaries in the past decade. Scientists have used protein design strategies to make de novo protein with specific function [1-20]. Our lab is developing a de novo safranine enzyme, a novel catalytic design capable of reducing nitroaromatic compounds. This de novo enzyme can also modified and used in the treatment of atherosclerosis and cancer. Compared with the natural enzymes currently

used in drug delivery techniques, the highly specific binding of our artificial enzymes could potentially avoid chemotoxicity and other undesired side effects.

The artificial organic cofactor, safranine O is a flavin-like molecule which has a much lower reduction potential than flavin and favors only two-electron chemistry [21]. It ensures to avoid all the free radical generating reactions that flavins perform. Using a computational de novo approach to design the binding sites for our safranine O cofactors, Prof. Vikas Nanda and his colleagues, made a combinatorial library of all available structures from the Protein Database [1,2,3]. A ProCAD algorithm was used to perform a statistical assessment on this library in order to pick consensus residues for the binding cavity. Then, keystone residues were fit to the α-helices, which were simply assembled using binary patterning [6,22]. Several iterations of saf proteins were made and analyzed for structural and binding properties [18]. Saf-X and safX-Loop are the latest iterations, and our binding studies show that they are indeed potential candidates for a fully functional artificial safranine enzyme.

2.3. Methodologies and experimental procedures.

2.3.1. Designing Saf Proteins.

All of the Saf proteins were designed in Prof. Vikas Nanda's lab, the Center for Advanced Biotechnology and Medicine and Department of Biochemistry, University of Medicine and Dentistry of New Jersey - Robert Wood Johnson Medical School, Rutgers University. Using a computational approach, ProCAD algorithms were applied to perform a statistical assessment and pick the consensus residues for the cofactor binding

pocket [1,2]. The helix backbone was constructed using simple binary pattering method [6,22].

Fei Xu in Vikas Nanda's lab designed the first set of saf proteins. For better binding affinity and specificity the most favorable protein scaffold for a safranine enzyme is a helix-loop-helix motif [1,20]. To encapsulate the safranine cofactor, a dimerised four-helix bundle with two α-helix strands connected with loops was created with an active binding site designed to bind safranine. Selection and optimization of the keystone residues was the first major step[1]. These consensus residues bind the amine groups of safranine cofactor with a hydrogen bond. Some of these residues must interact electrostatically with the positively charged nitrogen in the safranine cofactor, so serines and glutamates were selected as the potential residues. The first two glutamates were placed for electrostatic interactions and the other two for hydrogen bonding. Among the four serines selected, two of them were placed to take part in hydrogen bonding and the other two bonded with the above glutamates. Identifying optimal locations for the residues in the helix strands was the next step [1,2]. First, the safranine was flanked between two fictional helix strands, with the distance between optimized at 19 Å. Then, another two helixes were placed on the other two sides, resulting in a four-helix bundle with a radius of about 9.5 Å. At this stage in the design, all the residues except the serines and glutamate consensus are just repetitions of alanine. Keystone residues were placed on each strand in accordance with optimal distances. The hydrophobic cavity around the methyl group of the safranine cofactor ensures the fine-tuning of its electrochemical properties inside the enzyme complex. Approximations in energy calculations gave a small bend in helix orientation [1].

Binary patterning was used to satisfy the helix with a heptad repeat of a pentapeptide sequence such as this: ◆••••••, where (•) are polar and (◆) are non polar residues [6,22]. This pattern creates a right-handed amphiphilic α-helix with a hydrophobic surface on one side, which further drives the assembly of a α-helix bundle with a hydrophobic core inside. During the design evolution of the enzyme, each candidate structure was evaluated using nuclear magnetic resonance (NMR) imaging [1,20]. To enhanced NMR signals, the hydrophobic core was packed with asymmetric residues, using ROSETTA, a computational tool developed by Prof. David Baker's laboratory [19]. ROSETTA relies on the idea that the structure and stability information is encrypted in the local environment of each fragment of a larger protein molecule. It builds a small peptide of ten residues chosen by the statistical assessment of high-resolution PDB structures, and then reassembles these small peptide chains into larger ones. This approach reduces the conformational degrees of freedom in candidate structures [19]. In this step, we reduced the number of tryptophan and phenylalanine inside the hydrophobic core, which can be puzzling in the NMR structure elucidation. To evaluate the stability, the enzyme candidate was given a scoring value both in terms of van der Waals interactions and a statistical analysis of known residue interactions from protein data bank [1,23]. As a result of this analysis, the helix bundle radius was adjusted from 9.5 Å to 7.0 Å.

We then connected these four helices with three canonical loops. These loops enhance the folding of the protein into its tertiary structure. To properly fit the loops to the helices, a helix-loop-helix motif was extracted from an X-ray crystal structure (PDB ID: 1MFT) and superimposed onto our model of the saf bundle structure. Then the ϕ and ψ angles of the residues and the RMSD of the helical regions between the motif and model were

adjusted. During the loop fitting processes, there is a possibility of change in the conformation of some residues, which was repaired by moving the residues to another location. The energy minimization step was done to avoid any steric hindrance in the model [1,24]. The fine tuned finalized model of the saf helix bundle was designed to be of high affinity and specificity, attaining a tertiary structure suitable for electrochemical measurements and feasible for NMR experiments.

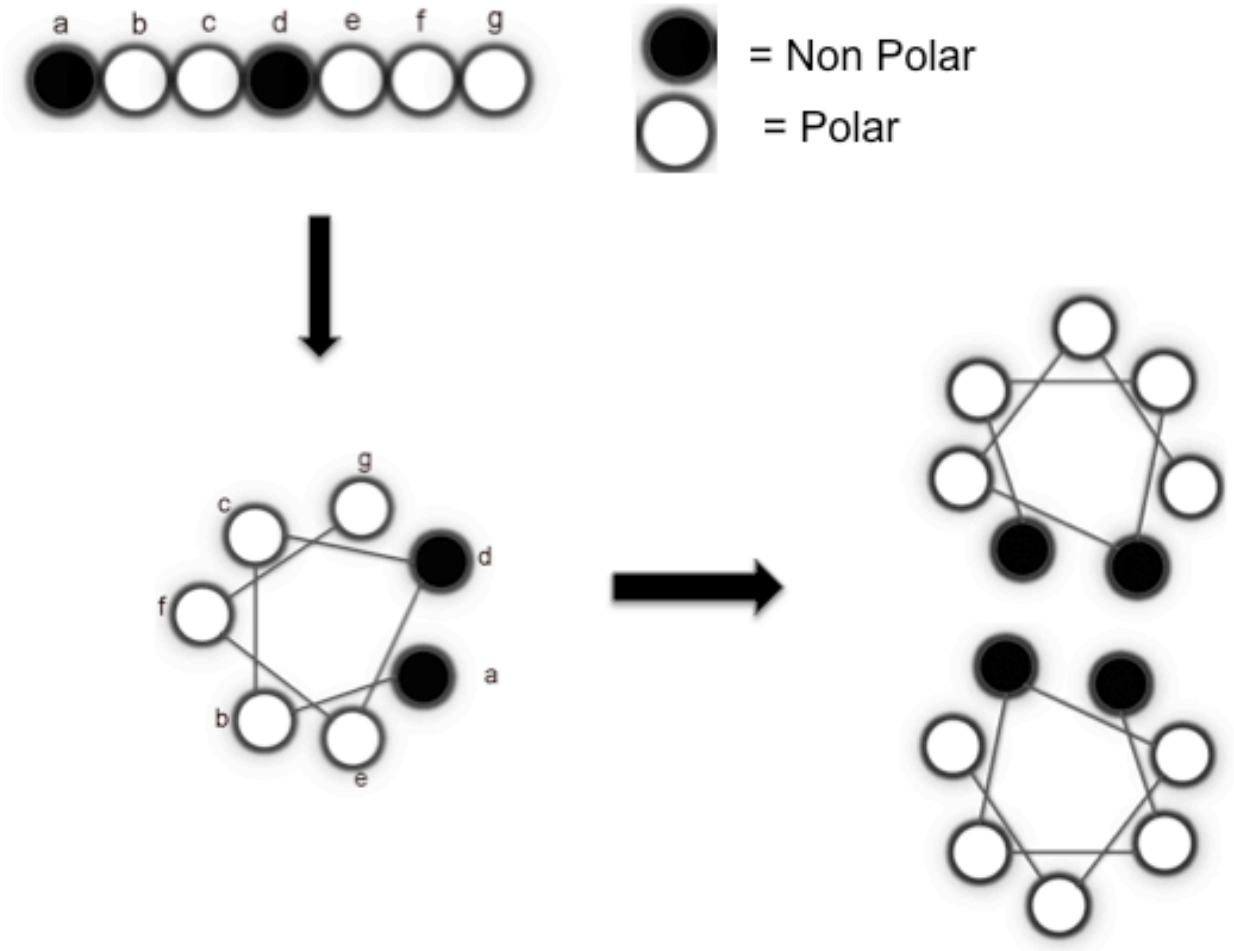

Figure. 2.1.Binary patterning. A hydrophobic surface will be created by repeating pattern of nonpolar (filled circles) and polar (open circles) residues. These surfaces can drive associations of helices, forming a hydrophobic core.

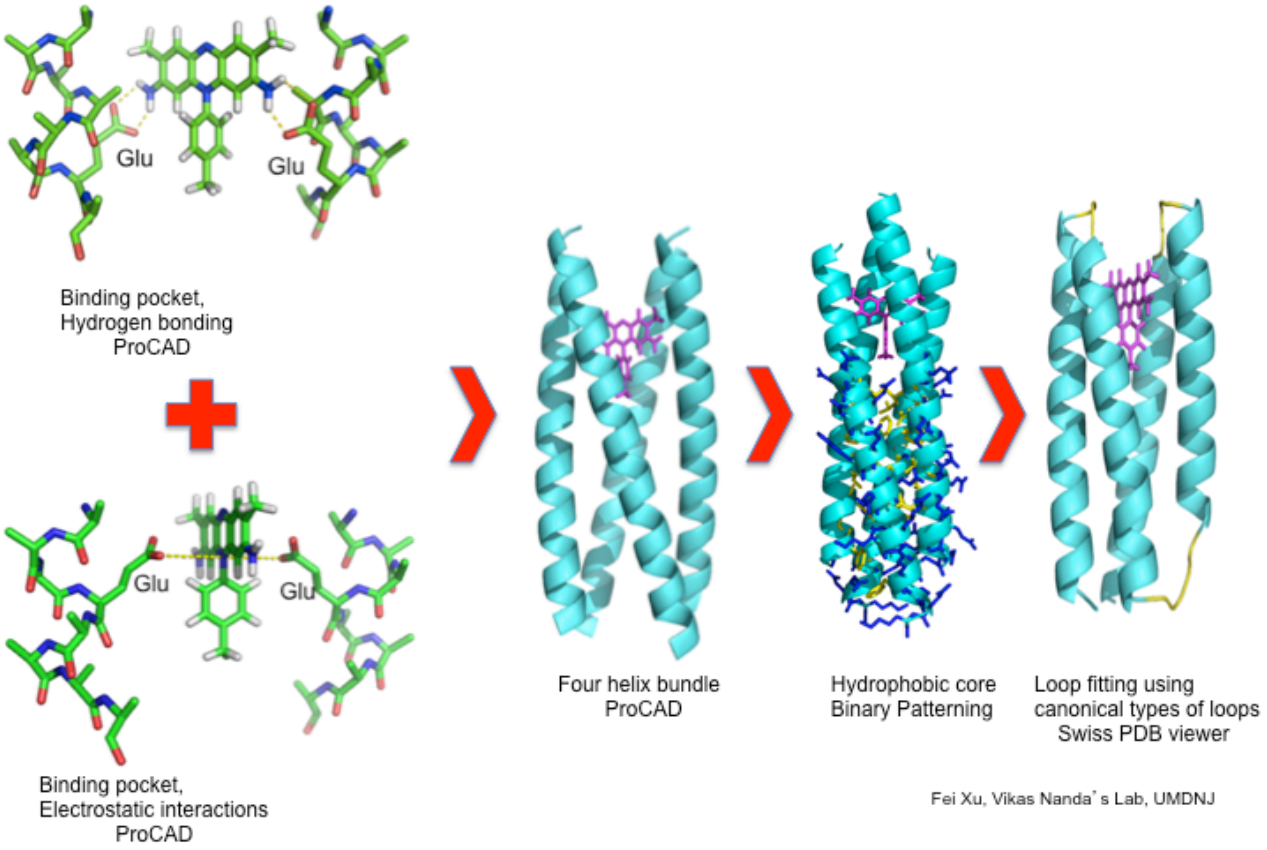

Figure.2.2. Our protein design algorithm.

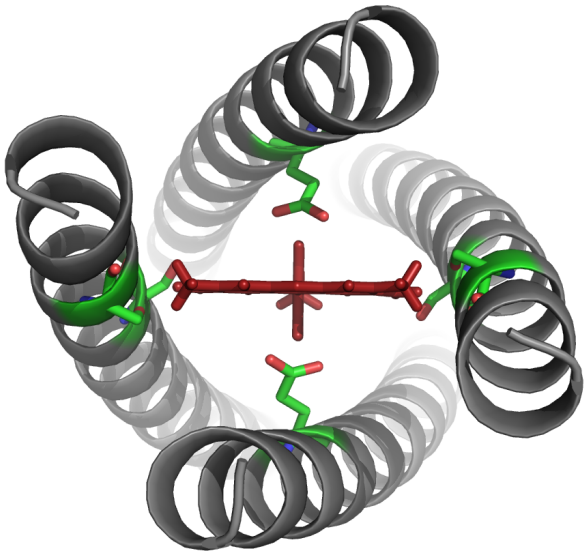

Figure 2.3. Safranine O inside a saf-protein model. Keystone glutamates are highlighted. (Courtesy: Prof. Vikas Nanda's lab, UMDNJ)

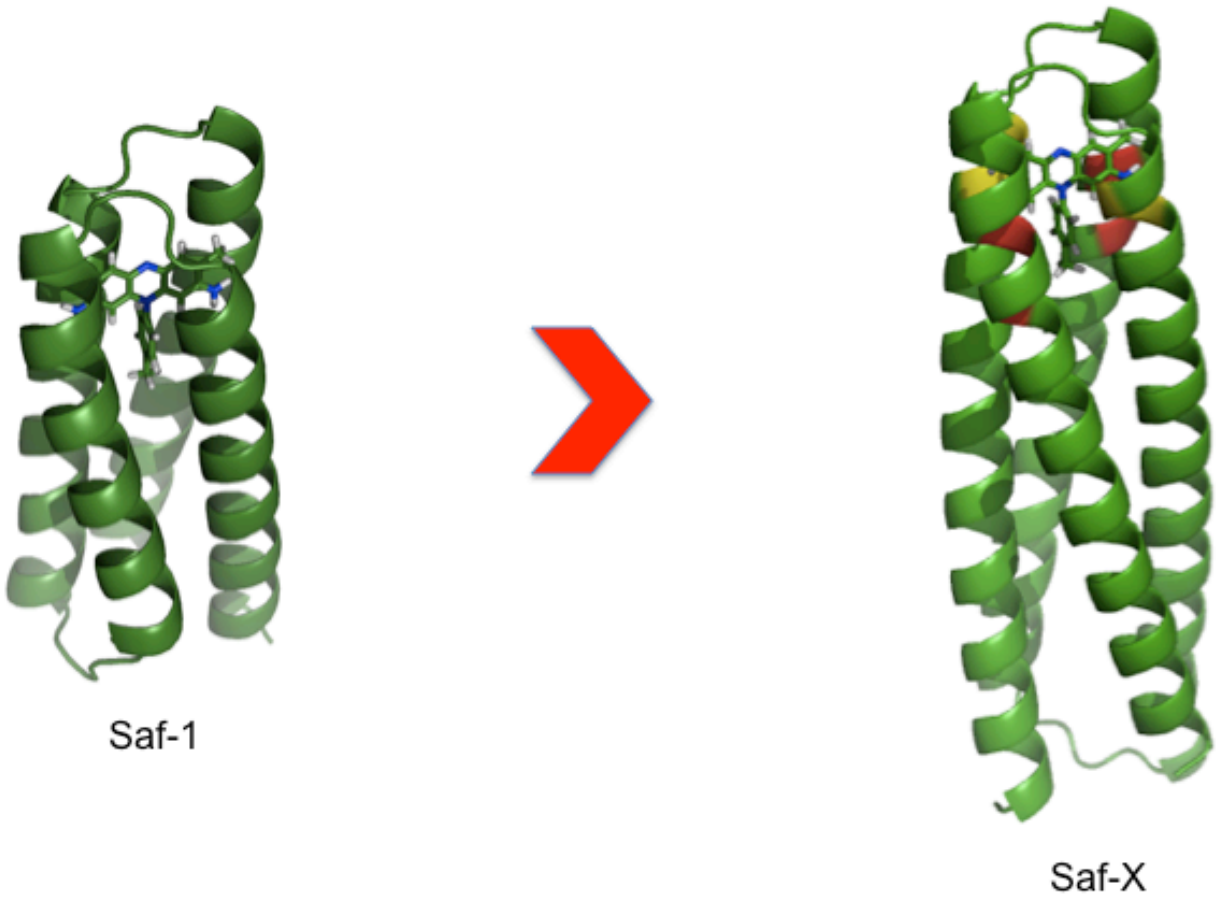

Figure 2.4. Saf-1 (first generation) and saf-X (last generation) protein binds to safranine O. (Courtesy: Prof. Vikas Nanda's lab, UMDNJ)

2.3.2. Expression and purification of recombinant protein from *E. coli*.

The DNA synthesized by DNA 2.0 was cloned into an expression vector and transformed into *E.coli* BL21agar plates with ampicillin selection [20,25,26]. The transformed BL21 was grown into colonies on overnight incubation at 37 °C. Then carefully selected cells from the agar plates were grown in a 100 ml LB media overnight at 37 °C. The next day, 100 ml LB cell media was transferred into 2L TPP media containing ampicillin, glucose and trace metals. The growth was monitored by the absorption of media at OD_{600} on 20 min. intervals. 0.5mM isopropyl-β-D-1-thiogalactopyranoside (IPTG) was used to induce the expression on the absorption of media reached close to 1. Cells were grown at room temperature for 5 h and harvested by centrifugation. The resulting cell pellets were re-suspended in lysis buffer together with DNAse I and PEFABLOC and incubated at 4°C for 30 min. on a rotor. The cells were French pressed in ice-cold conditions and centrifuged to collect the supernatant. The cell lysate was loaded into a nickel affinity column on a Biorad DuoFlow FPLC. Saf proteins with His tags bind to the nickel column and thus could be separated from the other proteins and eluted out by an elution buffer. The eluted protein was collected separately with the help of a Quadtec UV-Vis detector [20,25,26]. The denaturing of the protein was done by an 8M urea buffer. The His tagged saf proteins which were dialyzed into TEV working buffer needed to be cleaved by TEV cut protein for 6h at room temperature. Then, the protein was again loaded into the nickel column for another FPLC run. This time the cut TRX His-tagged protein would bind to the nickel column while the saf protein without His tags would be washed out first. Again the saf proteins were collected with the help of absorption a Quadtec UV-Vis detector. The

protein purity was tested on SDS-PAGE gel. The saf protein, stained with coomassie blue, was run along with a molecular marker to determine the size, purity and expression level. The pure protein was dialyzed in a 0.1 M redox buffer for further experiments. For ^{15}N-labelled expression, cells were grown at 37°C in M9 minimal media containing 1 g/L ^{15}N ammonium chloride to a OD_{600} of 1.0, induced with1 mM IPTG, and shaken at 25° C for an additional 7 h [20]. ^{15}N -labeled ammonium chloride was purchased from Cambridge Isotope Labs (Cambridge, MA).

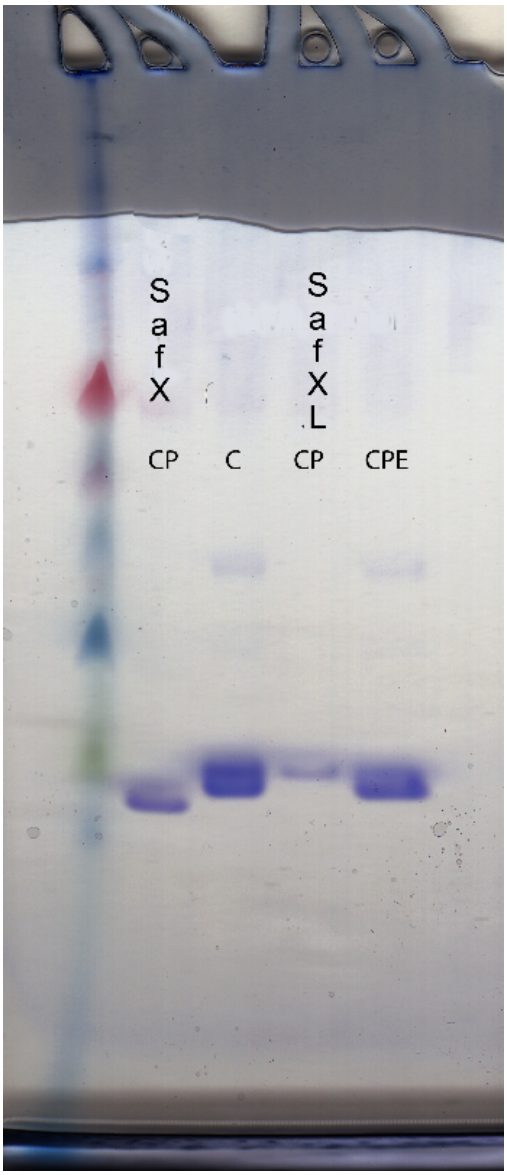

Figure 2.5. SDS-PAGE gel of saf-X and SafX-Loop.

2.3.3. Circular Dichroism.

Circular Dichroism (CD) measures the absorption of the protein using left or right handed polarized light. The spectrum is distinctive for each type of secondary conformation of the protein [27]. The difference in absorbance between left circularly polarized (LCP) and right circularly polarized light (RCP) is delta absorbance (ΔA), ($\Delta A = A_L - A_R$). CD is expressed in degrees of ellipticity (θ), with $\theta = \tan^{-1} \frac{b}{a}$ where b and a are major and minor axis of the resultant ellipse. The numerical relation between ellipticity (θ) and delta absorbance (ΔA) is $\theta = 32.98\ \Delta A$, where ΔA is a function of wavelength. An ellipticity of roughly 10 mdeg corresponds to a ΔA on the order of 3×10^{-4} [27]. The CD varies throughout a protein depending on which chromophore is in focus: peptide bonds have an absorption below 240 nm, aromatic amino acid side chains have an absorption range of 260 to 320 nm, and disulphide bonds have very weak bands around 260nm [27,28]. Cofactors can also be detected in a wide spectral range. Heme can have a strong signal at 410 nm with the rest of its spectral bands in a wide range between 350 to 650 nm, depending on the spin state and coordination of the Fe. Falvin varies with its oxidation state, with absorption in the 300 nm to 500nm range [30]. If a ligand has no intrinsic chirality, it can have an induced CD signal when it binds to a protein, achieving chirality due to the asymmetrical protein environment [30].

The absorption of a protein's peptide bond region (mostly 240nm and below) can be used to predict secondary structure. An n to π* transition has a broader but weaker band towards 220 nm, while a π to π* transition has strong band will be at 190 nm. In Saf α-helical bundles the percentage of helicity can be estimated using the CD signal values

arising at 208 nm and 222 nm. Conformational changes of saf protein over safranine O binding also can be observed by examining changes in different spectral regions [27,30]. Our CD spectra were recorded on a Jasco J-810 spectropolarimeter, at a temperature of 25 °C. Experiments were recorded in a range of 180 to 300 nm for secondary structure determination and for conformational change during ligand binding. The cell used was a quartz cuvette with a path length of 0.01 cm. In general, the ionic strength in the protein solution was kept very low so that the absorbance at 190 nm did not exceed 1. A Fourier transform algorithm was used to smooth all the spectra, and the background spectra were subtracted so that the resultant ΔA would only indicate the CD signals of the peptide bonds. The saf proteins were prepared with a concentration of 5 μM, and all experiments were run at 25 °C in 0.1 M redox buffer at pH 8.0.. The concentration was determined by ratio of absorbance (obtained on uv-vis diode-array spectrophotometer) of protein at 280 nm with specific extinction coefficient (ε) of each protein in accordance with Beers law. In ligand binding experiments, safranine O from a 1mM stock solution was added to an equimolar concentration of protein of interest into the same cuvette. Protein secondary structure percentages were calculated with K2D3 using data points ranging from 190 to 240nm [29].

2.3.4. Isothermal Calorimetry.

Protein ligand binding can be exothermic or endothermic. That is, a small amount of heating or cooling in the reaction medium always follows the binding. Isothermal calorimetry detects these small changes and serves as a measure of binding [31,32]. A solution containing reactant (binding partner) is maintained at constant temperature by a

thermostat as the titrant is added in small aliquots. The detection of the heat of reaction is directly dependent on the energy demanded by the thermostat to maintain a constant temperature in the solution. Recent instruments have a higher sensitivity, allowing them to measure the heat effects generated in a reaction in which reactants were in a range of 10 to 100 μM [31]. The injections of titrant continue until no further heat is generated or absorbed. At this point, the reactant in the cell has presumably reached complete saturation. The resultant spikes (spike correspond to the heat change of each titration) are integrated into an isothermal curve which can be analyzed for equilibrium constants (K_B) and thus, for standard Gibbs free energy (ΔG), enthalpy change (ΔH), entropy change (ΔS), also for the stoichiometry (*n*) of the binding. Heat capacity change (ΔCp) of the association reaction can be calculated from experiments run at different temperatures [31].

The mechanism of calorimeter is based on feedback that measures the difference of heat between the reference and the sample cell. The reference cell is under a constant external power, triggering the feedback circuit that also regulates the temperature of the sample cell. Normally the sample cell temperature would increase less than 0.1 °C/h during the progress of the experiment [32]. The rebound of feedback power from the resting baseline depends on the type of reaction. There is a decrease in the feedback power in the exothermic reactions and an increase in the case of endothermic reactions. Water is referenced against the system of interest in the sample cell. The titrant is injected using a long needled syringe continuously rotating throughout the experiment to ensure complete mixing. The heat produced as a result of the rotation becomes the part of the baseline. The heat of dilution during titration is corrected during analysis. The shape of the binding curve (C) is the product of binding constant K_B (M^{-1}) and molar concentration of

molecule being titrated (P) [31]. Most of our experiments were done with a C value between 10 to 100.

$C = K_B [P]$

The reversible association between protein (P) and ligand (L) can be represented as

$P + L \leftrightarrow PL$

And the binding constant K_B is

$$K_B = \frac{[PL]}{[P][L]}$$

[PL] is the complex, [P] is the protein and [L] ligand concentration.

The heat generated or absorbed due to each injection in the titration is directly proportional to the amount of the protein-ligand complex formed and can be stated as

$Q = V_0 \Delta H \Delta [PL]$

where Q is the heat associated with the reaction, V_0 is the volume of the sample cell, ΔH is the molar enthalpy of binding and Δ [PL] is the change in concentration of the complex.

All our binding titrations are done with Microcal (Northhampton, MA, USA), and the cell jacket temperature was kept at 25 °C throughout. HPLC purified safranine O taken in syringe was titrated against saf X loop and saf X in the sample cell. Experiments were run with protein and ligand in the same buffer and same pH. We used a pH 8 redox buffer with salt (KCl) concentrations varying from 0.1 to 1mM. We also did titrations in a Tris buffer at a pH of 7.5. Safranine O cofactor was titrated against HHHH aka H4 (not a

safranine O binding protein) in Tris buffer at pH 7.5 as a control experiment. To obtain a complete binding curve, the cofactor was titrated in a range of 10 to 100 mM in different experiments against all the proteins. Protein concentrations were varied between 0.1 to 100 mM. The protein volume injected in the sample cell was always 1.4 ml and the ligand in the syringe was approximately 0.4 ml, slightly more than needed for the whole titration. All proteins and ligands were degassed in a Thermovac at 25 °C. Each experiment was designed to run 2 or 10 μL/injection with a total time from 80 to 100 minutes. The sample cell was rinsed and soaked in the same buffer where the experiment was carried out. Proteins were loaded into the cell with extreme care to avoid bubbles in the solution. The total number of injections varied from 10 to 20. In every experiment first addition was smaller and eliminated during the analysis to adjust the equilibrium time for the whole titration. The binding peaks are obtained with μcal/sec against time in minutes. The peaks obtained were integrated and analyzed using Origin (Originlab Corporation). The integrated exothermic binding curve was obtained in kcal/mole of injectant against molar ratio after being corrected for heat of dilution.

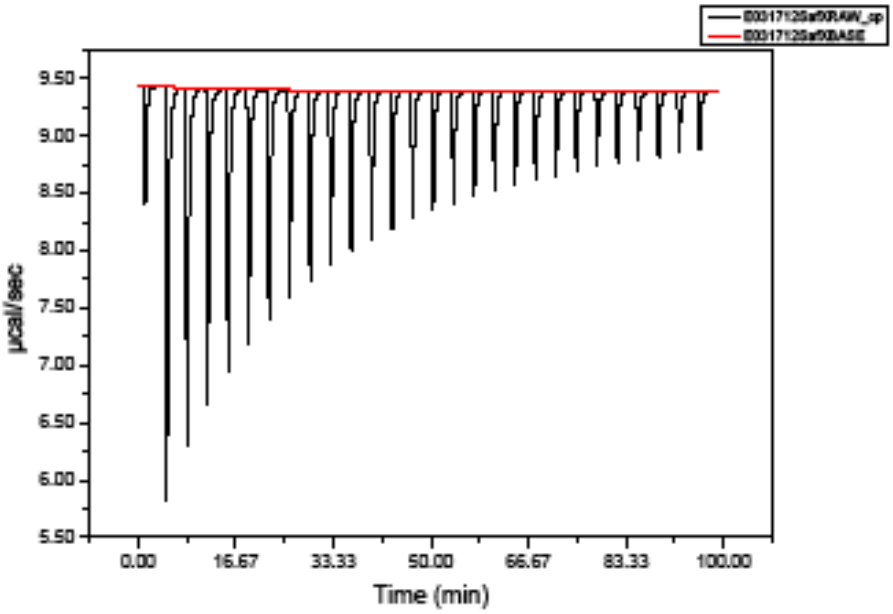

Figure.2.6. Raw data from ITC of safranine O against saf-X. Calorimetric experiments were later dropped from binding studies.

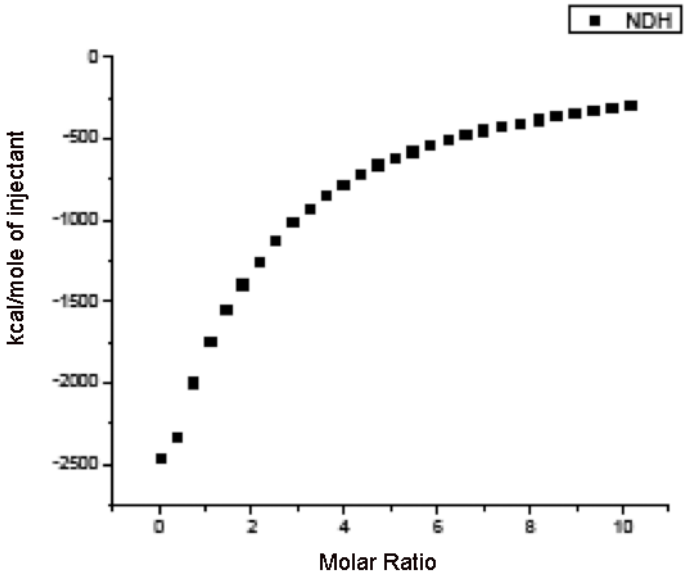

Figure.2.7. Integrated heat data from ITC of safranine O against saf-X. Calorimetric experiments were later dropped from binding studies.

2.3.5. Fluorescence Spectrophotometry.

Fluorescence occurs when photon is emitted during molecular relaxation from electronic excited states [33,34]. It involves the first absorption between the electronic levels and emission at a longer wavelength. The fluorescence wavelength differs from the incident light, so there is no background from the excitation source. Thus the sensitivity of fluorescence spectrophotometry measurement is much higher than absorption spectroscopy, able to detect even 10^{-7}M concentrations of fluorophores [34]. The excitation will be triggered by the photons with energies from the uv or blue-green range. Electronic levels are further divided into vibrational sublevels. According to Pauli exclusion principle, there have to be symmetric or antisymmetric spin states for electronic wave functions. The excitation of molecules occurs from the lowest vibrational level of the electronic ground state, which is a singlet state, to the accessible vibrational level of the next electronic excited singlet state. The fluorophore then rapidly relaxes to the lowest vibrational level of the electronic excited state on a timescale of femto to pico seconds. This is called the Stoke shift [34]. The timescale of the molecule, which remains in the lowest vibrational level of the electronic excited state is called the fluorescence lifetime, normally on the order of nanoseconds. The observed fluorescence emission is the decay from the excited electronic state to the allowable vibrational level of the electronic ground state. According to the Frank-Condon principle, the vibrational levels are not significantly altered during the absorption, excitation or emission [34]. This similarity in the vibrational level structures in the ground and excited states often results in identical features in the absorption and emission spectra.

$S_0 + hv_{ex} \rightarrow S_1$ [Excitation]

$S_1 \rightarrow S_0 + hv_{em} + heat$ [Fluorescence emission]

h is the Planck's constant and v is the frequency of light. S_0 is the ground state of the fluorophore and S_1 is the first electronic excited state.

The quantum yield (ϕ_F) is the efficiency of the fluorescence process. It is the ratio between the number of photons emitted and the number of photons absorbed. When every photon absorbed is emitted the quantum yield is 1.0 or 100%. Nevertheless, even fluorophores with 0.1 quantum yield are also considered fluorescent.

$$\phi_F = \frac{\#\ of\ photons\ emitted}{\#\ of\ photons\ absorbed}$$

Quantum yield can be also expressed in terms of the rate of fluorescent decay as follows:

$$\phi_F = \frac{k_{em}}{\sum_i k_i}$$

where k_{em} is the spontaneous emission rate and $\sum_i k_i$ is the sum of all excited-state decay.

The change in intensity, when light passes through sample, is correlated to Beer-Lambert law. The intensity change in the light is proportional to the number of excited molecules,

$$I = I_o\, e^{-\ln(10)\varepsilon_\lambda cl}$$

where ε_λ is the extinction coefficient at excited wavelength, c is the concentration of the sample and l is the path length of the light, I_o is the incident and I is the exited intensity of light. If the absorbance is low, we can express intensity as

$$I = I_o [1-\ln (10) \varepsilon_\lambda cl]$$

The fluorescence emission intensity (F_λ) of a fluorophore at a given wavelength is a function of the quantum yield (ϕ_F), the fraction of emission at that wavelength (f_λ) and the fraction of the radiation collected by the detector (z)

$$F_\lambda = \ln (10) \varepsilon_\lambda cl\, I_o \phi_F f_\lambda z$$

F_λ is also expressed in terms of the rate constant (k'), which accounts for the quantum yield.

$$F_\lambda = k' (I_o-I)$$

The difference in incident light (I_o) and the light exiting sample (I), is equal to the amount of absorbed light (A). According to the Beer-Lambert law

$$A = \varepsilon cl$$

$$\varepsilon\, cl = \log \frac{I_o}{I}$$

$$F_\lambda = k' I_o (1\text{-}10^{-\varepsilon\, cl})$$

This can be expanded in a McLaren series

$$F_\lambda = k' I_o (\ln (10)\, \varepsilon_\lambda\, cl - \frac{(\ln (10)\, \varepsilon_\lambda\, cl)^2}{2!} + \frac{(\ln (10)\, \varepsilon_\lambda\, cl)^3}{3!} + \cdots)$$

In a dilute solution, which has absorption of 0.05 at the excitation wavelength, the high order terms are insignificant and F_λ is approximately linear. But experimentally, the fluorescence does not always have a linear relation to the concentration. High concentrations of fluorophore and higher (I_o) excitation intensity can lead to higher fluorescence.

If, $\ln (10)\, \varepsilon_\lambda\, cl < 0.05$ then,

$$F_\lambda = k' I_o (\ln (10)\, \varepsilon_\lambda\, cl)$$

$F_\lambda = Kcl$

Experiments in high concentrations can lead to self-quenching and inner filter effects. It is better to maintain the concentration of fluorophore so that the absorbance is < 0.1 for a linear response in fluorescence emission [34].

The protein binding to the ligand can enhance a three-dimensional structural change. This structural change can cause a variation in the environment of a fluorophore. This environmental change can be marked by measurable deviations in the emission spectrum [33]. This can be a notable change in the fluorescence emission intensity (F_λ) or can be a shift in the emission wavelength (λ_{em}). If *n* is the moles of bound ligand per mole of protein:

$$n = \frac{[L]_{bound}}{[P]_{total}}$$

$[L]_{bound}$ is the concentration of ligand bound to protein and $[P]_{total}$ is the total protein concentration. If the changes in the fluorescence emission are linear in *n*, this can be used to determine the dissociation constant (K_d) of the protein for the ligand [33].

Safranine O has intrinsic fluorescence and can be excited at 522 nm with an emission at 581 nm. This was exploited during the binding studies. After binding to protein, fluorescence emission intensity (F_λ) was higher and also caused a shift in the emission wavelength (λ_{em}). When the titration was done by varying protein concentration in a minimum amount of safranine O, the emmission intensity increased with the amount of protein added and became constant after all the cofactor was used up in the binding. The

absorption of safaranine O was kept < 0.1. When the titration was done by varying safranine O with a fixed concentration of protein, there was also a linear increase in fluorescence emission intensity (F_λ), as well as a shift in emission wavelength (λ_{em}). Low-level concentrations of safranine O were used in aliquots for the binding study titrations. In higher concentrations of safranine O, the signals from non-specific protein cofactor interactions exceeded the binding signals.

All experimental data was recorded using an Olis fluorescence spectrophotometer. The temperature for all binding titrations was 25 °C, regulated with a thermostat. The increments of scan were 100 per second. Incoming light intensity was regulated with a slit of 0.6 and the outgoing slit was 1.24. The sample cell used was a quartz cuvette with 1cm path length. The spectrophotometer was tuned to higher voltage scan modes, in a range between 950 and 1100, when lower concentrations of safranine O were used in binding experiments. This was to ensure sufficient fluorescence emission intensity.

2.3.6. UV-Visible Spectroscopy-Redox Titrations.

In the ongoing redox titrations, UV-visible spectra are collected using an Olis computerized HP 8455UV/vis diode array spectrophotometer. Concentrated solutions of safranine O prepared in advance were diluted to1-2 μM into a solution containing >100 μM of the corresponding apoprotein. Reduction potentials are referenced to a standard hydrogen electrode [35]. All redox titrations are performed anaerobically using μL additions of freshly prepared sodium dithionite to adjust the solution potential to more negative values and potassium ferricyanide to more positive values [36]. The

reduction potentials obtained from apoprotein-safranine O solution are being compared against the redox titration of safranine O by itself [35,46].

Redox titrations are analyzed by monitoring the absorbance bands at 522 nm as the safranine O is reduced or oxidized [35]. The data is being analyzed with the Nernst equation using a z-value of 2.0

$$E = E^{o} - \frac{RT}{ZF} \ln \frac{[Saf.O]_{red.}}{[Saf.O]_{ox.}}$$

E is the ambient potential in the solution. E^o is the midpoint reduction potential of safranine O. R is the universal gas constant (8.31 $JK^{-1}mol^{-1}$). T is the absolute temperature. F is the Faraday constant (9.65 x 10^4 C mol^{-1}). Z is the number of electrons transferred in the reaction.

2.3.7. Nuclear magnetic Resonance Spectroscopy.

All NMR experiments were performed at 20°C on Varian Inova spectrometer operating at a 600MHZ and equipped with a triple resonance cryogenic probe capable of applying pulse field gradiants in the z-direction. Data was processed using the program NMR Pipe and analyzed using Sparky [37,38]. For structural specificity assays, sensitivity enhanced ^{1}H-^{15}N heteronuclear single quantum coherence (HSQC) spectra were collected on 50-100 μM holo- and apoprotein samples with sweep widths of 10,000 Hz for ^{1}H and 2000 Hz for ^{15}N utilizing GARP decoupling of ^{15}N during ^{1}H acquisition [39]. Chemical shifts were referenced to water at 4.77 ppm for ^{1}H. Lyophilized ^{15}N-labelled apoprotein samples were dissolved in 25 mM KaD_2PO_4. D_2O buffer pD 5.0

(pH meter reading + 0.4 pH units), a spectrum taken, and pD adjusted upwards by the addition of small amounts of KOD dissolved in D_2O. The observed ^{15}N chemical shifts were fit with the Henderson-Hasselbach equation

$$\delta_{obs} = \frac{\Delta\delta_{prot}}{1 + 10^{[pH-pKa]}} + \delta_0$$

where δ_0 is the neutral chemical shift of ^{15}N, δ_{prot} is the change in chemical shift due to protonation and pKa is the fitted acid dissociation constant.

2.4. Iterations of Saf protein and results.

2.4.1. Saf-1.

EELQRIAEAWERIWREVQQSSEKTSN-PEKKHAEQEEADELLRFAQKGSVS-

PQEFVEDAKAIAQRVQRSSEKTSN-PEKKQSEEREANELQNFAQWLEQAA

Sequence of saf-1 protein.

Saf-1 protein was designed by Fei Xu in Vikas Nanda's lab. The protein contains 99 residues with 11.5 kDa. The extinction coefficient (ε) is 17070$cm^{-1}M^{-1}$ [40]. It went through the native protocol of cloning, expression and purification. The CD studies showed that the apoprotein was not folded in solution. It also appeared that the protein was precipitating out of solution in higher concentrations. The preliminary binding studies by means of fluorescence spectroscopy show that there was a change in the fluorescence emission intensity (F_λ) and a slight shift of 3 nm in emission wavelength (λ_{em}). Nevertheless, we could not confirm whether it was partially bound or if there was non-specific binding to the aggregated protein.

Figure 2.8. Saf-1 and saf-2 (first generation) protein binds to safranine O. (Courtesy: Prof. Vikas Nanda's lab, UMDNJ)

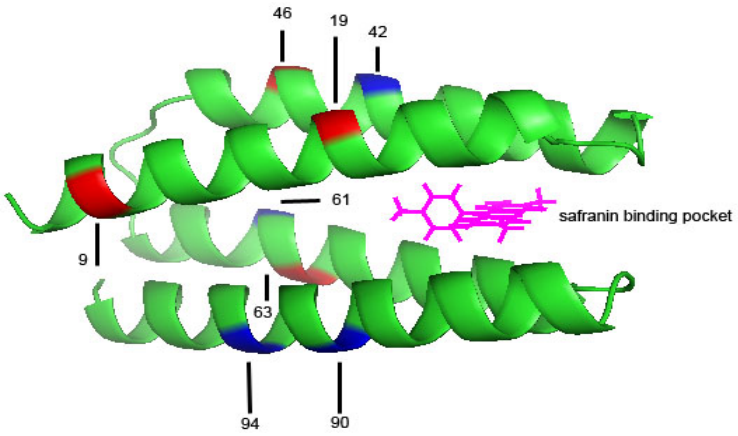

Figure 2.9. Saf-1 modification. Residues 9,19,46,63 are added for more negative charge and 42, 61, 94, 90 are for enhanced folding.

2.4.2. Saf-2.

EELQRIAEAWERIWREVQQSSEKTSN-PEKKHAEQEEADELLRFAQKGSVS-

PQEFVEDAKAIAQRVQRSSEKTTN-PEKKQSIEREANELQNFAQWLEQAA

Sequence of saf-2 protein.

Saf-2 went through a simple modification from Saf-1. We mutated the 73-rd positioned polar serine in saf-1 with polar threonine with chiral property. Additionally, the 81-st residue, which is a negatively charged glutamic acid in saf-1, was mutated to hydrophobic isoleucine (also chiral). The saf-2 protein contains 99 residues with 11.5 kDa. The extinction coefficient (ε) is 17070$cm^{-1}M^{-1}$ (same as saf-1). After these modest changes, we expected a better performance in folding and solubility. After expression, the protein was found largely insoluble in nickel column purification. Denaturing protocol was used to denature the protein and continue the process of purification. But it remained insoluble in TEV cleavage buffer. Attempts to regain the solubility by adding safranine O cofactor to the protein were unsuccessful.

2.4.3. Saf1-neutral.

EELQRIAEAWERIWREVQQSSEKTSN-PEKKHAEQEEAEELLRFAQKGSVS-

PQEFVEEAKAIAQRVQRSSEKTSN-PEKKQSEEREAQELQQFAQWLEQAA

Sequence of saf1-neutral protein.

With the help of Prof. Vikas Nanda , Master-student Jane Lau in our lab started working on a new saf-1 sequence modification, focusing on increasing the solubility and enhancing folding for better binding properties. The saf1-neutral has four major amino acid changes on possible helix-breaking residues: D42 (negatively charged aspartic acid) to E (negatively charged Glutamic acid), D61 to E, N90 (polar asparagine) to Q (polar glutamine) and N94 to Q, all for improving the folding. The saf1-neutral protein contains 99 residues with 11.6 kDa. The extinction coefficient (ε) is 17070$cm^{-1}M^{-1}$. The saf1-neutral expressed well and went through purification processes; however, in higher concentrations the protein was insoluble. CD data indicated that the protein was partially alpha helical. Fluorescence binding studies on saf1-neutral with safranine O cofactor showed no binding.

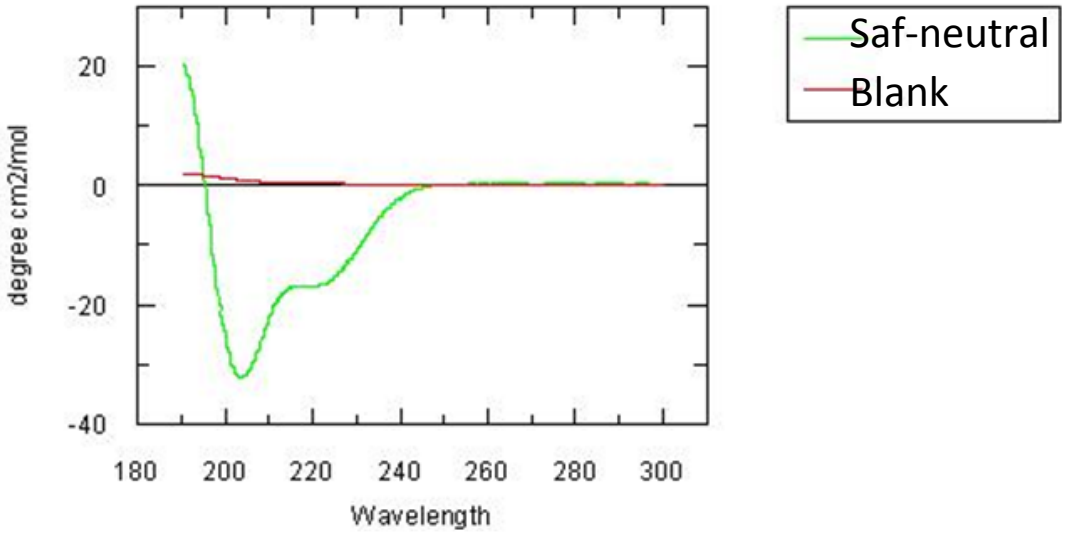

Figure.2.10. CD spectrum of Saf1-neutral, indicates that the protein is partially folded.

2.4.4. Saf1-minus.

EELQEIAEAWERIWEEVQQSSEKTSN-PEKKHAEQEEAEELLEFAQKGSVS-

PQEFVEEAEAIAQRVQRSSEKTSN-PEKKQSEEREAQELQQFAQWLEQAA

Sequence of saf1-minus protein.

Saf1-minus integrated all of the changes made in saf1-neutral together with the change of another four positively charged residues to negative residues: R9 (positively charged arginine) to E (negatively charged glutamic acid), R19 to E, R46 to E and K63 (positively charged lysine) to E. Removal of helix breaking residues and packing of negative charges on the helices was intended to keep the protein from aggregating. The overall charge of saf1-minus became -13. The saf1-minus protein contains 99 residues with 11.5 kDa. The extinction coefficient (ε) is 17070$cm^{-1}M^{-1}$, same as saf-1. CD experimental results showed that both the saf1-neutral and saf1-minus could have a partially alpha helical secondary structure. Initial binding studies on saf1-minus showed little or no binding of safranine cofactor. H4 (aka HHHH) is a protein from Koder lab with an overall charge of -16, but lacking the safranine O binding pocket. Control binding studies of safranine O with H4 showed the same type of behavior as with saf1-minus, suggesting that any kind of fluorescence intensity fluctuation in our binding studies was due to non-specific binding.

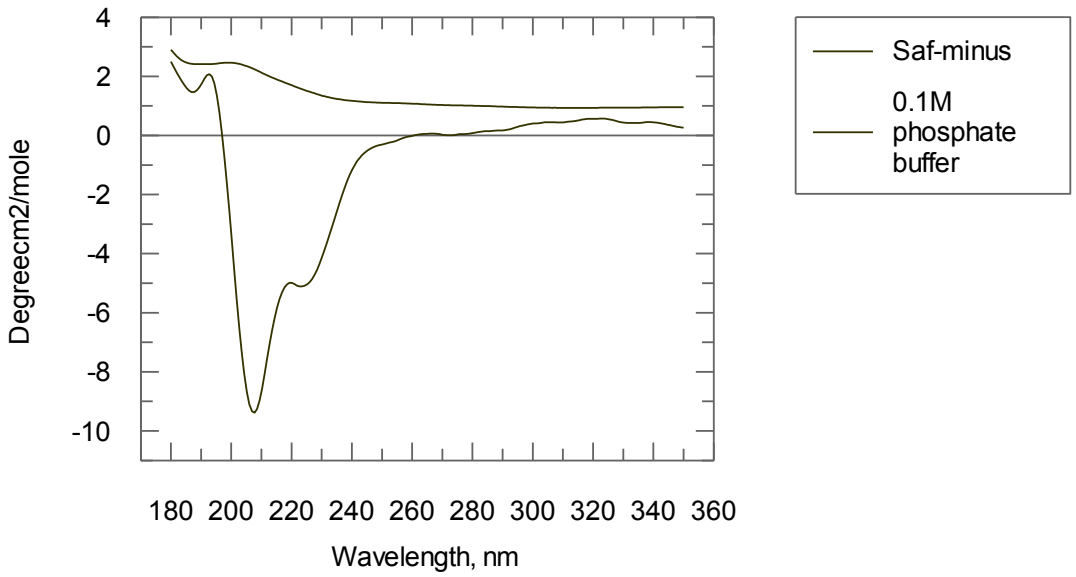

Figure. 2.11. CD spectrum of Saf-minus, indicating that the protein is partially folded.

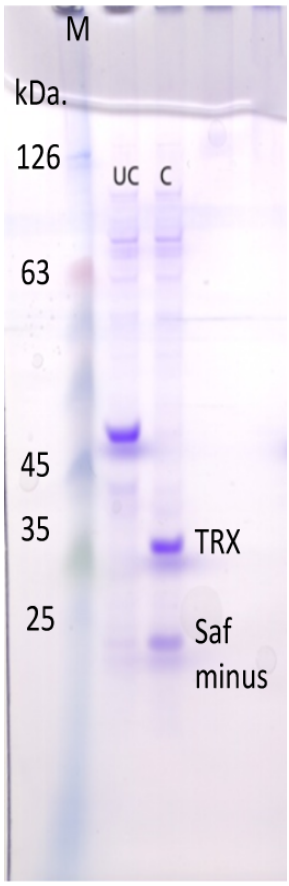

Figure. 2.12. SDS-PAGE gel of saf1-minus.

2.4.5. Saf-X.

EQLAQRLAQVVEEIQRFAEAIERIAREVQKSSEKTSNPQARKEEEAEADDLQRIAQKLQ

QLAQDLQRFAQKGSTSPQEFREDFEQISQRLQEVVEDVKAIAQRVQRSSEKTSNPQAKQ

SEEREANDIQNVAQWFEQAAQKLQAFAQE

Sequence of saf-X protein.

Saf-X protein was designed in Prof. Vikas Nanda's lab. The idea was to elongate the helix turns of saf1-minus by increasing the number of residues, increasing folding and hence improve binding [41]. The overall charge of Saf-X became -7. The saf-X protein contains 147 residues with 16.9 kDa. The extinction coefficient (ε) is 5690$cm^{-1}M^{-1}$. CD experiments showed typical α-helix peaks. A large negative peak of the n to π* transition at 222nm and a π to π* transition was split into two transitions because of exciton coupling. This transition consisted of a negative band at 208nm and a strong positive band at 192 nm. This proved that saf-X was well folded in the solution. Secondary structure percentage calculation shows that saf-X consisted of 83.86% α-helix. Adding 1 equivalent of safranine O to the saf-X in CD deepened the negative bands. The complex secondary structure contained 93.26% α-helix. Isothermal calorimetric experiments were not informative about binding. Titrations were done in different experiments with a range of 10μM to 1mM of saf-X against 10μM to 1mM safranine O. All of the experimental results showed non-completion of reaction. The buffer used was redox buffer at pH 8 for protein and the ligand. Switching of buffer to Tris at pH 7.5 made no change in the

isotherm. As a control, titration of safranine O against H4 (overall charge is -16) was done and the same kind of isotherm as in the saf-X titrations was found. Safranine O cofactor has an intrinsic positive charge. The saf-X protein was packed with negatively charged residues. It was definite that non-specific binding signals were higher than binding signals and such titrations are always incomplete. We modified the experiments with an increase in the salt concentration of the buffer. Titrations were held in range from 0.1M to 1M KCl in redox buffer. Slight improvements were made in the isotherm. But the titrations became extremely difficult, as the rotating syringe baffled in the high salt buffer. Most of the time, the experiments were stopped without completion of the reaction. ITC experiments became extremely difficult in high salt concentrations. Fluorescence measurements were done titrating the protein solution (redox buffer pH 8) to minimum concentration of safranine O (0.5 μM in redox buffer). Also titration of safranine O against 1 μM saf-X in redox buffer pH 8 was done. In both cases, measurements started with safranine O alone in the buffer and the change in intensity and shift of 583nm peak was monitored throughout the experiment. Titration of the protein against minimum cofactor gives a binding curve break at 1 to 1.2 equivalents. Calculations from Grafit showed a dissociation constant (Kd) approximately 0.03×10^{-6}M [42,43]. Safranine O titrated against minimum concentration of saf-X yielded more linear increments of intensity and breaks at almost 1 to 1.2 equivalent of cofactor, with Kd approximately 0.01×10^{-6}M. This experiment was repeated several times with buffers of different concentrations of KCl. Salt concentrations ranging from 0.1 to 2 M were tested in each titration. Concentrations between 1.5 and 2M KCl were ideal to get good binding curves. Redox titration was done to find the reduction potential of safranine O in

saf-X medium and compared with safranine O reduction potential. An NMR-HSQC titration of 1 equivalent safranine O against saf-X resulted in dispersion of peaks from apo to holo spectra, indicating the structural change of saf-X during binding.

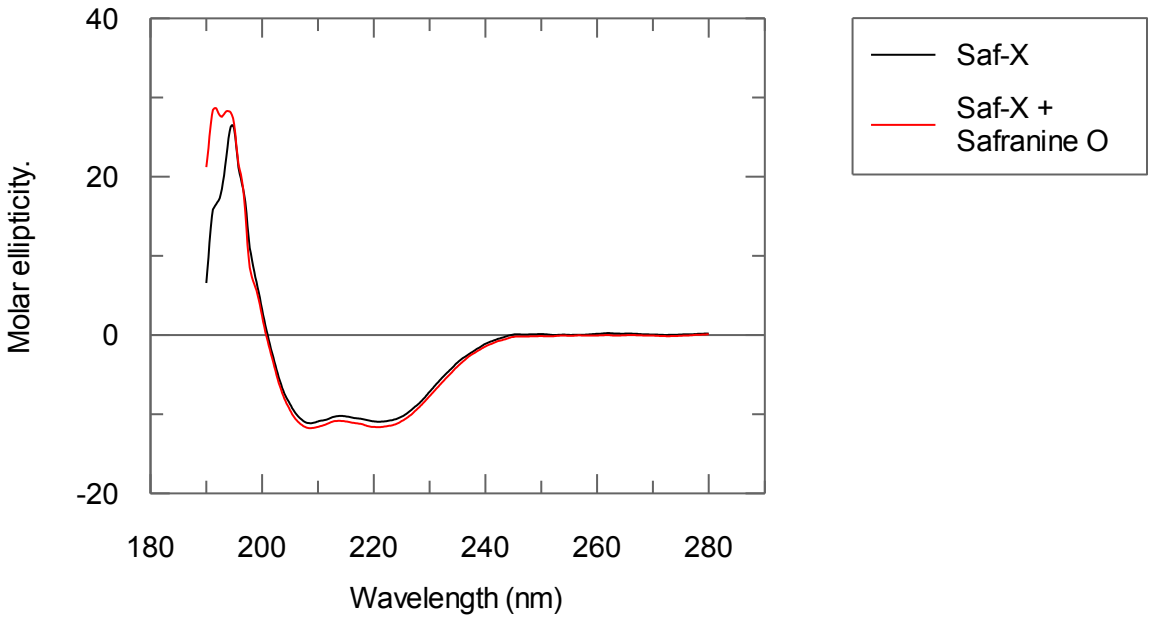

Figure.2.13. CD spectra of saf-X and complex of saf-X and safranine O.

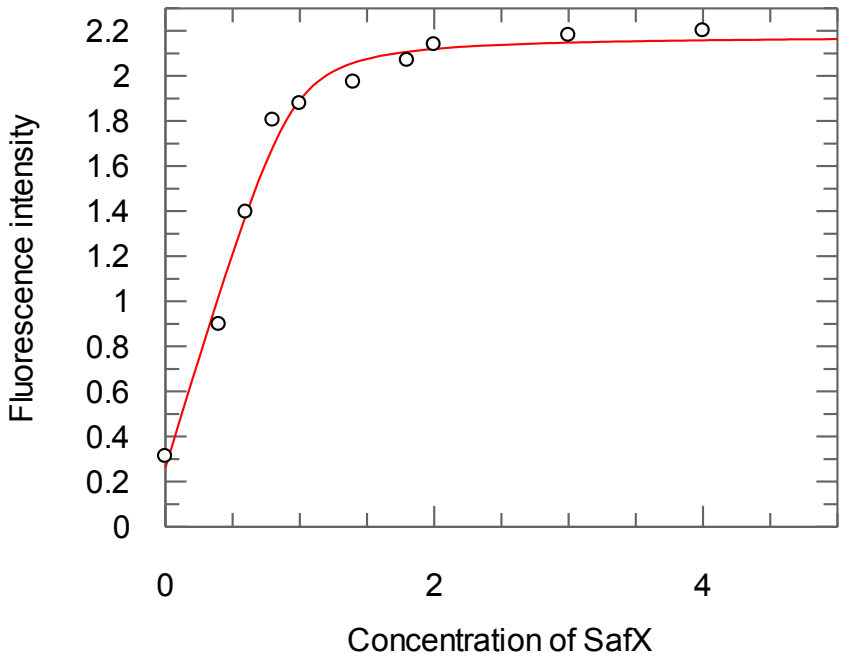

Parameter	Value	Std. Error	
Capacity of saf cofactor	0.9422	0.1130	
Kd	0.0351	0.0359	sub µM
Abs of unbound	0.2777	0.0805	
additional abd of bound	2.2930	0.9518	

Figure. 2.14.Binding curve obtained from titrating saf-X protein against 1µM safranine O.

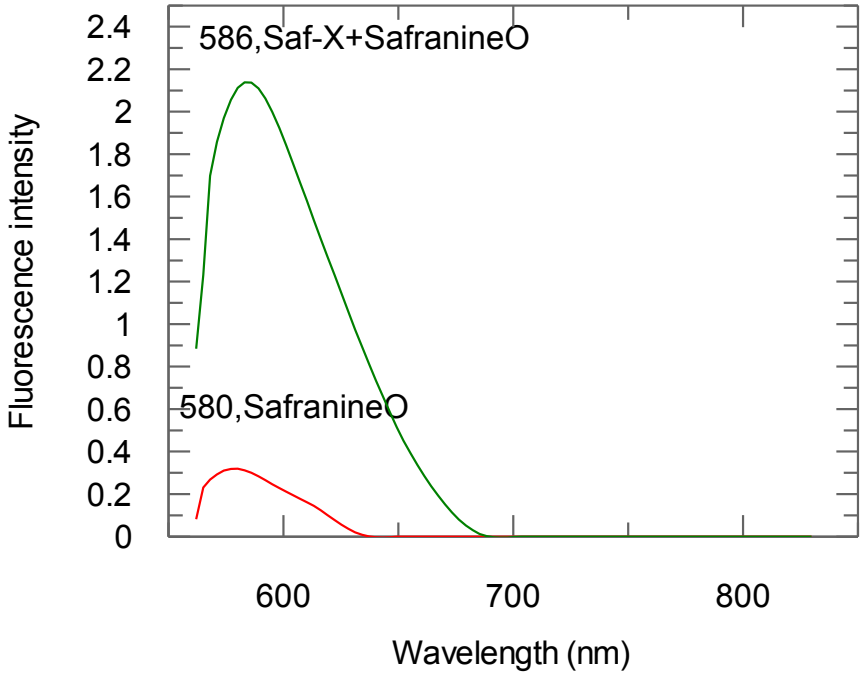

Figure. 2.15. Fluorescent peaks saf O alone and complex of 1 equivalent protein-cofactor obtained from titrating saf-X protein against 1μM safranine O.

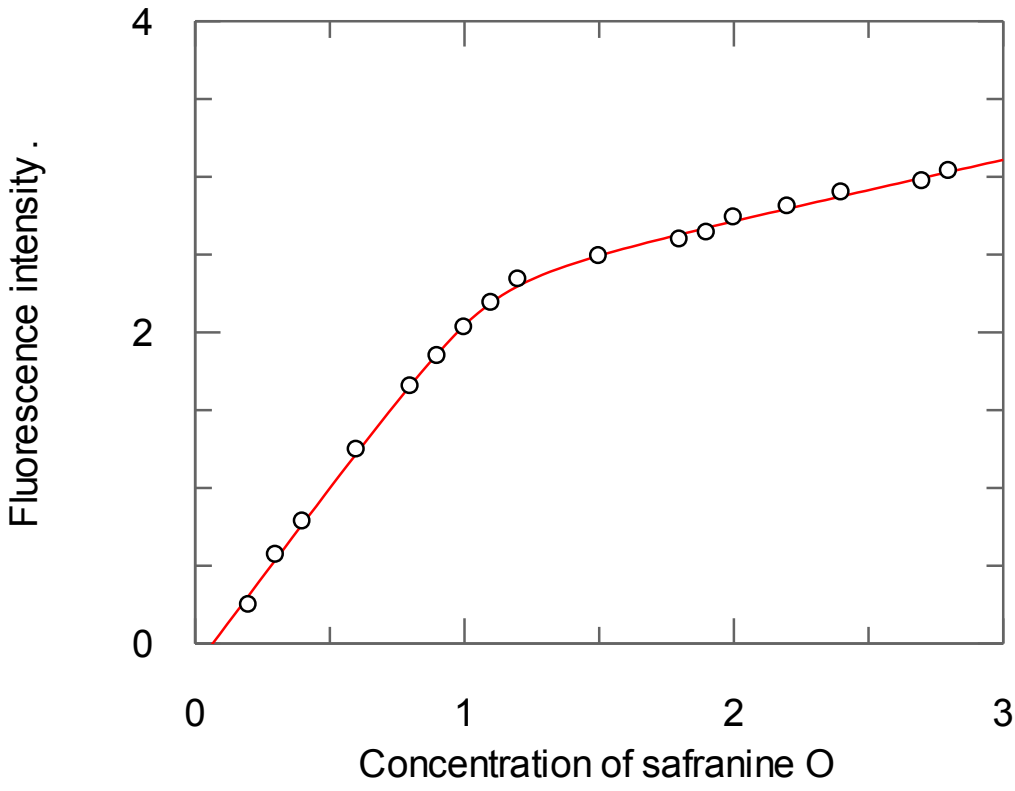

Parameter	Value	Std. Error	
Capacity	1.0894	0.0279	
Kd	0.0126	0.0073	sub µM
Abs of unbound	0.3810	0.0341	
additional abd of bound	1.6493	0.1643	
start abs	-0.1528	0.0377	

Figure. 2.16. Binding results obtained from titrating safaranine O cofactor against 1µM saf-X protein.

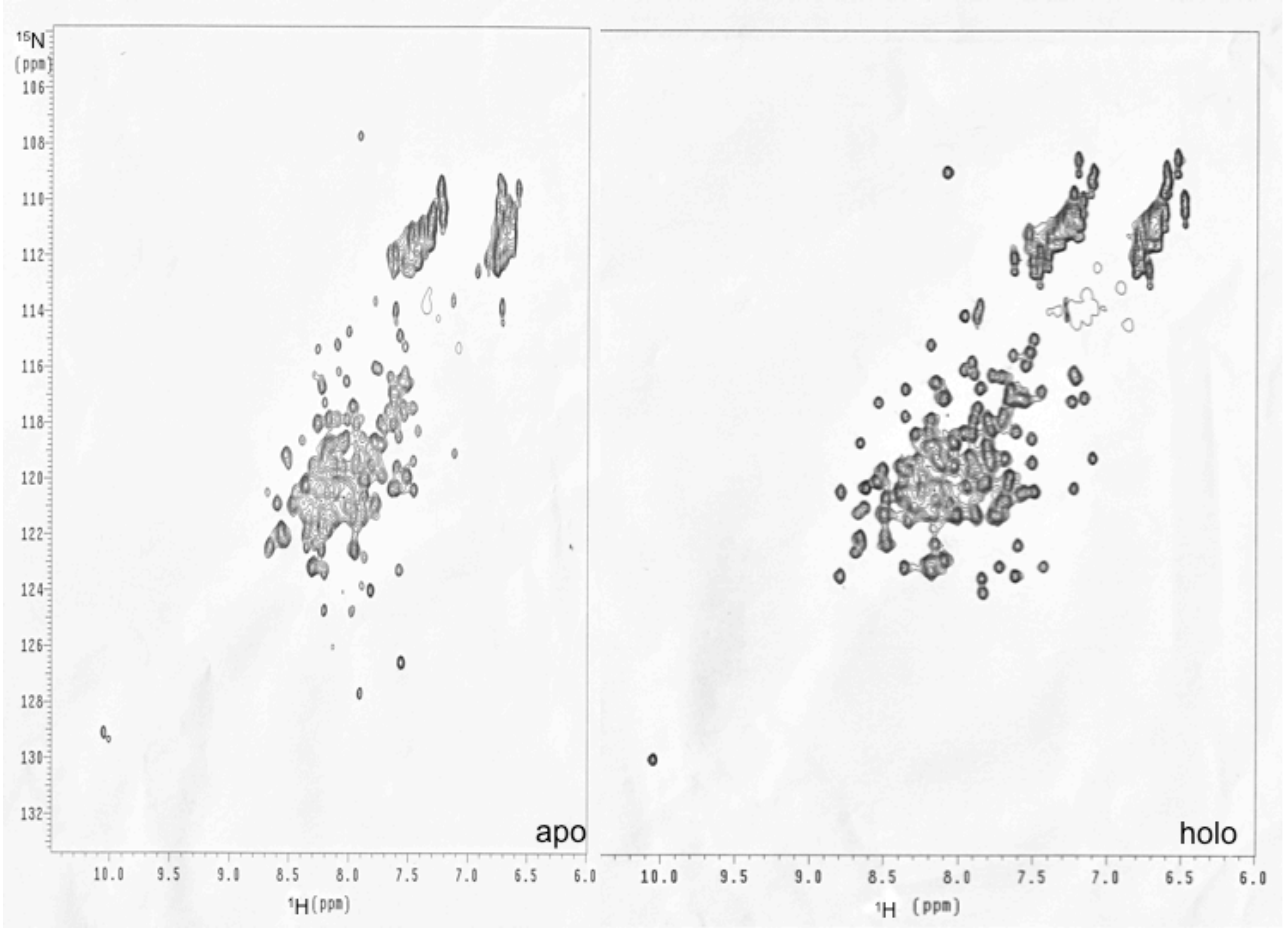

Figure. 2.17. NMR-HSQC titration. Spectra obtained from titrating safaranine O cofactor against saf-X protein. The holo is much more dispersed upon binding the cofactor.

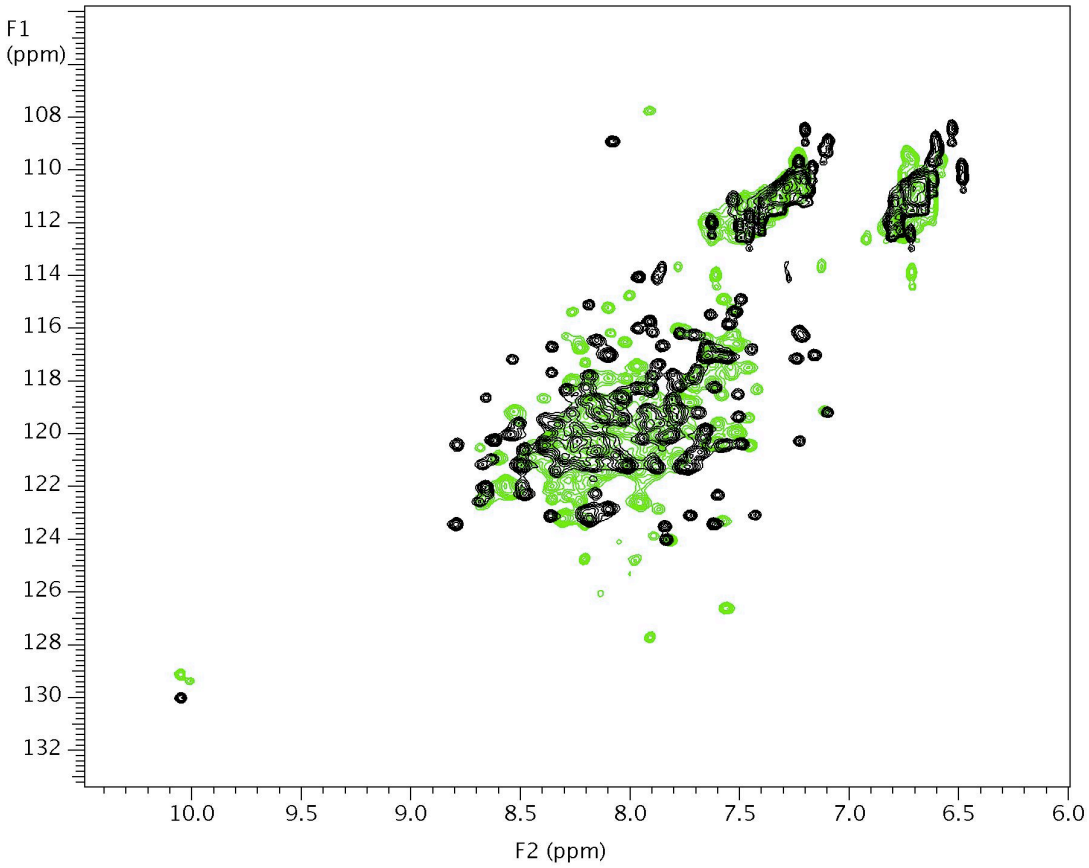

Figure. 2.18. NMR-HSQC titration. Spectra obtained from titrating safaranine O cofactor against saf-X protein. The holo is overlaid on apo.

2.4.6. SafX-Loop.

EQLAQRLAQVVEEIQRFAEAIERIAREVQKSSEKGGSNSGSGGPQARKEEEAEADDLQR
IAQKLQQLAQDLQRFAQKGGSSTGSGGPQEFREDFEQISQRLQEVVEDVKAIAQRVQRS
SEKGGSSGGSGGPQAKQSEEREANDIQNVAQWFEQAAQKLQAFAQE

Sequence of safX-Loop protein.

SafX-Loop is a loop modification of saf-X. Together with the elongation of the helical-turns in saf-X, we swapped three short loops with longer canonical loops (GGSNSGSGG, GGSSTGSGG, GGSSGGSGG) from Koder lab. This was done to increase the flexibility of the helices for better binding. The safX-Loop protein contains 164 residues with 17.9 kDa. The extinction coefficient (ε) is 5690$cm^{-1}M^{-1}$ (same as saf-X). CD results showed typical α-helix peaks. A large negative peak of the n to π* transition at 222nm and a π to π* transition was split into two transitions because of exciton coupling. This transition consisted of a negative band at 208nm and a strong positive band at 192 nm. This showed safX-Loop was well folded in the solution. Secondary structure percentage calculation showed that safX-Loop consists of 41.86% α-helix. Adding 1 equivalent of safranine O to the safX-Loop in CD, deepens the negative bands and a decrease in 192 positive band is observed. The complex secondary structure contained 53.01% α-helix. Isothermal calorimetric experiments were not informative about binding like saf-X studies. Titrations were done in different experiments with a range of 10μM to 1mM of safX-Loop against 10μM to 1mM safranine O. In all experiments, the reactions were

incomplete. The buffer used was redox buffer at pH 8 for the protein and the ligand. Switching of buffer to Tris at pH 7.5 gave almost same isotherm. Control titrations of safranine O against H4 (overall charge is -16) were done. The isotherms of H4, SafX-Loop and saf-X titrations were almost the same and incomplete. Here our conclusion was same as in case of saf-X, such that the titration of intrinsic positive charged safranine O with negatively charged packed safX-Loop leads to non-specific binding signals. We increased the salt concentration of the buffer, and did titrations in the range from 0.1M to 1M KCl in redox buffer. As in the case of saf-X, slight improvements were made in the isotherm. Titrations became difficult as the rotating syringe stopped in the middle of the experiment because of high salt in the buffer, forcing us to stop the ITC experiments. Fluorescence measurements were done titrating protein solution (redox buffer pH 8) into a minimum concentration of safranine O (0.5 μM in redox buffer). Also, safranine O was titrated against 2 μM safX-Loop in redox buffer pH 8. Measurements were started with safranine O alone in the buffer and the change in intensity and shift of the 583nm peak was monitored. Titration of the protein against a minimum concentration of cofactor gave a binding curve break at 10 to 12 equivalents. Calculations from Grafit showed dissociation constant (Kd) of approximately 0.8×10^{-6}M [42,43]. Safranine O titrated against 2 μM safX- Loop yielded linear increments of intensity and a break at 1.2 to 1.4 equivalent of cofactor. Kd for that was approximately 0.1×10^{-6}M. This experiment was repeated several times with buffers of different concentrations of KCl. Salt concentrations ranging from 0.1 to 2 M were tested in each titration. Above 1.5 to below 2M KCl were found ideal to get a good binding curve. Redox titration was done to find the reduction

potential of safranine O in safX-Loop and compare it with safranine O reduction potential.

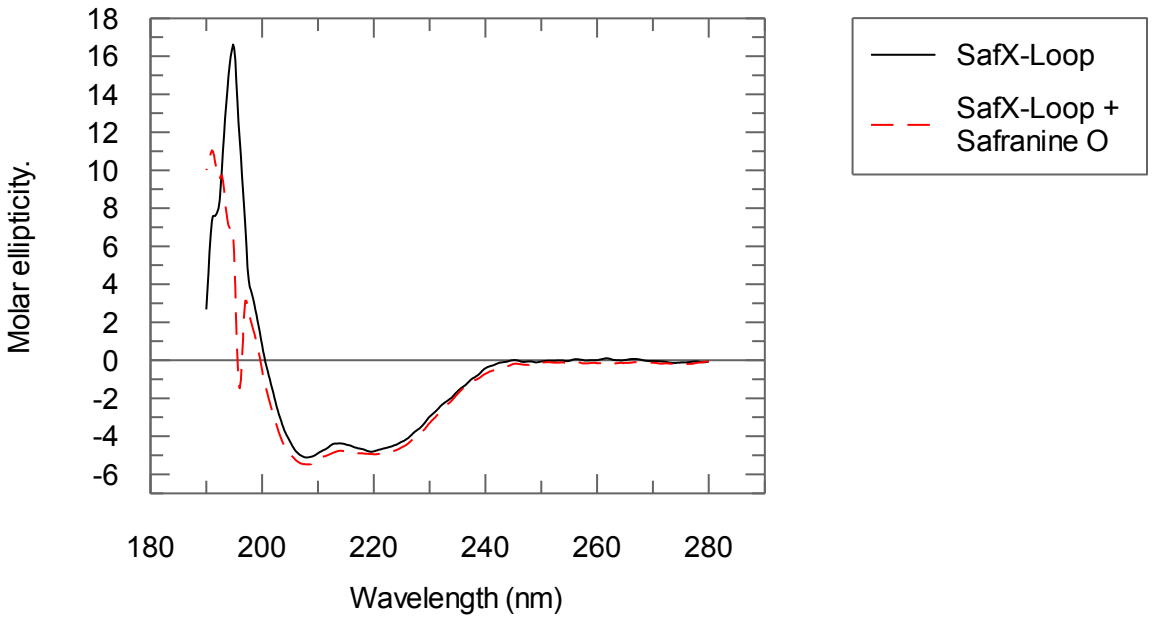

Figure.2.19. CD spectra of safX-Loop (solid line) and complex of safX-Loop and safranine O (dotted line).

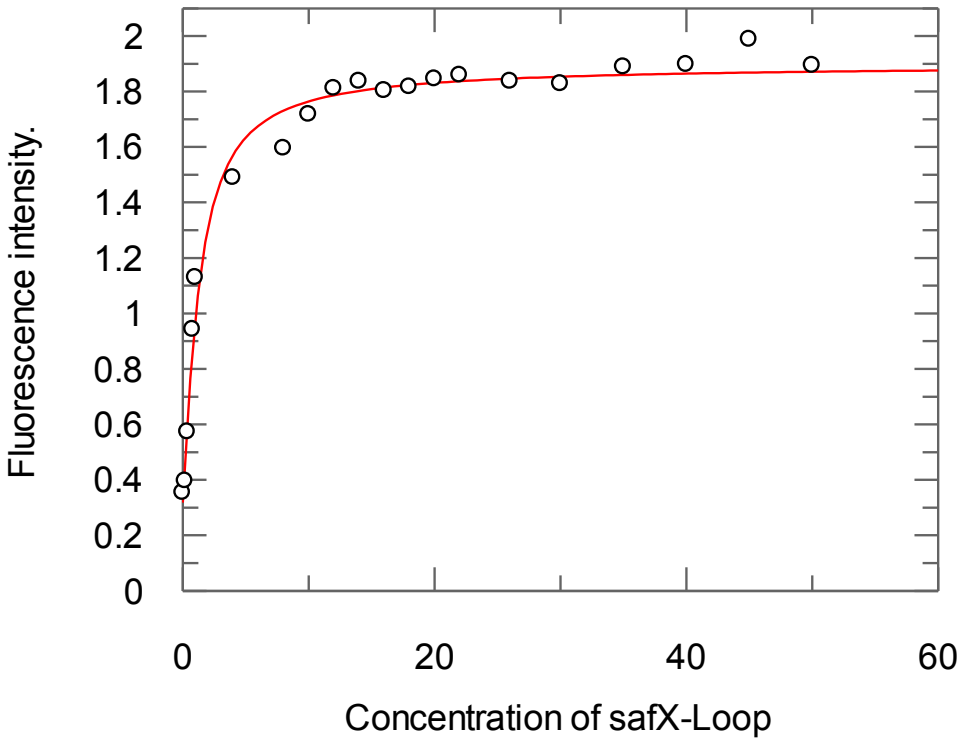

Parameter	Value	Std. Error
Capacity of saf cofactor	0.9385	0.0862
Kd	0.8489	0.1916
Abs of unbound	0.3392	0.0624
additional abd of bound	1.9111	0.4881

20-fold weaker!

Figure. 2.20. Binding curve obtained from titrating safX-Loop protein against 1μM safranine O.

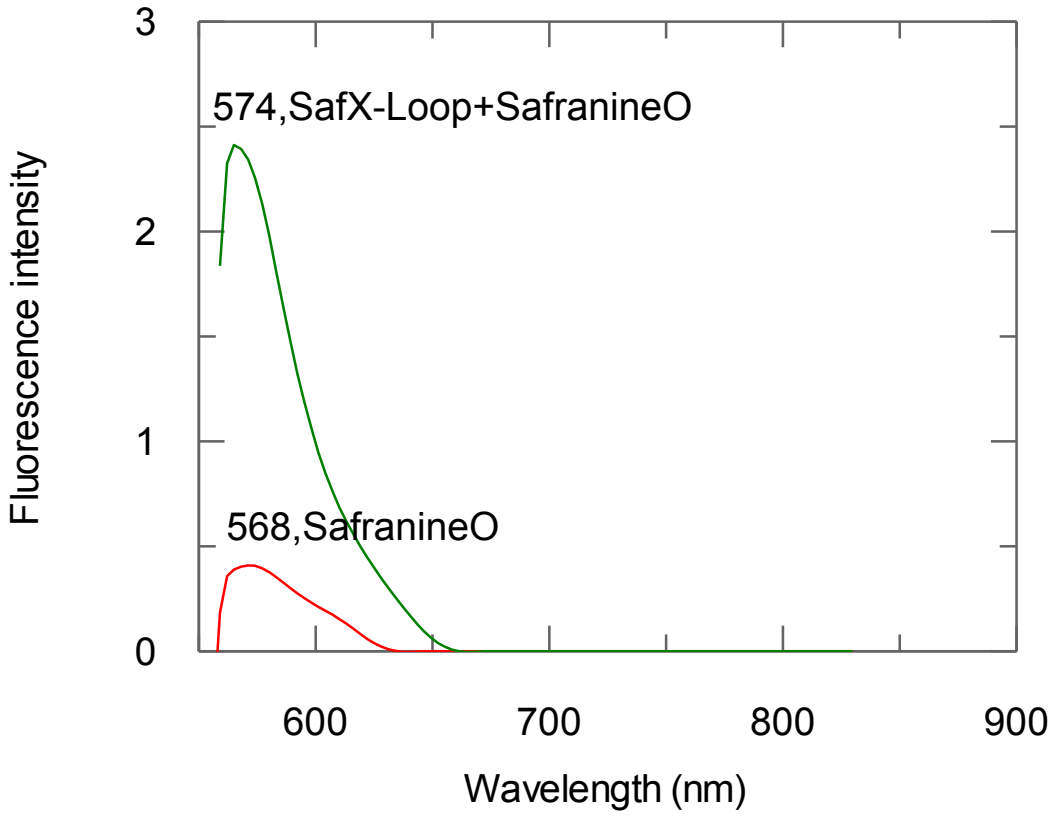

Figure. 2.21. Fluorescent peaks saf O alone and complex of 1 equivalent protein-cofactor obtained from titrating safX-Loop protein against 1μM safranine O.

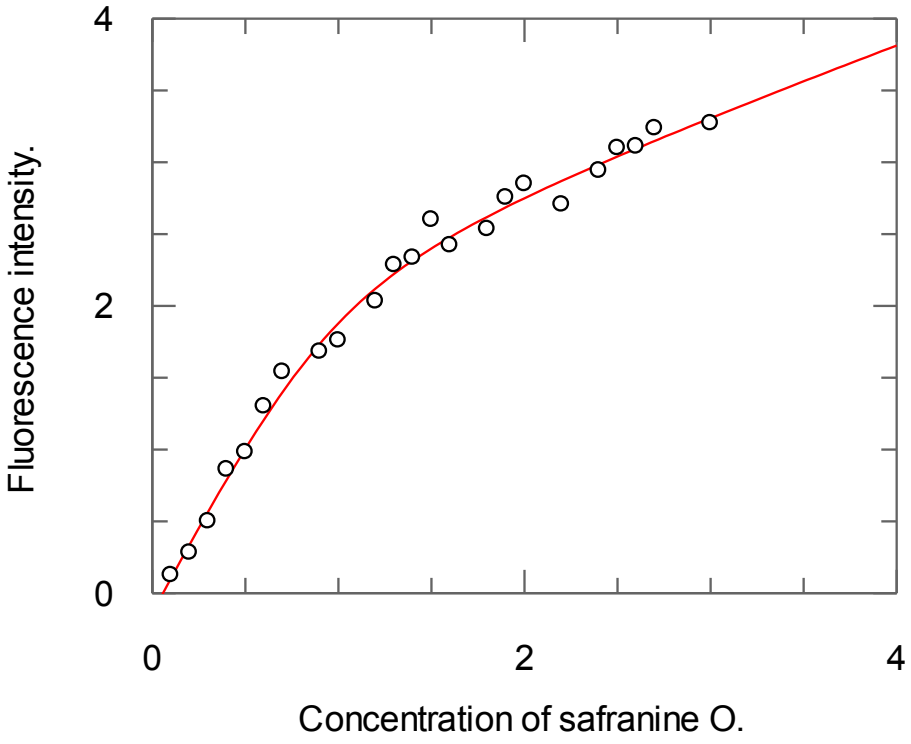

Parameter	Value	Std. Error
Capacity	0.9887	0.1170
Kd	0.1088	0.1174
Abs of unbound	0.4726	0.1911
additional abd of bound	2.2090	0.8522
start abs	-0.1399	0.0424

10-fold weaker!

Figure. 2.22. Binding results obtained from titrating safaranine O cofactor against 1μM safX-Loop protein.

2.4.7. Saf X-Mutant.

EQLAQRLAQVVEEIQRFAEAIERIAREVQKSSEKTSNPQARKEAEAAADDLQRIAQKLQ

QLAQDLQRFAQKGSTSPQEFREDFEQISQRLQEVVEDVKAIAQRVQRSSEKTSNPQAKQ

SAERAANDIQNVAQWFEQAAQKLQAFAQE

Sequence of safX-Mutant protein.

SafX-Mutant is a binding pocket knockout version of saf-X protein. We mutated four important glutamic acid residues to alanine: two for electrostatic interactions and the other two for hydrogen bonding. They are E44 to A, E47 to A, E120 to A and E123 to A. The safX-Mutant contains 147 residues with 16.7 kDa. The extinction coefficient (ε) is 5690$cm^{-1}M^{-1}$ (same as saf-X). The mutated sequence was sent for the DNA synthesis and the binding experiments with safranine O are still to be investigated. These will serve as a control for the binding experiments of saf-X and safX-Loop.

2.5. Conclusions.

Our saf protein evolution shows that simple design modifications made by applying basic rules of protein engineering made significant improvement [1-20]. Our first design lacked a folded structure and showed very little response to ligand, but the changes we made to improve folding in the second iteration made the protein insoluble and impossible to purify. Packing of negative charges on the periphery of the helix eased the purification

hurdles. Mutating the helix breaking residues improved folding and solubility. But the improvement was not good enough for binding, and the protein came out of solution in high concentrations. The choice to increase the turns in the helix was a huge leap forward in our engineering design [41]. As a result of this structural change, we have significantly enhanced binding in the latest generation of saf proteins, saf-X and safX-Loop.

Calorimetric studies were the perfect choice for obtaining Kd. Binding titrations stumbled in charge interaction between the intrinsically positive safranine O and negatively charged advanced generation proteins. In isothermal calorimetric experiments we had to use >10μM concentration of ligand, because experiments with low concentrations of protein or ligand gave a signal similar to water - water mixing [31,32]. Normal titrations ended up with an isotherm of an incomplete reaction. Control experiments with H4 (an artificial protein structure with no safranine O binding pocket), also gave the same results. The safranine O – protein non-specific binding signals superseded any binding signal possible. High salt concentration titrations had an unexpected ending, when the salt stalled the syringe rotation.

Fluorescence spectroscopic analyses gave a better insight into the binding of saf-X and safX-Loop to safranine O [33,34]. Kd for all the binding curves were elucidated by the tight binding equation [43]. Upon binding, safranine O fluorescence emission intensity (F_λ) was higher and also caused a shift in emission wavelength (λ_{em}). Titrations with high concentrations of ligand resulted in deviation of the binding trend. High salt concentration in buffer was helpful for slowing down the non-specific interaction of protein and ligand. Increase in the salt may support enhanced folding in proteins. The safaranine O had a higher binding affinity towards the saf-X than the safX-Loop. The

difference in Kd is the contribution of change in conformational entropy associated with the protein [44]. Comparison of CD studies shows that saf-X is better folded than safX-Loop [27]. The factors that affect the binding entropy are largely from change in conformational entropy and change in solvation entropy. Binding causes partial or entire removal of solvents from the binding pocket, hence the solvation entropy changes are always favorable [44,45]. Additionally, the binding event occurs with the expense of conformational degrees of freedom for both ligand and protein, thus conformational entropy change has adverse effects. . NMR-HSQC titration of safranine O against saf-X shows dispersion of peaks from apo to holo spectra. This is an evidence of the cofactor binding with protein [44,45].

2.6. Future developments.

Structural studies assisted by NMR in complex formation are a further development in safaranine enzymes. Enzyme kinetics also needs to be investigated. A wide variety of nitroaromatic substrate binding and catalytic functionality need to be considered. NAD(P)H assisted enzymatic catalytic studies are also of special importance in safarnine enzymes. Tuning the functionality is another major milestone. Safranine enzymes need to modify binding and functionality in accordance with different suggested applications.

2.7. Bibliography.

1. Nanda, V., and Koder, R. L. *Nature Chemistry*. **2010**. 2, 15-24.

*2. Ronald L. Koder, P. Leslie Dutton. Dalton Trans., **2006**, 3045-3051.*

3. Koder, R. L., Anderson, J. L. R., Solomon, L. A., Reddy, K. S., Moser, C. C., and Dutton, P. L. *Nature.* . **2009**. 458, 305-309.

*4. Stephen Betz, Robert Fairman, Karyn O'Neil, James Lear, Wililiam Degrado. Phil. Trans. R. Soc. Lond. B , **1995**, 348, 81-88.*

*5. Yinan Wei, Tun Liu, Stephen L. Sazinsky, David A. Moffet, Istvan Pelczer, Michael H. Hecht. Protein Science, **2003**, 12, 92-102.*

*6. Satwik Kamtekar, Jarad M. Schiffer, Huayu Xiong, Jennifer M. Babik, Michael H. Hecht. Science, **1993**, 262, (5140), 1680-1685.*

*7. J. A. Silverman, R. Balakrishnan, P. B. Harbury. PNAS, **2001**, 98, (6), 3092-3097.*

*8. G. V. Semisotnov, N. A. Rodionova, O. I. Razgulyaev, V. N. Uversky, A. F. Gripas, R. I. Gilmanshin. Biopolymers, **1991**, 31, 119-128.*

*9. Beth Allyn Krizek, Barbara T. Amann, Valda J. Kilfoil, Denise L. Merkle, Jeremy M. Berg. J. Am. Chem. Soc., **1991**, 113, 4518-4523.*

*10. Amit R. Reddi, Tabitha R. Guzman, Robert M. Breece, David L. Tierney, Brian R. Gibney. J. Am. Chem. Soc., **2007**, 129, 12815-12827.*

*11. Shiluan Yi, Brian L. Boys, Anne Brickenden, Lars Konermann, Wing-Yiu Choy. Biochemistry, **2007**, 10, 1021-1031.*

*12. Byoung-Chul Lee, Tammy K. Chu, Ken A. Dill, Ronald N. Zuckermann. J. Am. Chem. Soc., **2008**, 2117-2125.*

13. Ilan Samish, Christopher M. MacDermaid, Jose Manuel Perez-Aguilar, and Jeffery G. Saven. *Annu. Rev. Phys. Chem.* **2011**.62:129-149.

14. C.A. Floudas, H.K. Fung, S.R. McAllister, M. Mönnigmann, R. Rajgaria. *Chemical Engineering Science.* **2006.** 61, 966 – 988.

15. Almer M. Van der Sloot, Christina Kiel1, Luis Serrano and Francois Stricher. *Protein Engineering, Design & Selection.* **2009**. 22 .9. 537–542.

16. Navin Pokala and Tracy M. Handel. *Journal of Structural Biology.* **2001**.134, 269–281.

17. Shaun M Lippow, and Bruce Tidor. *Current Opinion in Biotechnology.* **2007**, 18,1–7.

*18. Brian. R. Gibney, Francesc Rabanal, Jack J. Skalicky, A. Joshua Wand, P. Leslie Dutton. J. Am. Chem. Soc., **1999**, 121, 4952-4960.*

*19. Kuhlman, B. and Baker, D. Proc. Natl Acad. Sci. USA. **2000**. 97, 10383-10388.*

20. Koder, R. L., Valentine, K. G., Cerda, J. F., Noy, D., Smith, K. M., Wand, A. J., and Dutton, P.L. *Journal of the American Chemical Society.* **2006**. 128, 14450-14451.

21. Clarke, W.M. *Oxidation Reduction Potentials of Organic Systems*. ed. **1960**. The Williams and Wilkins Co., Baltimore.

22. West MW and Hecht MH. *Protein Science*. **1995**. 4, 2032-2039.

23. Lazar, G.A., Desjarlais, J.R and Handel, T.M. *Protein Sci.* **1997**. 6,1167-1178.

24. Looger, L.L and Hellinga, H.W. *J. Mol. Biol.* **2001**. 307,429-445.

25. Moore, J. T., Uppal, A., Maley, F., and Maley, G. F. *Protein Expression and Purification 4*. **1993**. 160-163.

26. Mainiatis, T., Fritsch, E. F., and Sambrook, J. *Molecular Cloning: A Laboratory Manual*. 1982.Cold Spring Harbor Laboratory, Cold Spring Harbor, NY.

27. Sharon M. Kelly, Thomas J. Jess, Nicholas C. Price. *Biochimica et Biophysica Acta*. **2005**. 1751,119 – 139.

28. Niels, C. K., Anne-Marie, K.,Susan, E. D.,Jan, H and Steen, I.H. *Biochem. J.* **1993**. 292,921-925.

29. Andrade, M.A., Chacon, P., Merelo, J.J., and Moran, F. *Protein Eng*.**1993**. 6,383-390.

30. Joseph A. D'Anna Jr., Gordon Tollin. *Biochemistry*. **1972**. 11, 1073–1080.

31. Remo Perozzo, Gerd Folkers and Leonardo Scapozza. *Journal of Receptors and Signal Transduction*. **2004**. 24,1-52.

32. Geoffrey A. Holdgate and Walter H. J. Ward. *DDT*.**2005**.10, 1543-1550.

33. Matias Moller and Ana Denicola. *Biochemistry and Molecular Biology Education.* **2002.**30, 309–312.

34. Peter TC So, Chen Y Dong. *Encyclopedia Of Life Sciences*. **2002** Macmillan Publishers Ltd.

35. Huang, S. S., Koder, R. L., Lewis, M., Wand, A. J., and Dutton, P. L. *Proceedings of the National Academy of Sciences of the United States of America.* **2004**. 101, 5536-5541.

36. Dutton, P. L. *Methods in Enzymology*. 1978. *54*, 411-435.

37. Delaglio, F., Grzesiek, S., Vuister, G., Zhu, G., Pfeifer, J., and Bax, A. *J. Biomol. NMR*. **1995**. 6 , 277-293.

38. Goddard, T. D., and Kneller, D. G. *Sparky*. **2007**. The University of California, San Francisco.

39. Kay, L. E., Keifer, P., and Saarinen, T. *J. Am. Chem. Soc.* **1992**.114,10663-10665.

40. Pace, C. N., Vajdos, F., Fee, L., Grimsley, G., and Gray, T. *Protein Science.***1995**.4,2411-2423.

41. Yinan Wei, Tun Liu, Stephen L. Sazinsky, David A. Moffet, István Pelczer, and Michael H. Hecht. *Protein Sci*. **2003.** 12,92–102.

42. Leatherbarrow, R.J. *Grafit Version 7.0,* **2012**. Erithacus Software Ltd., Staines, U.K.

43. Robert A. Copeland. Enzymes: A Practical Introduction to Structure, Mechanism, and Data Analysis. 2000. Wiley-VCH, Inc., NY, U.S.A.

44. Nidhi Singh and Arieh Warshel. *Proteins*. **2010**.78, 1724–1735.

45. Raik Grunberg, Johan Leckner, and Michael Nilges. *Structure*. **2004.** 12, 2125–2136.

46. Richard C. Stewart and Vincent Massey. *The Journal of Biological Chemistry*.**1985.** 260, 13639-13647.

Chapter 3.

Manipulating reduction potentials in an artificial safranine cofactor (*p*-Methoxy safranine).*

3.1. Summary.

Safranines hold great promise as artificial flavin-like electron transfer cofactors with tunable properties. We report the design and chemical synthesis of the p-methoxy derivative of safranine O using a new synthetic route based on the Ulmann condensation. Spectroelectrochemical comparison of the purified parent safranine and this derivative demonstrates that the modification increases its two-electron reduction potential by 125 mV, or 5.75 kcal/mol. This modification also causes redshifts in the absorbance and fluorescence spectra of the cofactor, suggesting that it may find future utility in arrayed sensor applications.

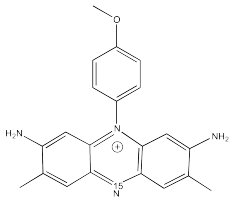

Figure.3.1. Methoxy safranine.

* This chapter is adapted from **Gheevarghese Raju**, Joseph Capo, Bruce R. Lichtenstein, Jose F. Cerda, Ronald L. Koder. Manipulating reduction potentials in an artificial safranin cofactor. *Tetrahedron Letters,* **2012**, 53, 1201- 1203.

3.2. Introduction.

The combination of natural and designed proteins with artificial cofactors is a rapidly expanding focus of modern enzyme design efforts [1-4]. The anticipated benefit of this combination is that a cofactor energetically and structurally optimized to perform the catalytic task at hand will aid the enzyme design or re-engineering effort by removing the necessity for the enzyme to "tune" the cofactor reactivity for the desired task [5-7]. The properties to be optimized may include reduction potentials, substrate or ligand affinity, hydrophobicity, chemical reactivity, or photophysical properties [8].

Progress to date has primarily been in the area of metalloproteins, especially the replacement of heme residues with synthetic porphyrins [9-12]. There are few reports of artificial proteins that incorporate artificial bioorganic cofactors [13, 14]. Despite the fact that more than a tenth of known cofactor-containing enzymes are flavoenzymes [15], there have been no reports thus far of artificial flavin enzymes which utilize artificial flavin-like cofactors and likewise no reports of the synthesis of flavin-like cofactors created for use in such a manner. We have reported the synthesis and characterization of riboflavin derivatives with differing hydrophobicity [16, 17], but these lack desirable properties such as changes in reduction potential.

Reduction midpoint potentials, both one- and two-electron, play a large role in determining the chemical reactivity of flavin cofactors [18-21], and flavoproteins observed in nature have been shown to modulate the reduction potentials of their bound cofactors by more than half a Volt [15]. For this reason, we have set out to create a series of flavin-like cofactors in which small changes in the cofactor structure engender large changes in its reduction potentials. Safranines are ideal candidates for this as the

phenazine moiety is similar in size and shape to that of isoalloxazine (see Figure 3.1.) The reported two-electron reduction midpoint potential of safranine O, -290 mV vs SHE [22], is 100 mV, or 2.3 kcal/mol more negative than that of riboflavin [23]. Furthermore the N(10) phenyl substituent of Safranine O is conjugated to the phenazine, raising the possibility that the reduction potential of the molecule may be simply altered by modifications of this ring.

The safranine mauveine was the first synthetic dye, created by Perkin in 1856 [1]. It was synthesized by the oxidation of crude aniline, itself derived from the nitration and reduction of a benzene-toluene mixture, and purified in a 5% yield from a mixture of products containing a variety of oligoanilines [24]. Soon after dozens of safranine derivatives were created using similarly uncontrolled oxidative condensations of various arylamines and diamines [2, 25]. Modern industrial safranine dyes are still synthesized in this manner [24].

In this report we describe our initial effort to create a general synthetic route towards safranine O analogues modified at the para position of the N(10) phenyl ring using a stepwise synthesis in which the phenyl substituent is incorporated as aniline. Given the large number of commercially available aniline derivatives, we hoped such a synthetic route may lead to a similarly large scope of safranine products. Furthermore, given our recent demonstration that the chemical shift tensor of the isoalloxazine N(5) nitrogen in flavin compounds is very informative as to the chemical reactivity imparted upon flavins by their environments [1, 26], we desired to created a route which enables the ready and inexpensive incorporation of isotopically labeled nitrogen at the equivalent N(5) position in the phenazine ring of these analogues.

3.3. Methodologies and experimental procedures.

3.3.1. Materials and chemical synthesis.

Safranine O was purchased from Aldrich. All reactions were carried out under an inert atmosphere. Commercial reagents were used without further purification unless otherwise noted. For analytical thin-layer chromatography, precoated glass silica gel plates (EMD silicagel 60 F_{254}) were used. All products were purified using silica gel (Analtech 30-75 μm) and/or by recrystallization. Melting points were determined using a Fisher-Johns melting point apparatus and are uncorrected. NMR spectra were recorded in $CDCl_3$ with TMS as an internal standard at room temperature on a Varian Inova operating at 500 MHz for ^{1}H, 125 MHz for ^{13}C and 50 MHz for ^{15}N. When necessary, two-dimensional homonuclear correlation (COSY) spectra were run in order to confirm assignments.

Our approach is outlined in Scheme 1. 5-iodo-2-methylaniline **1** was quantitatively protected with *tert*-butyldicarbonate [2] and then condensed with p-anisidine **3** using copper iodide, 2,2'-bipyridine and three equivalents of potassium *tert*-butoxide in dry toluene forming triarylamine **4** [25]. Initial attempts using 1,10-phenanthroline as a copper ligand and potassium hydroxide as a base resulted in low yields, so the rigid phenanthroline ligand was replaced with the more flexible bipyridine ligand [5], and the stronger, more hindered, tert-butoxide base was used to replace potassium hydroxide [3].

The next step was nitrosative cyclization [27]. Directly cyclization of **4** proved unsuccessful as the acidic conditions required deprotect the amines forming azo compounds from the free amines and the nitrite. We thus replaced the Boc protecting groups with acid-stable phthalate protecting groups in a single step reaction [7] forming **5**

in an 86% isolated yield. **5** was cyclized with ^{15}N-sodium nitrite in a 17/3 mixture of acetic acid/tetrahydrofuran at 0°C forming **6** in a 55% yield. Reductive deprotection of **6** resulted in the purple final product **7** in a 40% isolated yield. The low yield in the final two steps was compensated for in part by the fact that the isotopic label was introduced in the second to last step. This greatly reduced label loss in comparison to other possible approaches in which either the label is introduced at the beginning, entailing a geometrically growing loss of expensive labeled material, or the extremely low yield uncontrolled oxidative condensation methods currently in use.

Similar syntheses with other aniline starting materials demonstrate that this reaction pathway is limited in scope: anilines with methyl, cyano or hydrogen groups at the position *para* to the amine had reduced yields of 52, 24 and 38% respectively in the condensation step, and all had negligible yields (<5%) of cyclization. The latter is likely due to the fact that these are not as activating as the methoxy for electrophilic substitution at the position *meta* to the amine.

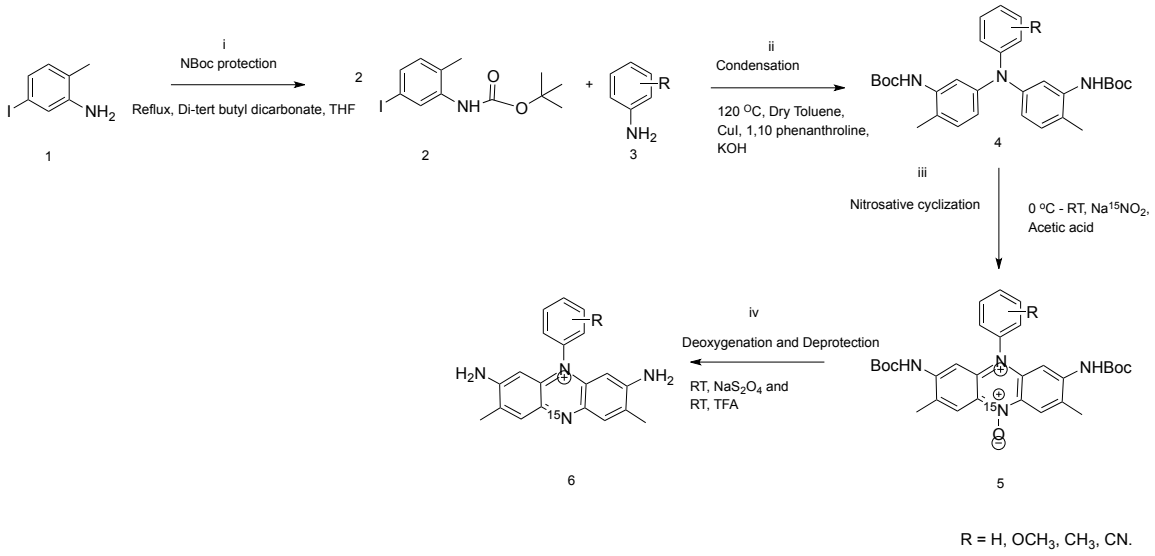

Scheme. 3.1. First synthesis scheme of safranine analogues.

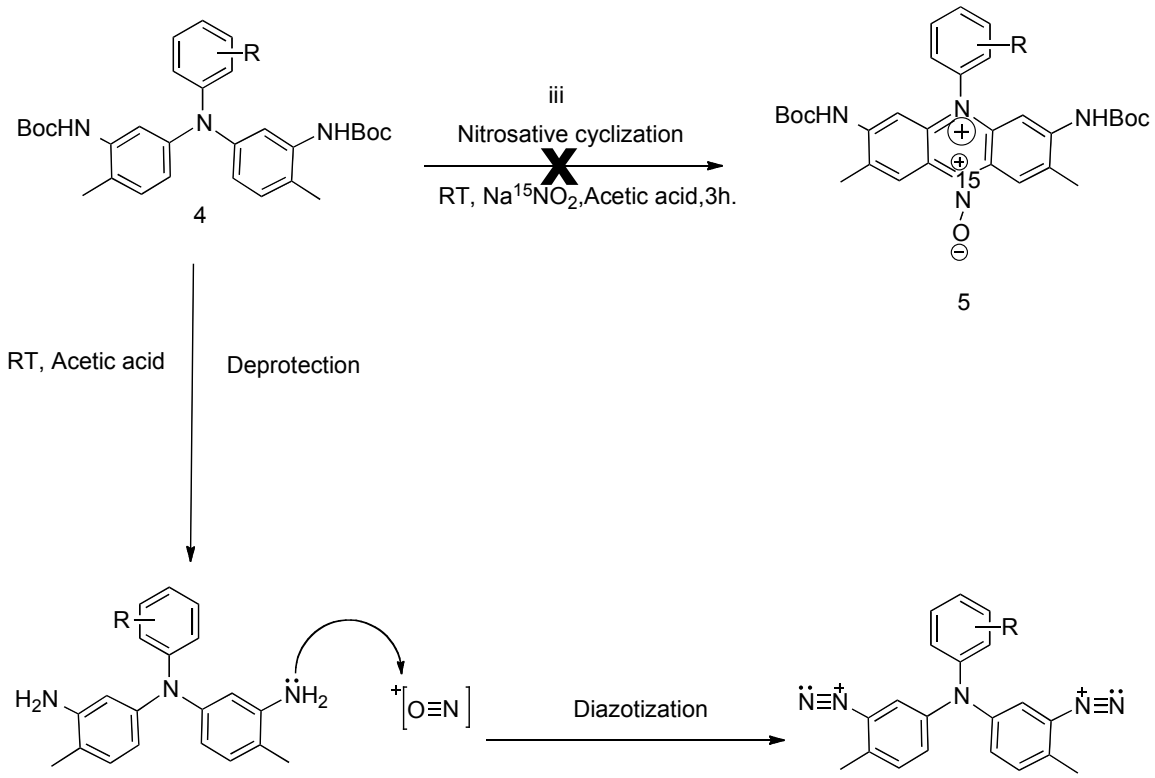

Scheme.3.2. Plausible reason for failure of first synthesis scheme.

Protection of amine with NBoc	Aniline derivatives	Ullmann Condensation	Nitrosative Cyclization	Deoxygenation and Deprotection of Amine
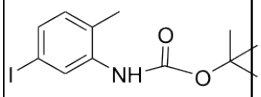	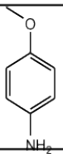	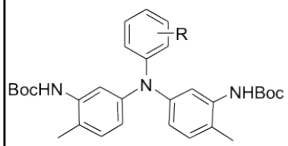	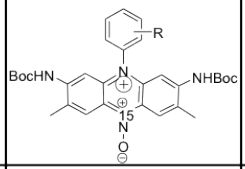	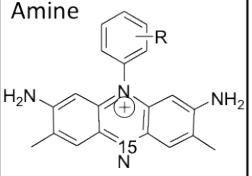
85.3%		33.89%	No Reaction	No Reaction
	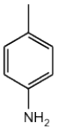	21.4%	No Reaction	No Reaction
	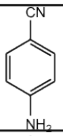	3.8%	No Reaction	No Reaction
	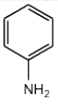	6.9%	No Reaction	No Reaction

Table.3.1. Reaction yield from first synthesis scheme.

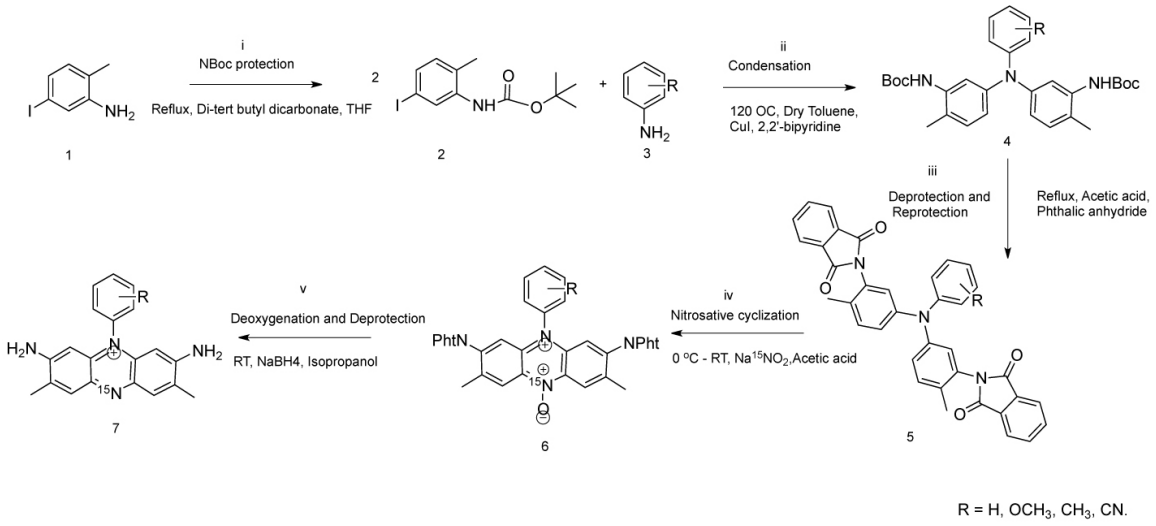

Scheme.3.3. Second synthesis scheme of safranine cofactors.

Protection of amine with NBoc	Aniline derivatives	Ullmann Condensation	Deprotection of Nboc and Protection of amine with phthalate	Nitrosative Cyclization	Deoxygenation and Deprotection of Amine
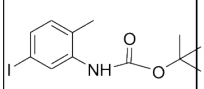	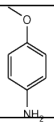	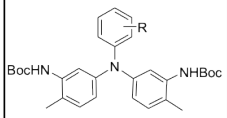	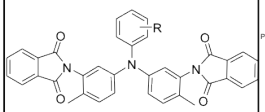	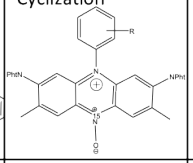	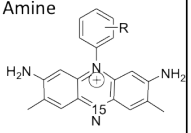
85.3 %		78.3%	86%	55%	40%
	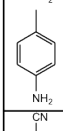	51.6%	80.2%	5%	29%
	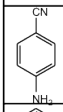	23.5%	70.7%	No Reaction	No Reaction
		37.9%	75%	6.4%	15%

Table.3.2. Reaction yield from second synthesis scheme.

3.3.2. HPLC purification.

Final purifications of both safranine O and its methoxy derivative were performed using a Shimadzu HPLC equipped with two LC-6AD pumps and a multiwavelength photodiode array detector with a scanning range of 200-800 nm. Preparative scale purification was performed at room temperature using a 250 x 20 mm 10μm Proto 300 C18 column (Higgins Analytical) at a flow rate of 12 ml/min. Buffer A consisted of 9:1-water/methanol (v/v) and 5% phosphoric acid, pH 2. Buffer B consisted of methanol. For safranine O, the applied gradient was from 48 to 72% of Buffer B over 20 min. For the methoxy derivative, the gradient was from 42.5 to 60% Buffer B over 20 min. Retention times of were 11.3 min for Safrinine O and 12.5 min for the methoxy derivative.

3.3.3. Specrtrophotometry analysis (UV-visible and Fluorescence).

Compound **7** was compared to a commercial sample of safranine O, the latter of which had to be purified using both normal- and reversed-phase chromatography in succession as it was very impure despite Aldrich's claim of >95% purity [9]. Safranines were dissolved in 0.2M sodium phosphate, 0.2M NaCl, pH 7.0. Solutions were degassed using several cycles of applied vacuum followed by flushing with argon. Oxidized spectra were collected and then the safranines were reduced using sodium hydrosulfite. The oxidized and two-electron reduced spectra of **7** are both significantly red-shifted in comparison to the base compound safranine O, and the fluorescence emission maximum is likewise shifted by 44 nm (See Figure 3.2 and 3.3). Neither compound is fluorescent in the reduced state. These spectral differences are advantageous, as they mean the compounds can be separately monitored in mixed solutions of the two species, or in mixed complexes

of the two cofactors with one or more proteins, as has been proposed for biochemical sensor arrays [21].

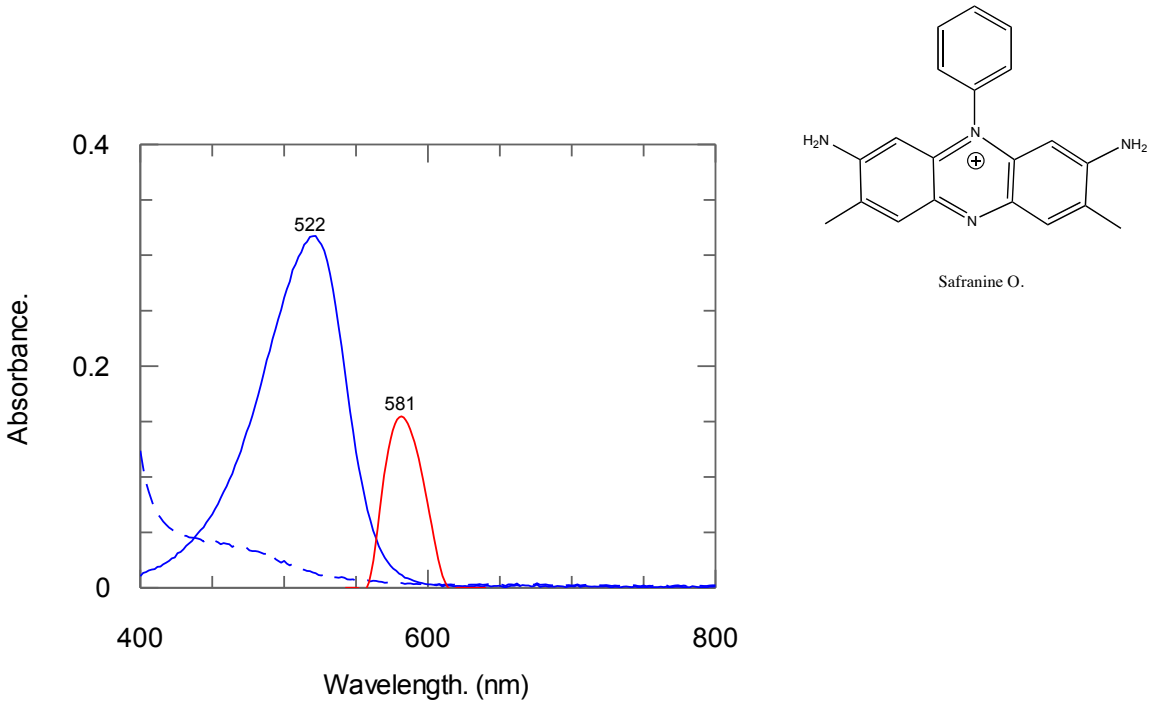

Figure 3.2. Absorbance spectra of oxidized (solid line, 522 nm), reduced (dotted line) and fluorescence emission (solid line, 581 nm) spectra of oxidized and reduced safranine O.

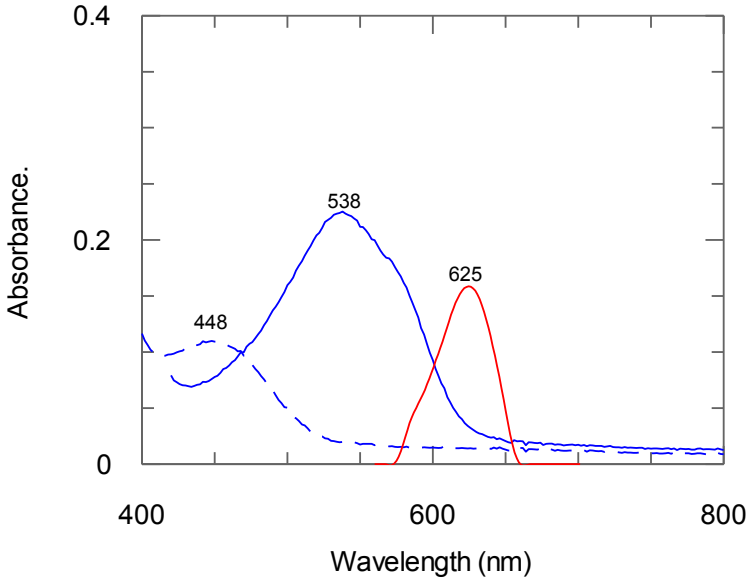

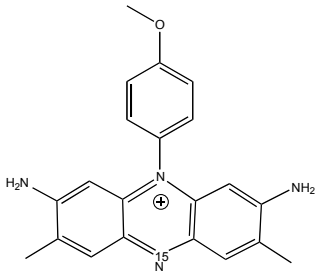

Methoxy Safranine.

Figure 3.3. Absorbance spectra of oxidized (solid line, 538 nm), reduced (dotted line) and fluorescence emission (solid line, 625 nm) spectra of oxidized and reduced p-methoxysafranine.

3.3.4. Spectroelectrochemical analysis.

We performed spectroelectrochemical analysis of the two proteins using the apparatus described previously [13]. Briefly, the cell is a 10mm quartz cuvette that contains a pair of gold slides that serve as the working electrode, a platinum wire auxiliary electrode, and an Ag-AgCl reference microelectrode (Microelectrodes Inc). The gold working electrode was coated with 1-mercaptohexanol by soaking the slides in a 1-proponal solution containing 1-mercaptohexanol 1% (v/v) for 20 hours. The applied potential is set by using a PWR-3 Power Module potentiostat (Bioanalytical Systems Inc.). Spectra were collected in a PerkinElmer Lambda 35 UV/Vis spectrometer. Safranines were dissolved in water containing 0.2M sodium phosphate, 0.2M NaCl, pH 7.0. The applied potentials are referenced against Ag-AgCl which is +210 mV (NHE). Solutions were equilibrated at each potential for at least ten minutes before spectra were collected. Absorbance values at the oxidized maximum were used to calculate the fractional oxidation at each potential and these data were fit with the Nernst equation.

Figure 3.5 and 3.7 depicts the data obtained for the two compounds in pH 7.0 buffer solution. **p**-Methoxysafranine **7** has a reduction potential 125 mV higher than that of safranine O. Each displays two-state behavior, directly transforming from the oxidized state to the two-electron reduced state during the titration. No semiquinone spectral intermediates are observed. The two-electron nature of these reductions are further evinced both by the presence of isosbestic wavelengths in each titration and by the fact that the fits to the titration data each report a 2.0 ± 0.1 electron reduction. Thus a protein containing **7** as a cofactor will have 125 mV, or 5.75 kcal/mol, more driving force

for two-electron oxidative reactions such as the oxidation of nicotinamide cofactors such as NADH and NADPH.

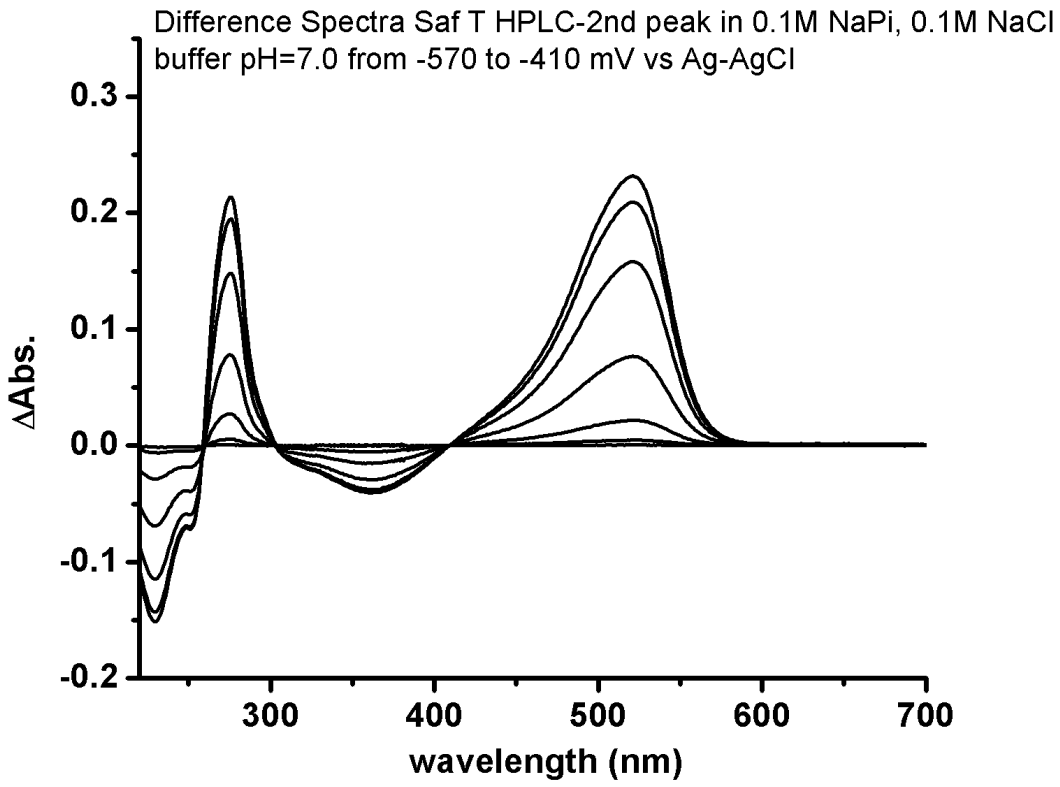

Figure 3.4. Difference spectra (oxidized –reduced) of safranine O.

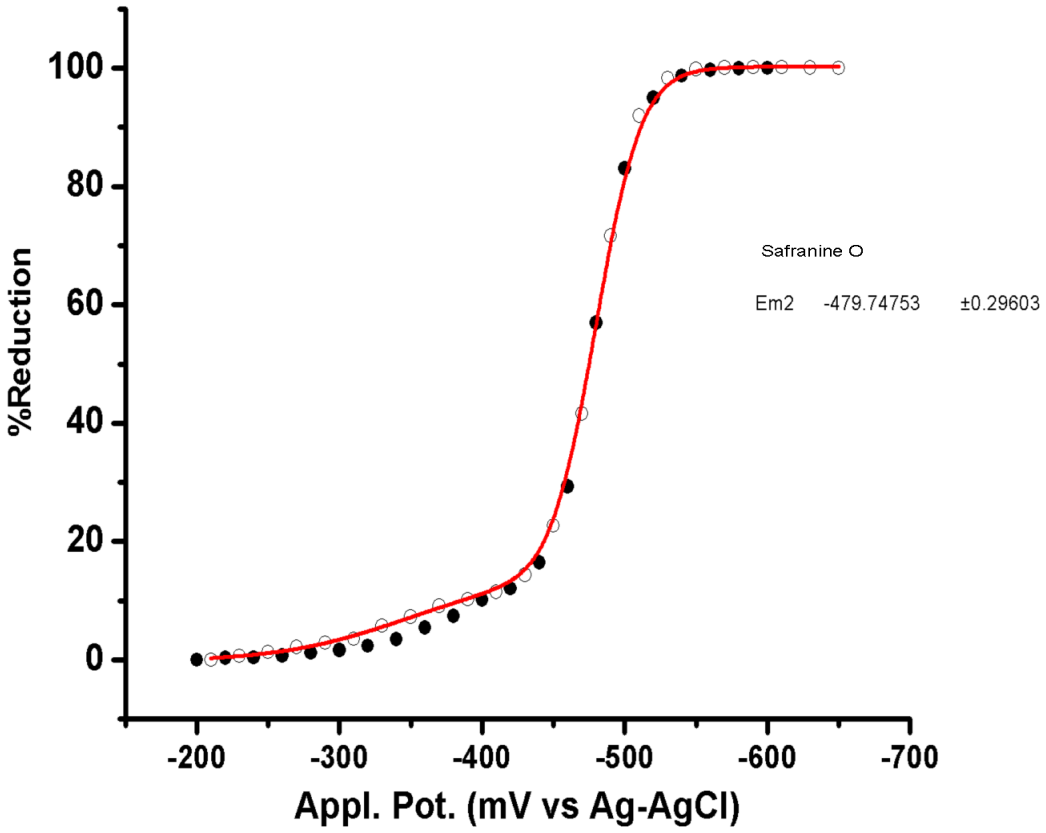

Figure.3.5. Spectroelectrochemical data of safranine O. The applied potentials are referenced against Ag-AgCl which is +210 mV (NHE). The data were fit with the Nernst equation.

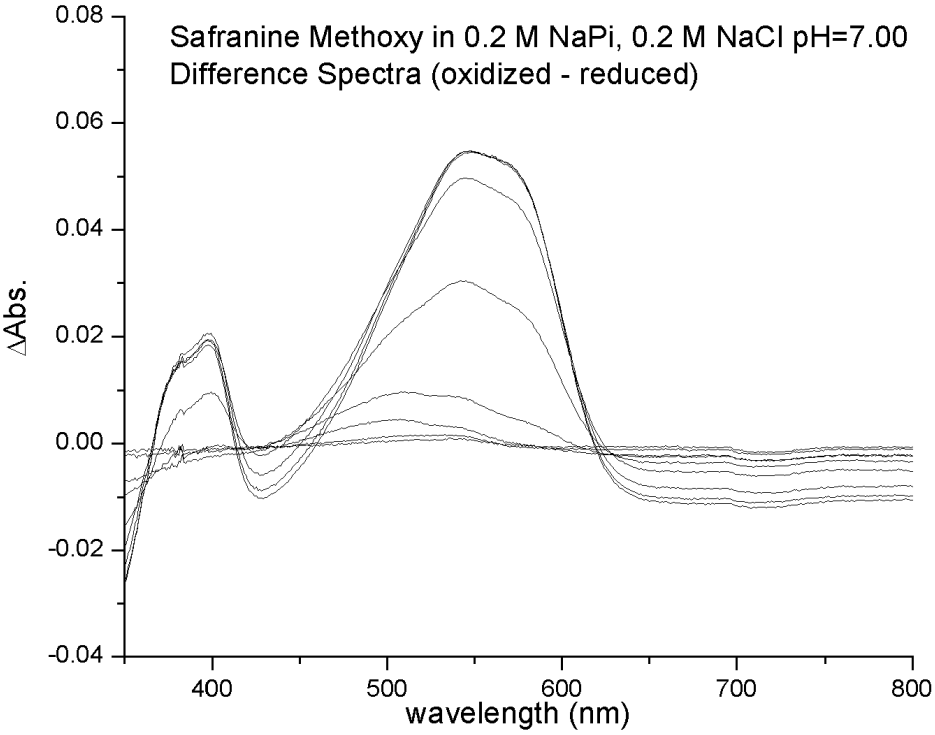

Figure. 3.6. Difference spectra (oxidized –reduced) of p-methoxysafranine.

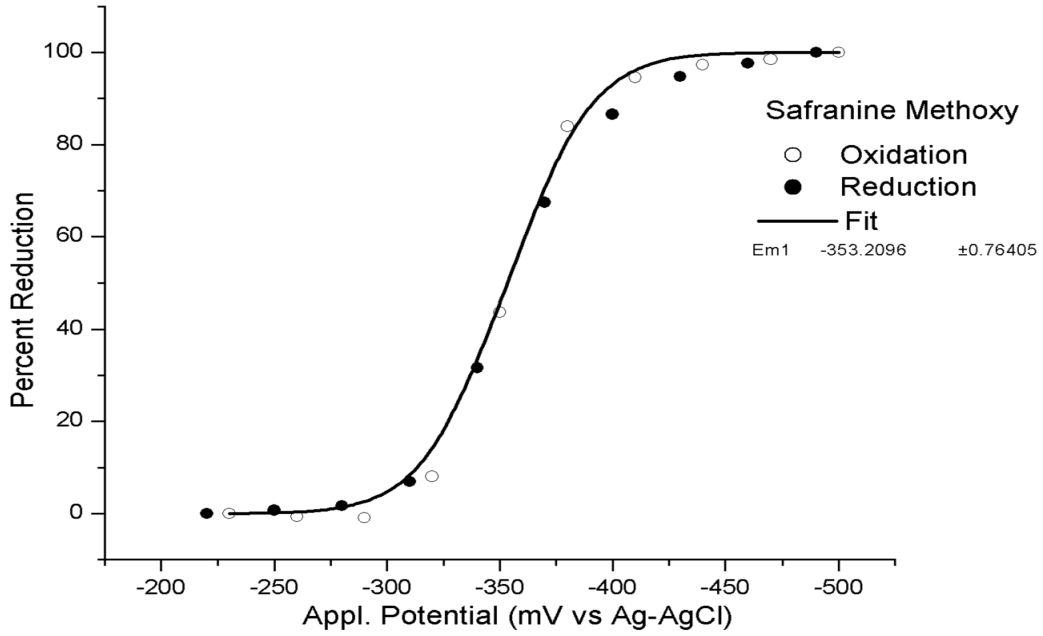

Figure.3.7. Spectroelectrochemical data of p-methoxysafranine. The applied potentials are referenced against Ag-AgCl which is +210 mV (NHE). The data were fit with the Nernst equation.

3.4. Spectra analysis data.

N-tert-butoxycarbonyl-5-iodo-2-methylaniline (2). A solution of 5-iodo-2-methylaniline (1g, 42.91mmol) and 2-tert butyldicarbonate (1.03g, 47.19 mmol) in THF (10 ml) was stirred at reflux temperature for 2 hours. Solvent was then removed in vacuo, the residue dissolved in ethyl acetate and this solution was washed successively with 1M citric acid solution and brine. The organic phase was dried over $MgSO_4$ and concentrated in vacuo. The resultant yellow-white solid was crystallized from hexane to give white solid **2** (1.22g, 85.3%). mp 119° C (hexane); R_f 0.8 (3:1, hexane/ethylacetate); λ_{abs}max ($CDCl_3$) 246 nm; ESIMS: *m/z* 356.1 (M^++1), 372.1(M^++K). ^{1}H-NMR ($CDCl_3$,500MHz): δ 1.52 [9H, s, C(C*H*$_3$)$_3$], 2.18 [3H, s, C*H*$_3$), 6.21 [1H, bs, **o**-Ph*H*], 6.84 [1H, d, *J* = 7.81 Hz, **m**-Ph*H*], 7.30 [1H, dd, *J* = 7.8, 1.47 Hz, **p**-Ph*H*], 8.25 [1H, bs, N*H*]. ^{13}C-NMR ($CDCl_3$, 125MHz): δ 17.67 [*C*H$_3$], 28.44 [C(*C*H$_3$)$_3$], 81.14 [*C*(CH$_3$)], 128.88 [*C*(5)], 131.85 [*C*(4)], 132.10 [*C*(2)], 132.41 [*C*(1)], 132.56 [*C*(6)], 137.83 [*C*(3)], 152.73 [NH*C*O].

Tert-butyl 5,5'-(4-methoxy phenylazanediyl) bis (2-methyl-5,1-phenylene)dicarbamate (4). P-anisidine **3** (300mg, 2.44mmol) was added to a solution containing **2** (1.7g, 5.11mmol), KO$_t$-Bu (819.76mg, 7.31mmol), CuI (18.5mg, 0.097mmol) and 22'bipyridine(15.2mg, 0.097mmol) in dry toluene (7ml) and then stirred at 120° C for 4h. The reaction was filtered and concentrated in vacuo. The crude product was purified by flash chromatography [4:1 hexane/ethylacetate, 1% triethylamine] resulting in 1.01g (78.3%) of a golden yellow oil. R_f 0.27 (4:1, hexane/ethylacetate, 1% triethylamine); λ_{abs}max ($CDCl_3$) 304 nm, ESIMS: *m/z* 534.3 (M^++1), 556.2(M^++Na). ^{1}H-

NMR ($CDCl_3$,500MHz): δ 1.43 [9H, s, C(CH_3)$_3$], 2.17 [3H, s, CH_3], 3.78 [3H, s, OCH_3], 6.12 [2H, bs, C(4)*H*], 6.66 [1H, d, *J* = 2.44 Hz, **o**-Methoxy*Ph*], 6.67 [1H, d, *J* = 1.96 Hz, **m**-Methoxy*Ph*], 6.95 [2H, d, *J* = 8.2 Hz, C(6)*H*], 7.04 [2H, d, *J* = 8.2 Hz, C(3)*H*], 7.35 [2H, bs, N*H*]. ^{13}C-NMR ($CDCl_3$, 125MHz): δ 17.44 [*C*H_3], 28.50 [C(*C*H_3)$_3$], 55.67 [O*C*H_3], 81.5 [*C*(CH_3)],114.81 [*C*(6)] , 117.07 [**m**-Methoxy*Ph*], 119.38 [*C*(4)] , 122.18 [*C*(2)], 126.85 [*C*(3)], 130.92 [**o**-Methoxy*Ph*], 136.86 [*C*(1)], 141.20 [*C*(5)], 147.10 [diPhN*C*-MethoxyPh], 153.20 [*C*=O], 155.89 [**p**- Methoxy*Ph*].

2,2'-(5,5'-(4-methoxyphenylazanediyl)bis(2-methyl-5,1-phenylene))diisoindoline-1,3-dione (5). Deprotection and phthaloylation of the amino groups in **4** was performed in a single step. 2.1 equivalents of phthalic anhydride (932.7 mg, 6.29 mmol) was added to **4** (1g, 2.99 mmol) and the reactants stirred in 15 ml of glacial acetic acid at 119° C for 4h. The resultant dark brown colored solution was subsequently washed with saturated sodium bicarbonate and then brine, dried over $MgSO_4$, filtered and concentrated in vacuo. The resultant yellow oil was purified using flash chromatography [1:1 hexane/ethylacetate, 1% triethylamine] resulting in 1.5g, (86%) of a light yellow oil. R_f 0.7 (1:1, hexane/ethylacetate, 1% triethylamine); λ_{abs}max (CDCl3) 302 nm; ESIMS : m/z 594.4 (M++1), 616.4 (M++Na); ^{1}H-NMR (CDCl3 ,500MHz): δ 2.11 [6H, s, CH3] , 3.76 [3H, s, OCH3], 6.82[1H, bs, C(4/4')H], 6.84 [1H, bs, C(4/4')H], 6.92[2H, d, J = 1.96 Hz, C(3/3')H], 7.1 [1H, d, J = 2.45 Hz, C(6/6')H], 7.11 [1H, d, J = 2.44 Hz, C(6/6')H], 7.15 [2H, d, J = 8.6 Hz, o-MethoxyPh], 7.19 [2H, d, J = 8. 3Hz, m-MethoxyPh], 7.76 [4H, dd, J = 2.93, 5.38 Hz, αH-Isoind], 7.91[4H, dd, J = 2.93, 5.37 Hz, βH-Isoind]. ^{13}C-NMR (CDCl3, 125MHz): δ 17.58 [CH3], 55.67 [OCH3], 115.61 [C(6)] , 122.96 [m-MethoxyPh], 123.70 [C(4)], 123.94 [αC-Isoind], 127.67 [C(2)], 129.99 [C(3)],

131.37 [4C-Isoind], 131.84 [o-MethoxyPh], 132.27 [βC-Isoind], 134.48 [C(1)], 140.04 [C(5)], 146.65 [diPhN-C-MethoxyPh], 156.68 [p- MethoxyPh], 167.45 [1, 3 C dione].

2,8-bis(1,3-dioxoisoindolin-2-yl)-10-(4-methoxyphenyl)-3,7-dimethylphenazine-10-ium 5-oxide (6).

5 (100mg, 0.17mmol) was dissolved in 17 ml acetic acid and 3ml of dry THF and the solution cooled to 0° C with ice. ^{15}N labeled sodium nitrite (60 mg, 0.85 mmol) was added all at once, the ice was removed, and the solution was stirred while warming to room temperature for 3h. After completion of the reaction was monitored by TLC the resultant deep red solution was washed with saturated sodium bicarbonate solution and then brined, dried over $MgSO_4$, filtered and concentrated in vacuo.. The resultant dark red oil was purified using flash chromatography [1:1 hexane/ethylacetate, 1% triethylamine] resulting in 57.7mg (55%) of a sticky orange solid. R_f 0.4 (1:1, hexane/ethylacetate, 1% triethylamine); λ_{abs}max (CDCl3) 450 nm; ESIMS: m/z 623.3 (M++1), 640.3 (M++H2O);^{1}H-NMR (CDCl3, 500MHz): δ 2.12 [6H, s, CH3], 3.83 [3H, s, OCH3], 6.84 [1H, d, J = 2.44 Hz, C(4/6)H], 6.98 [1H, d, J = 2.44 Hz, C(4/6)H], 7.01[1H, d, J = 2.44 Hz, C(1/9)H], 7.03[1H, dd, J = 2.93, 8.8 Hz, C(1/9)H], 7.14 [2H, d, J = 8.3 Hz, m-MethoxyPh], 7.26 [1H, dd, J = 0.98, 8.8 Hz, o-MethoxyPh], 7.28 [1H, dd, J = 2.92,5.85 Hz, o-MethoxyPh], 7.67 [1H, dd, J = 3.41, 5.37 Hz, αH-Isoind], 7.82 [1H, dd, J = 2.93, 5.37 Hz, βH-Isoind]; ^{13}C-NMR (CDCl3, 125MHz): δ 17.89 [CH3], 56.4 [OCH3], 110.51 [m-MethoxyPh], 122.51 [C(1)], 123.48 [αC-Isoind], 124.14 [C(5)], 131.28 [C(6)], 131.75 [o-MethoxyPh], 132.20 [C(4)], 132.41 [4C-Isoind], 132.62 [βC-Isoind], 133.06 [C(3)], 134.68 [C(2)], 145.27 [diPhN-C-MethoxyPh], 157.49 [p-MethoxyPh], 167.44 [1,3 C dione]; ^{15}N-NMR (CDCl3, 50 MHz): δ 371.49

3,7-diamino-5-(4-methoxyphenyl)-2,8-dimethylphenazin-5-ium (7). **6** (10mg, 0.016mmol) was dissolved in isopropanol (10ml) cooled to 0° C. $NaBH_4$ (3.03 mg, 0.08 mmol) was added and the solution stirred for 24 h at room temperature. When TLC indicated that **6** had been completely consumed, glacial acetic acid was added dropwise until fuming subsided. The flask was then fitted with a condenser and heated to 80° C for 2h. The crude solution was filtered, concentrated in vacuo and then lyophilized in the dark for 48 h to remove trace amounts of acetic acid. The reaction mixture was purified by flash chromatography [6:3:1 isopropanol/ethylacetate /5% aqueous acetic acid] yielding a purple powder (2.2mg, 40%). Rf 0.3 (6:3:1 isopropanol/ethylacetate /5% aqueous acetic acid). Further purification was done by HPLC as described below. λ_{abs}max (20 mM KH_2PO_4, 100 mM KCl, pH=8) 538nm; λ_{em}max (20 mM KH_2PO_4, 100 mM KCl, pH=8) 623nm; ESIMS: m/z 347.2 (M++1); ^{1}H-NMR (CDCl3, 500MHz): δ 2.23[6H, s, CH3], 3.94 [3H, s, OCH3], 6.56 [2H, bd, C(1/9)H], 6.58[2H, bd, C(1/9)H], 6.92 [2H, bd, C(4/6)H], 6.94[2H, bd, C(4/6)H], 7.53[4H, dd, J=3.42, 5.86 Hz, m-MethoxyPh], 7.63[4H, dd, J=3.42, 5.86 Hz, o-MethoxyPh]; ^{15}N-NMR (CDCl3, 50 MHz): δ 380.66.

3.5. Conclusions.

In conclusion, we have developed a synthetic route to a flavin-like cofactor, a safranine O analogue which incorporates a single substitution at a point far removed from the phenazine headgroup at which reduction occurs. This route enables the inexpensive incorporation of an isotopic reporter atom at the reduction site. This analogue displays

large differences in both reduction potentials and photophysical properties from its parent compound.

3.6. Future developments.

We are currently exploring in more detail the pH-dependent oxidation-reduction potentials of both one- and two-electron reduction of both molecules in solution, and investigating their properties when complexed with artificial proteins designed to bind and activate them.

3.7. Bibliography.

1. Cui, D.T., et al., *(15)N Solid-State NMR as a Probe of Flavin H-Bonding.* Journal Of Physical Chemistry B, 2011. **115**(24): p. 7788-7798.
2. Muchowski, J.M. and M.C. Venuti, *Ortho functionalization of N-(tert-butoxycarbonyl)aniline.* Journal of Organic Chemistry, 1980. **45**(23): p. 4798-4801.
3. Kelkar, A.A., N.M. Patil, and R.V. Chaudhari, *Copper-catalyzed amination of aryl halides: single-step synthesis of triarylamines.* Tetrahedron Letters, 2002. **43**(40): p. 7143-7146.
4. Nanda, V. and R.L. Koder, *Designing artificial enzymes by intuition and computation.* Nature Chemistry, 2010. **2**(1): p. 15-24.
5. Manifar, T., et al., *Copper(I)-medliated ligand-accelerated Ullmann-type coupling of anilines with aryliodides: Ligand selection and reaction kinetics for synthesis of tri-p-tolylamine.* Industrial & Engineering Chemistry Research, 2005. **44**(4): p. 789-798.
6. Koder, R.L. and P.L. Dutton, *Intelligent design: the de novo engineering of proteins with specified functions.* Dalton Transactions, 2006. **25**: p. 3045-3051.
7. Osby, J.O., M.G. Martin, and B. Ganem, *An exceptionally mild deprotection of phthalimides.* Tetrahedron Letters, 1984. **25**(20): p. 2093-2096.
8. Lu, Y., *Design and engineering of metalloproteins containing unnatural amino acids or non-native metal-containing cofactors.* Current Opinion In Chemical Biology, 2005. **9**(2): p. 118-126.

9. Meth-Cohn, O. and M. Smith, *What did W.H. Perkin actually make when he oxidized aniline to obtain mauveine?* Journal of the Chemical Society-Perkin Transactions 1, 1994(1): p. 5-7.

10. Fry, H.C., et al., *Computational Design and Elaboration of a de Novo Heterotetrameric alpha-Helical Protein That Selectively Binds an Emissive Abiological (Porphinato)zinc Chromophore.* Journal of the American Chemical Society, 2010. **132**(11): p. 3997-4005.

11. Bender, G.M., et al., *De novo design of a single-chain diphenylporphyrin metalloprotein.* Journal Of The American Chemical Society, 2007. **129**(35): p. 10732-10740.

12. Zhuang, J.Y., et al., *Evaluating the roles of the heme a side chains in cytochrome c oxidase using designed heme proteins.* Biochemistry, 2006. **45**(41): p. 12530-12538.

13. Lichtenstein, B.R., et al., *Reversible proton coupled electron transfer in a peptide-incorporated naphthoquinone amino acid.* Chemical Communications, 2009(2): p. 168-170.

14. Sharp, R.E., et al., *Design, synthesis, and characterization of a photoactivatable flavocytochrome molecular maquette.* Proceedings of the National Academy of Sciences of the United States of America, 1998. **95**(18): p. 10465-10470.

15. Massey, V., *The chemical and biological versatility of riboflavin.* Biochemical Society Transactions, 2000. **28**: p. 283-296.

16. Koder, R.L., et al., *A flavin analogue with improved solubility in organic solvents.* Tetrahedron Letters, 2007. **48**(31): p. 5517-5520.

17. Cerda, J.F., et al., *Hydrogen bond-free flavin redox properties: managing flavins in extreme aprotic solvents.* Organic & Biomolecular Chemistry, 2008. **6**: p. 2204-2212.

18. Schopfer, L.M., M.L. Ludwig, and V. Massey, *A working proposal for the role of the apoprotein in determining the redox potential of the flavin in flavoproteins: correlations between potentials and flavin pKs*, in *Flavins and Flavoproteins*, B. Curti, S. Ronchi, and G. Zanetti, Editors. 1990, Walter de Gruyter: New York.

19. Koder, R.L., et al., *Flavin thermodynamics explain the oxygen insensitivity of enteric nitroreductases.* Biochemistry, 2002. **41**(48): p. 14197-14205.

20. Zhang, L., et al., *Manipulating cofactor binding thremodynamics in an artificial oxygen transport protein.* Biochemistry, 2011. **50**. p. 10254-10261.

21. Iordanov, V.P., et al., *Integrated sensor arrays for bioluminescence and fluorescence bio-chemical analysis.* Proceedings of IEEE Sensors 2004, 2004. **2**: p. 810-3.

22. Clarke, W.M., *Oxidation Reduction Potentials of Organic Systems*1960, Baltimore: The Williams and Wilkins Co.

23. Draper, R.D. and L.L. Ingraham, *A potentiometric study of the flavin semiquinone equilibrium.* Archives of Biochemistry and Biophysics, 1968. **125**: p. 802-808.

24. Heichert, C. and H. Hartmann, *On the Formation of Mauvein: Mechanistic Considerations and Preparative Results.* Zeitschrift Fur Naturforschung Section B-a Journal of Chemical Sciences, 2009. **64**(6): p. 747-755.

25. Goodbrand, H.B. and N.X. Hu, *Ligand-accelerated catalysis of the Ullmann condensation: Application to hole conducting triarylamines.* Journal of Organic Chemistry, 1999. **64**(2): p. 670-674.

26. Koder, R.L., et al., *^{15}N Solid-state NMR provides a sensitive probe of oxidized flavin reactive sites.* Journal of the American Chemical Society, 2006. **128**: p. 15200-15208.

27. Yoneda, F., et al., *Syntheses of Isoalloxazines and Isoalloxazine 5-Oxides - New Synthesis of Riboflavin.* Journal of the American Chemical Society, 1976. **98**(3): p. 830-835.

Chapter 4.

A novel synthetic route for artificial safranines and spectral studies.

4.1. Summary.

Safranines are flavin-like artificial cofactors, which are capable of transferring electrons [1-4]. We have developed a novel synthesis route, generating a variety of safranine analogues differing in photophysical and electrochemical properties. These cofactors are energetically engineered to perform catalytic reactions at higher rates, easing the effort of artificial enzyme engineering for desired tasks. We have also incorporated an isotopic nitrogen on phenazine ring which helps to track the cofactor chemistry inside the enzyme, lending insight during the enzyme engineering process.

4.2. Introduction.

Artificial proteins are designed for binding both natural and artificial cofactors [5-7]. There has been much effort put toward designing artificial enzymes with metal-porphyrins as cofactors, but less toward the design of enzymes with bioorganic cofactor molecules [6,7,27-30]. Natural flavoenzymes are involved in numerous metabolic processes, and their flavin cofactors have unique properties making flavoenzymes especially useful in the chemical reactions of the biological world [9]. Flavins can exist in multiple oxidation states and, hence they can execute both one- and two- electron transfer reactions, making them versatile in different reaction scenarios [16]. In chapter 3,

we reported our success at making an artificial flavin-like cofactor, a safranine analogue, modulated for its reduction potential [8]. In current chapter we report our new synthesis scheme for making a bunch of artificial safranine cofactors. These novel cofactors are made only to perform one kind of chemistry. The higher reduction potentials of these cofactors lend extra driving force to reactions like the oxidation of nicotinamide cofactors such as NADH and NADPH.

The phenazine moiety of safranine resembles the isoalloxazine of flavin. The reported two-electron reduction midpoint potential of safranine O, -290 mV vs SHE [22], is 100 mV, or 2.3 kcal/mol more negative than that of riboflavin [11]. Our novel synthetic route conjugates a phenyl ring at the N(10) position, which can then be altered, resulting in a range of reduction potentials. Moreover, this synthesis enables the inexpensive incorporation of isotopically labeled nitrogen at the N(5) position in the phenazine ring of the safranine analogues [8]. The isotopic chemical shift of the nitrogen translates the chemical reactivity imparted upon the cofactor by its environment [12]. The tunable photophysical properties of these safranine analogues are another outcome of our synthesis that extends their applications to areas such as biochemical sensors.

4.3. Methodologies and experimental procedures.

4.3.1. General procedures and materials.

All chemicals were purchased from Sigma-Aldrich. For ^{15}N-labelled reactions, ^{15}N -labeled sodium nitrite ($^{15}NaNO_2$) was purchased from Cambridge Isotope Labs (Cambridge, MA). Reactions were purged with dry nitrogen gas, ensuring an inert atmosphere. Synthesis grade or ACS grade reagents were used for all reactions. For

purification, HPLC grade reagents and water were used. Reactions were monitored by thin-layer chromatography. Different ratios of hexane-ethyl acetate with triethylamine solvent mixtures were used for TLC. Final TLC products were run in an isopropanol-ethyl acetate-aqueous acetic acid mixture. TLC pre-coated silica gel plates were purchased from EMD silica gel 60 F_{254}. All products were purified using flash column chromatography. Hexane-ethyl acetate with a triethylamine mixture gave good separation in flash column purifications. Only final products were purified in an isopropanol-ethyl acetate-aqueous acetic acid mixture. Silica gel (pore size is 30-75 μm) for flash column chromatography was purchased from Analtech. NMR spectra were recorded on a Varian Inova spectrometer operating at 500 MHz for ^{1}H, 125 MHz for ^{13}C and 50 MHz for ^{15}N. For confirming NMR assignments, two-dimensional homonuclear correlation (COSY) was done.

4.3.2. Allyl protection of primary amine.

Primary amines are extremely reactive and can cause interference in synthetic transformations because of the nitrogen atom with basic and nucleophilic lone pair electrons. To protect this primary amine is the first step of any multistep synthesis, if one of the reactant has a primary amine moiety. Selection of the protecting groups is also very important. They must be stable in the reaction medium for multiple steps of synthesis, despite changes in acidity, alkalinity, temperature and duration. Also, they need to be inert to other reactive species taking part in the reaction. In our synthetic route, condensation and nitrosative cyclization are two key steps. These reactions have different conditions. Condensation has to be done in fairly high temperature and a highly alkaline medium [14-18]. On the contrary, the next step is nitrosative cyclization, which takes

place at ice cold or room temperature and in an acidic medium. In the first design of the synthesis of safranine, we tried t-butyl carbamate (Boc) to protect the amine [13]. It served the purpose well in the first condensation step. Boc was removabale by trifluoroacetic acid (TFA) [13]. In the second step, which is acidic in nature, Boc broke down and the amine was exposed to the nitrosonium ion in the medium [8]. This led to the diazotization reaction and exterminated the cyclization. To overcome this situation we switched to phthalic anhydride as the primary amine protecting group. Phthalimide can survive in acidic conditions [19]. But this added two more steps to the overall synthesis. The protecting and deprotecting steps of the phthalic anhydride group also affected the yield. Only the methoxy analogue of safranine came out of that synthesis with descent yield. All other derivatives yielded less than 30%. The electron density of the fourth carbon on each toluidine ring in triarylamine needed to be high in order to engage with the nitrosonium ion, but the electron withdrawing groups in the para position of the N(10) phenyl reduced the electron density of the two toluidines connected to it. This reflected in the overall yield of the synthesis. The protecting group of primary amine could have also engaged in electron donation. This may have enhanced the reaction. The Hammet constant of $-NH\text{-}CO\text{-}CH_3$ at σ para position of phthalimide is 0.00, which means the phthalic group had no effect in the reaction other than just protecting the primary amine [20]. All these reasons led to a redesign of the synthesis route for our safranine analogues. The new protecting group needed to be stable in condensation (basic condition, high temperature) and nitrisative cyclization (acidic condition, cold or room temperature). This could reduce two steps in the overall synthesis. Also it needed to enhance the electron

density on targeted carbons on the phenyl rings. By selecting an allyl group protection scheme, we were able to avoid the problems with the previous methods.

Allyl protection is upheld as an alternative for Boc and Fmoc protection reactions as in peptide synthesis [21]. This is mainly because of the mild palladium catalyzed deprotection [23]. A solution of 5-iodo-2-methylaniline and allyl bromide with an alkali metal carbonate (potassium carbonate, K_2CO_3) in a polar aprotic solvent (anhydrous dimethylformamide, DMF) was stirred at 80 °C for 2 hours [21]. The solvent was then removed in vacuo, the residue dissolved in hexane-ethyl acetate mixture and purified by flash column chromatography, yielding 75% of product.

4.3.3. Condensation.

Condensation with p-anisidine in the synthesis of the methoxy analogue of safranine in the previuos chapter used copper iodide, 2,2'-bipyridine and three equivalents of potassium *tert*-butoxide in anhydrous toluene forming triarylamine [8,14-18]. In the first scheme, the rigid phenanthroline ligand was replaced with the more flexible bipyridine ligand, and the stronger, more hindered, *tert*-butoxide base was used to replace the potassium hydroxide [8]. Initial attempts using 1,10-phenanthroline as a copper ligand and potassium hydroxide as a base resulted in low yields [8]. The presence of *tert*-butoxide could have initiate a rearrangement of allyl group in the reaction, so sodium hydride (NaH) was used as a base instead of potassium *tert*-butoxide. This change also resulted in a considerable increase in the triarylamine yield.

Aniline and its derivatives such as para-anisidine, para-toluidine, 4-aminobenzonitrile, 2,3,4,5,6 pentafluoroaniline were added to a solution containing N,N-diallyl-5-iodo-2-methylaniline, sodium hydride, Copper(1)iodide (CuI) and 22'bipyridine in anhydrous

toluene and then stirred at 120° C for 4h. The reaction was filtered and concentrated in vacuo. The crude product was purified by flash chromatography (4:1 hexane/ethylacetate, 1% triethylamine), resulting in golden yellow oil. Isolated yields of condensation were >60% with aniline, >71% with para-anisidine, ≈70% with para-toluidine, 60% with 4-aminobenzonitrile, 72% with 2,3,4,5,6 pentafluoroaniline, respectively.

4.3.4. Nitrosative cyclization.

In an effort to correct diazotization problems with the first scheme, Boc protecting groups were replaced with acid-stable phthalate protecting groups [13,19]. Direct cyclization of triarylamine with Boc had proved to be unsuccessful, as the acidic conditions required to deprotect the amines forming azo compounds from the free amines and the nitrite. But in current scheme, allyl protection of the amine was inert towards cyclization, and it stayed stable in the acidic condition. It also helped simplified the previous scheme by two steps. All triaryarylamine derivatives were dissolved in 17 ml acetic acid and 3ml of dry THF and the solution cooled to 0° C with ice. ^{15}N labeled sodium nitrite was added all at once, the ice was removed, and the solution was stirred while it was warmed at room temperature for 3h [8,22]. After the completion of the reaction as monitored by TLC, the resultant deep red solution was washed with saturated sodium bicarbonate solution and then brined, dried over $MgSO_4$, filtered and concentrated in vacuo. The resultant dark red oil was purified using flash chromatography [1:1 hexane/ethylacetate, 1% triethylamine] resulting a sticky orange solid. The respective phenazinium-oxide yields were 51% with phenylphenazinium-oxide, 54% with methoxyphenyl-phenazinium-oxide, 49% with para-tolyl-phenazinium-oxide, 57% with cyanophenyl-phenazinium-oxide, 62% with 2,3,4,5,6 perfluorophenyl-phenazinium-oxide. As in the previous shemes, the isotopic label was

introduced in the nitrosative cyclization step. To prevent loss of the isotopic material and lower yields by uncontrolled oxidative condensations, we introduced the labeling only at the end step of the scheme as in previous chapter. In the latest scheme, all the phenazinium-oxide analogues showed considerable increase in isolated yield after the nitrosative cyclization.

4.3.5. Deoxygenation and allyl deprotection.

The reductive deprotection was a one step reaction. Palladium based mild deprotection served the purpose [23]. Resultant phenazenium-oxide analogues were dissolved in anhydrous dicholoromethane. Tetrakis(triphenyl phosphidine)palladium was added with NN'-dimethyl barbituric acid and the solution stirred for 2 hours at 35° C. The crude solution was filtered, concentrated in vacuo. The reaction mixture was purified by flash chromatography [6:3:1 isopropanol/ethylacetate /5% aqueous acetic acid]. The respective diamino-dimethyl-phenazinium yields were >22% with phenylphenazinium, 24% with methoxyphenyl-phenazinium, 35% with para-tolyl-phenazinium, 30% with cyanophenyl-phenazinium, 45% with 2,3,4,5,6 perfluorophenyl-phenazinium. Further purification was done by HPLC for the right safranine isomer as described below.

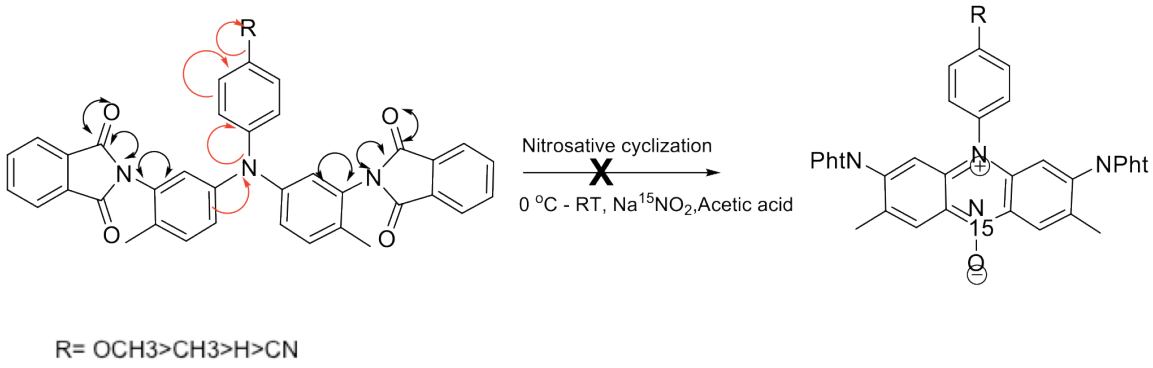

Scheme. 4.1. Plausible reason for low yield in second synthesis scheme. The Hammet constant of –NH-CO-CH_3 at σ para position is 0.00. [*Lange's Hand Book of Chemistry (2005, Sixteenth Ed., -James G Speight)*]

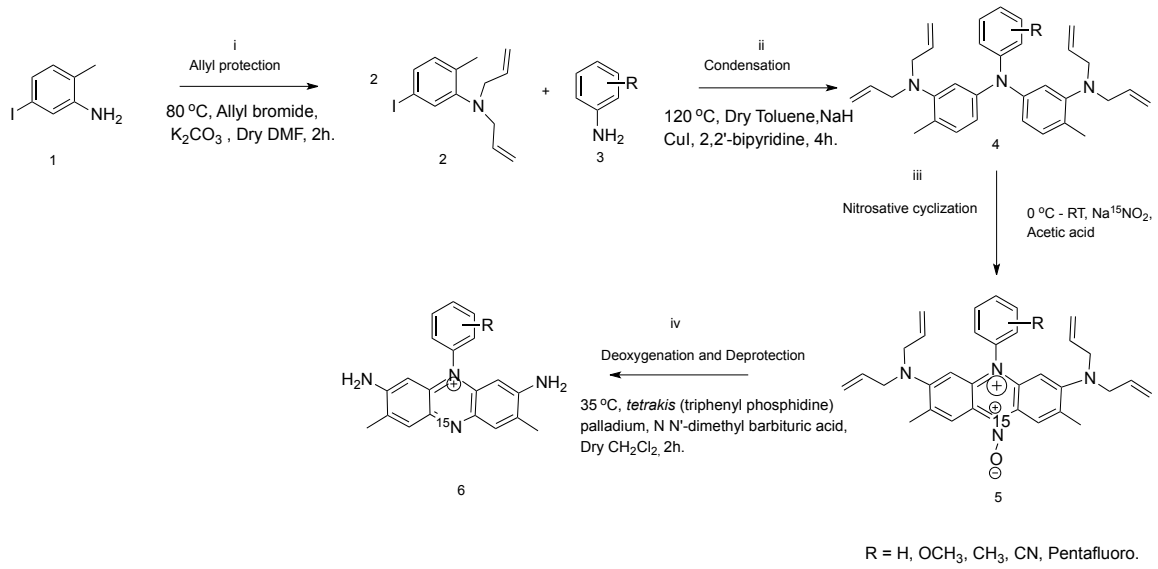

Scheme.4.2. Third synthesis scheme of safranine analogues.

Protection of amine with Allyl bromide	Aniline derivatives	Ullmann Condensation	Nitrosative Cyclization	Deoxygenation and Deprotection of Amine
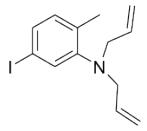		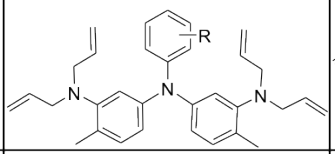	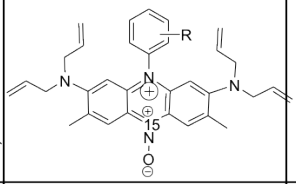	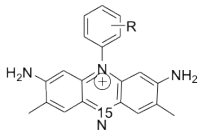
75.5%	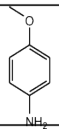	71.5%	54%	24%
	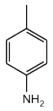	69.6%	49%	35%
	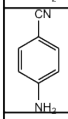	60%	57%	30%
		60.2%	51%	22.5%
	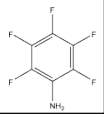	72.0%	62%	45%

Table.4.1. Reaction yield from third synthesis scheme.

4.3.6. HPLC purification.

The final purifications of all safranine analogues were performed using a Shimadzu HPLC equipped with two LC-6AD pumps and a multiwavelength photodiode array detector with a scanning range of 200-800 nm. Preparative scale purification was performed at room temperature using a 250 x 20 mm 10μm Proto 300 C18 column (Higgins Analytical) at a flow rate of 12 ml/min. An inline degasser removed the gas from all the eluents used. Samples were injected 500 μl. manually. The eluent system used was a water and methanol gradient with 5mM tetrabutyl ammoniumhydroxide (TBA) as an ion pairing reagent purchased from Sigma-aldrich. TBA solution was prepared from a stock solution consisting of 0.1 M TBA and 0.1 M potassium hydroxide purchased from Spectrum that was brought to a pH of 7 with phosphoric acid. For the methoxy derivative, the gradient was from 42.5 to 60% Buffer B over 20 min. The respective retention time of the diamino-dimethyl-phenazinium derivatives (final safranine analogues) was between 10 to 15 minutes. The appropriate peak was collected with the help of a fraction collector and removed the solvent in vacuo. Then it was lyophilized to remove the water, resulting a dry powder. A ^{1}H NMR (500 MHz) in D_2O and mass spectrometry were performed on peak collected from HPLC for further conformation [8].

4.3.7. UV-visible spectrophotometry.

UV-visible spectra were collected using an Olis computerized HP 8455UV/vis diode array spectrophotometer. Safranines were dissolved in 0.2M monopotassium phosphate, 0.1M KCl, pH 8.0. Solutions were degassed using several cycles of applied vacuum

followed by flushing with dry nitrogen [8, 24]. Oxidized spectra were collected, and then the safranines were reduced using sodium hydrosulfite. All of the safranine analogues showed an absorption ≈ 570 nm.

4.3.8. Fluorescence spectrophotometry.

All experiments were recorded using Olis DM 45 fluorescent spectrofluorimeter with a spectral range ≤ 210-800nm. The instrument is equipped with a 75 Watt Xenon arc lamp and has single grating monochromators for highest throughput. Safranines were dissolved in 0.2M monopotassium phosphate, 0.1M KCl, pH 8.0. Solutions were degassed using several cycles of applied vacuum followed by flushing with dry nitrogen. The temperature for all measurements was 25 °C, regulated with a thermostat. The scan increments were 100 per second. Incoming light intensity was regulated with a 0.6 slit, and the outgoing slit was 1.24. The sample cell used was a quartz cuvette with a 1cm path length. The machine was tuned to higher voltage scan modes in a range between 950 to 1100 when lower concentrations of safranine O were used. This was done to ensure the sufficient fluorescence emission intensity. The fluorescence emission wavelength (λ_{em}) maximum was 601nm with para-tolyl-phenazinium (*p*-methylsafranine, excitation wavelength was 570nm), 607nm with cyanophenyl-phenazinium (cyanosafranine, excitation wavelength was 570nm), 617nm with 2,3,4,5,6 perfluorophenyl-phenazinium (pentafluorosafranine, excitation wavelength was 560nm). None of the compounds were fluorescent in the reduced state. These spectral differences are advantageous, as they can be separately monitored in mixed solutions of the two species, or in mixed complexes of the two cofactors with one or more proteins, as has been proposed for biochemical sensor arrays [8].

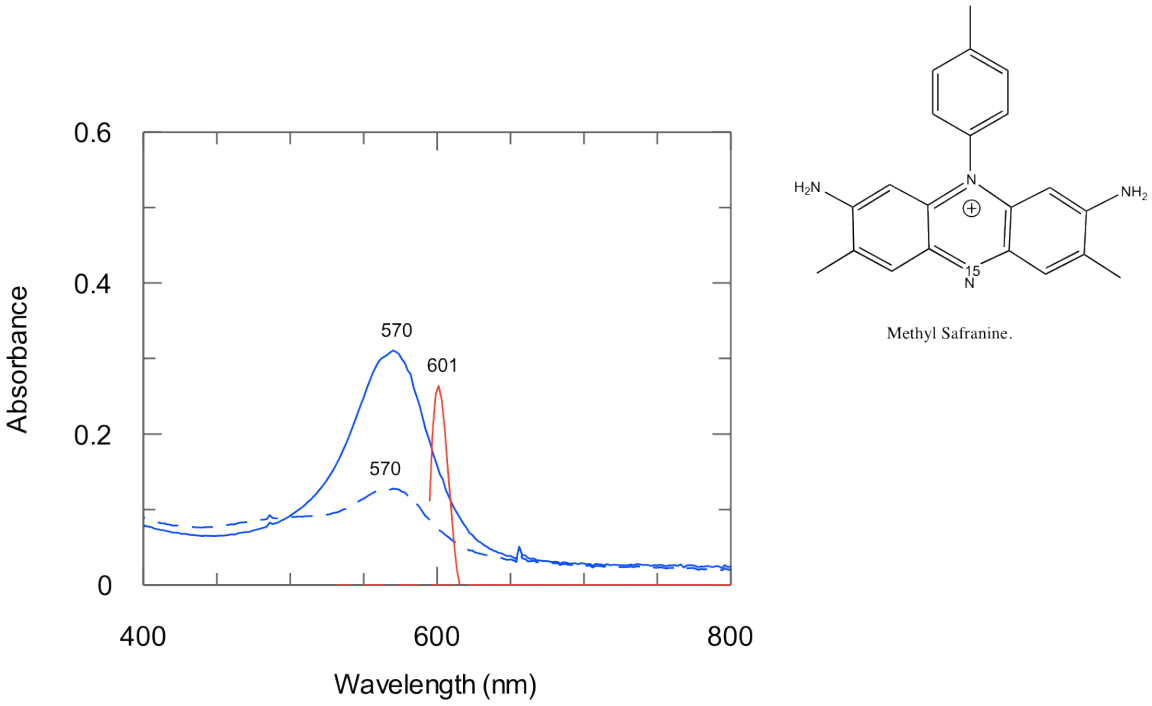

Figure.4.1. Absorbance spectra of oxidized (solid line, 570 nm), reduced (dotted line, 570 nm) and fluorescence emission (solid line, 601 nm) spectra of oxidized p-methylsafranine.

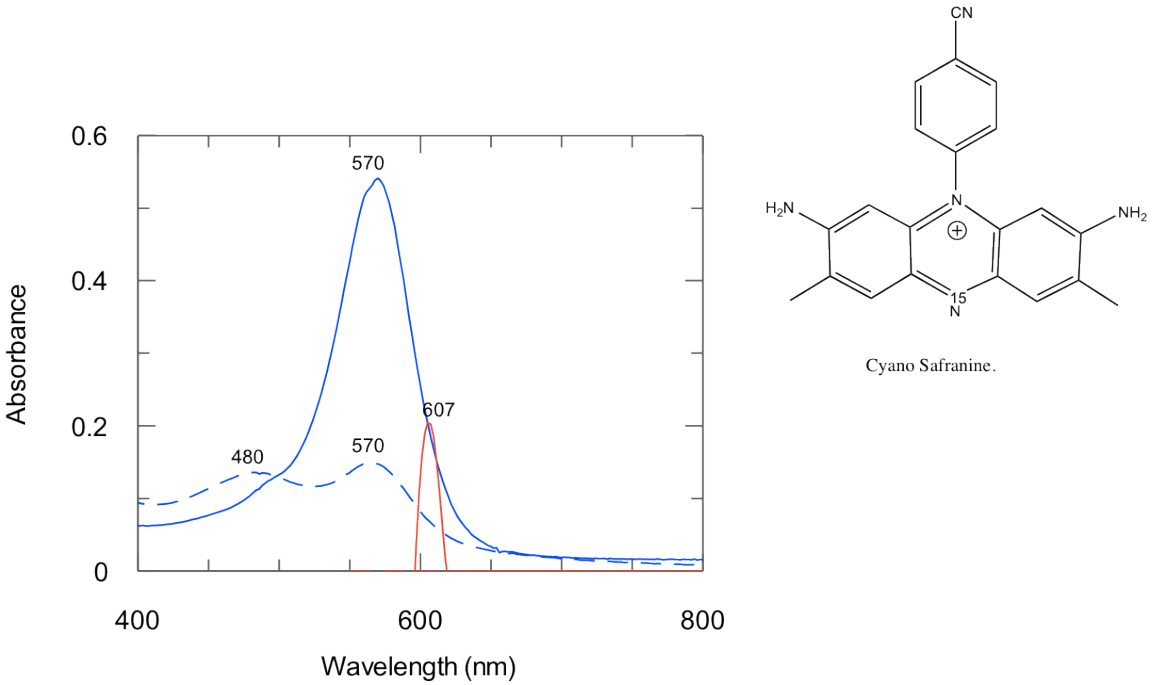

Figure.4.2. Absorbance spectra of oxidized (solid line, 570 nm), reduced (dotted line, 570 nm) and fluorescence emission (solid line, 607 nm) spectra of oxidized p-cyanosafranine.

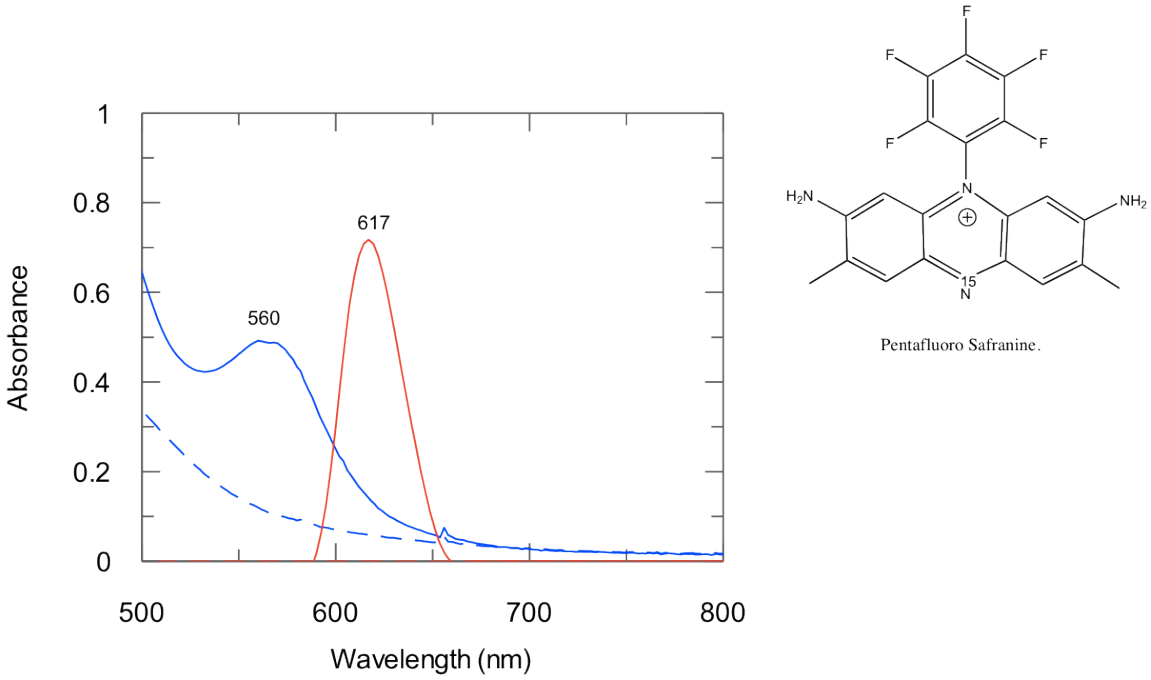

Figure.4.3. Absorbance spectra of oxidized (solid line, 560 nm), reduced (dotted line) and fluorescence emission (solid line, 617 nm) spectra of oxidized pentafluorosafranine.

Safranine analogue	Wavelength (nm) of maximum absorbtion. [oxidized form]	Wavelength (nm) of maximum absorbtion. [reduced form]	Wavelength (nm) of Fluorescence emission. [oxidized form]	Wavelength (nm) of Fluorescence emission. [reduced form]
Safranine O	522	522	581	No Fluorescence
p-Methoxysafranine	538	448	625	
Cyanosafranine	570	480, 570	607	
p-Methylsafranine	570	570	601	
Pentafluorosafranine	560	480	617	

Table.4.2. Absorption and fluorescence emission spectral details of safranine analogues.

4.3.9. ^{15}N-Nuclear magnetic resonance spectroscopy.

Previous research has established that the chemical shift tensor of the isoalloxazine N(5) nitrogen in flavin compounds is very informative as to the chemical reactivity imparted upon flavins by their environments. N(5) and O geometry, hydrogen bonding and protonation status can restrain the energy and distribution of HOMO electron density in the delocalized frontier orbitals of flavin [12]. Optical and fluorescence spectral shifts will give very little information on these confined local changes that correlates to enzyme activities. Isotropic shifts in solution represent the variations of electron distribution. Paramagnetic deshielding is mainly from orbital coupling of HUMO and LUMO. Hence it is specifically associated with the orbitals involved in cofactor reactivity. It is more accentuated in conjugated systems, particularly at N sites. The chemical shifts should relate to such reactivity [12]. This inspired us to create a synthetic route which enables the inexpensive incorporation of isotopically labeled nitrogen at the equivalent N(5) position in the phenazine ring of safranine analogues [8,12].

All NMR experiments were performed at 20°C on a Varian Inova spectrometer operating at 50 MHz If there are electron donating groups present in the phenazinium ring, it leads to an increased shielding and an upfield isotropic shift. On the contrary, if there is an electron withdrawing group attached, that would lead to deshielding, hence a downfield shift. ^{15}N-NMR (D_2O, 50 MHz) of safranine analogues are : δ414.84 with para-tolyl-phenazinium (*p*-methylsafranine), δ401.87 with cyanophenyl-phenazinium (cyanosafranine), δ523.57 with 2,3,4,5,6 perfluorophenyl-phenazinium (pentafluorosafranine).

Safranine analogue.	^{15}N – NMR (CD_3OD, 50 MHz)
p-methoxy safranine	δ 380.66
p-methyl safranine	δ 414.84
Pentafluoro safranine	δ 523.57
Cyano safranine	δ 401.87

Table. 4.3. ^{15}N chemical shifts of safranine analogues.

4.3.10. Spectroelectrochemical analysis.

Natural flavoproteins regulate the reduction potentials of flavin by more than half a Volt. Scientific research shows that small molecular structural changes cause large fluctuations in reduction potentials [25,26]. This inspired us to create a series of flavin-like cofactors with small functional group changes. Safranines have a phenazine moiety similar in size and shape to that of isoalloxazine in flavin. We investigated whether modifying the N(10) phenyl substituent of safranine, which is conjugated to the phenazine, would alter the reduction potential of the molecule.

Spectroelectrochemical analysis was done on all safranine analogues. Safranines were dissolved in buffer containing 0.2M sodium phosphate, 0.2M NaCl, pH 7.0. The applied potentials were referenced against Ag-AgCl which is +210 mV (NHE). The spectra were collected in a PerkinElmer Lambda 35 UV/Vis spectrometer. The applied potential was set by using a PWR-3 Power Module potentiostat (Bioanalytical Systems Inc.). The safranine solutions were equilibrated at each potential for at least ten minutes before spectra were collected. The electrochemical cell is a 10mm quartz cuvette containing a pair of gold slides that serve as the working electrode, a platinum wire auxiliary electrode, and a Ag-AgCl reference microelectrode (Microelectrodes Inc). The gold working electrode was coated with 1-mercaptohexanol by soaking the slides in a 1-proponal solution containing 1-mercaptohexanol 1% (v/v) for 20 hours. The absorbance values at the oxidized maximum were used to calculate the fractional oxidation at each potential and this data was fit with the Nernst equation.

$$E = E^{o} - \frac{RT}{ZF} \ln \frac{[Saf]_{red.}}{[Saf]_{ox.}}$$

E is the ambient potential in the solution. E^o is the midpoint reduction potential of safranine. R is the universal gas constant (8.31 $JK^{-1}mol^{-1}$). T is the absolute temperature. F is the Faraday constant (9.65 x 10^4 C mol^{-1}). Z is the number of electrons transferred in the reaction.

To quantify the change in free-energy (ΔG) the equation is

$$\Delta G = -nF\,\Delta E$$

where n is the number of electrons and ΔE is the difference between the oxidant and the reductant couples, and F is Faradays constant (23.0 $kcalV^{-1}mol^{-1}$).

The reduction potentials of safranine analogues are more negative than safranine O. The reduction potentials are: *p*-methylsafranine: -109.35mV, pentafluorosafranine: -123mV, cyanosafranine: -106.9 mV. Safranine O, p-methoxysafranine and *p*-methylsafranine display two-state behavior, directly transforming from the oxidized state to the two-electron reduced state during the titration. Thus, an enzyme containing the following cofactors, pentafluorosafranine with 5.67 kcal/mol, *p*-methylsafranine with 5.04 kcal/mol, and cyanosafranine with 4.93 kcal/mol, will have more driving force, respectively, for oxidative reactions like the oxidation of nicotinamide cofactors such as NADH and NADPH.

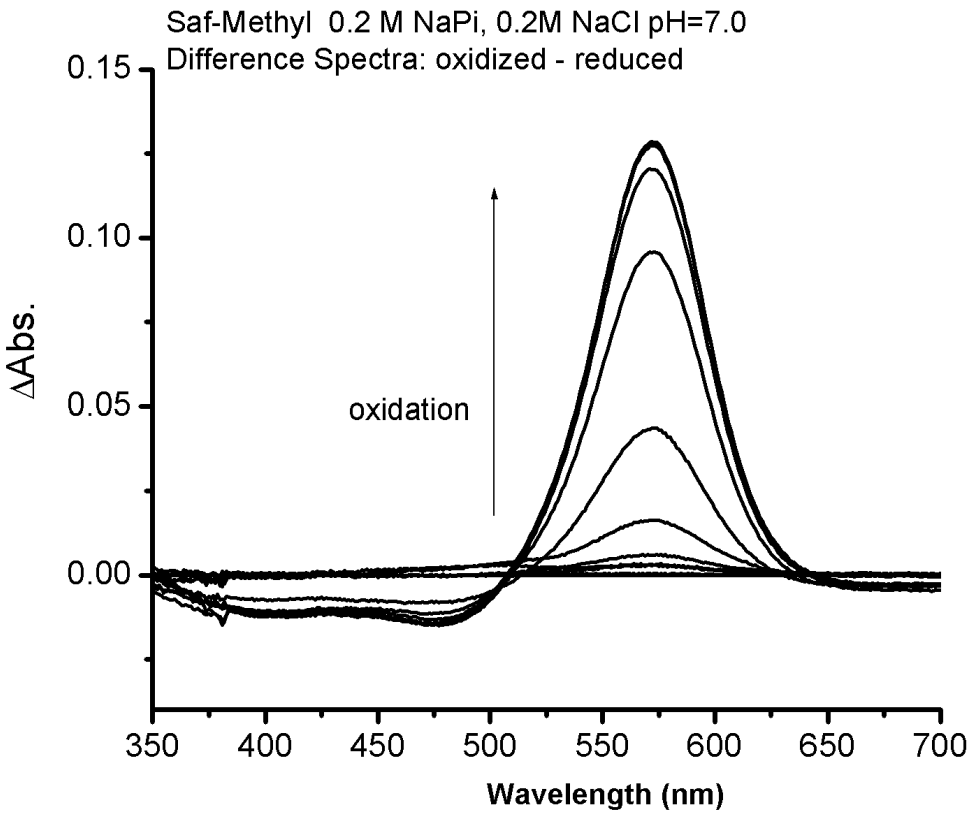

Figure 4.4. Difference spectra (oxidized –reduced) of p-methylsafranine.

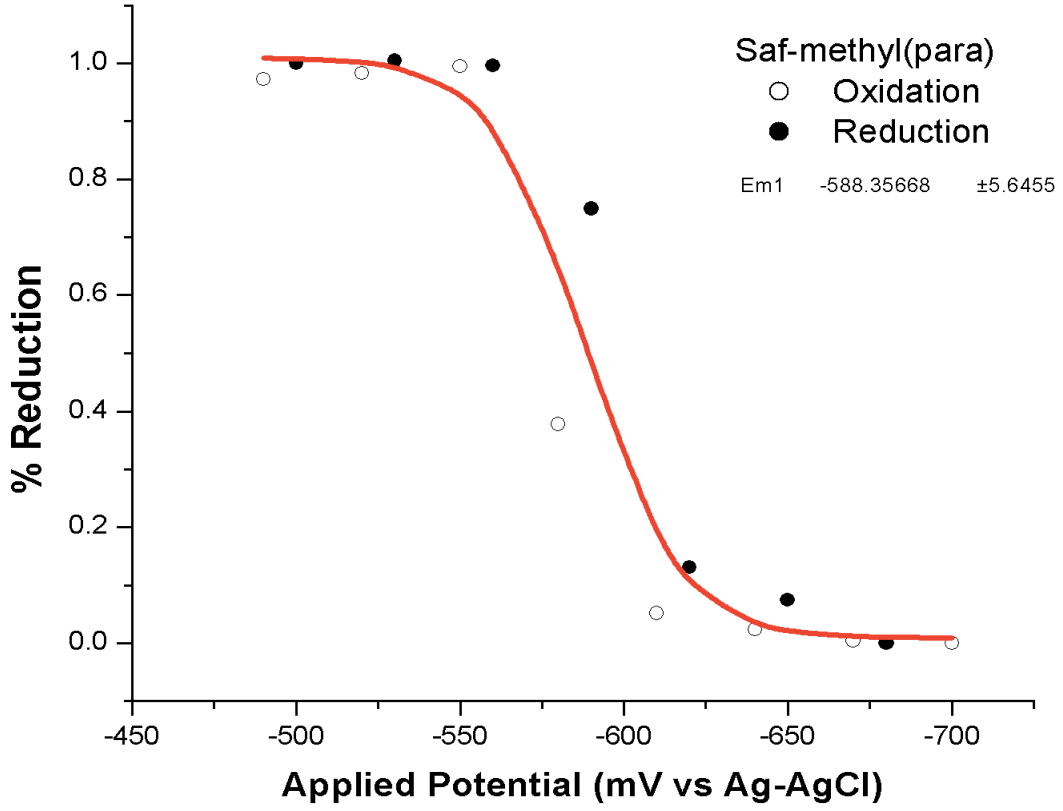

Figure.4.5. Spectroelectrochemical data of p-methylsafranine. The applied potentials are referenced against Ag-AgCl which is +210 mV (NHE). The data were fit with the Nernst equation.

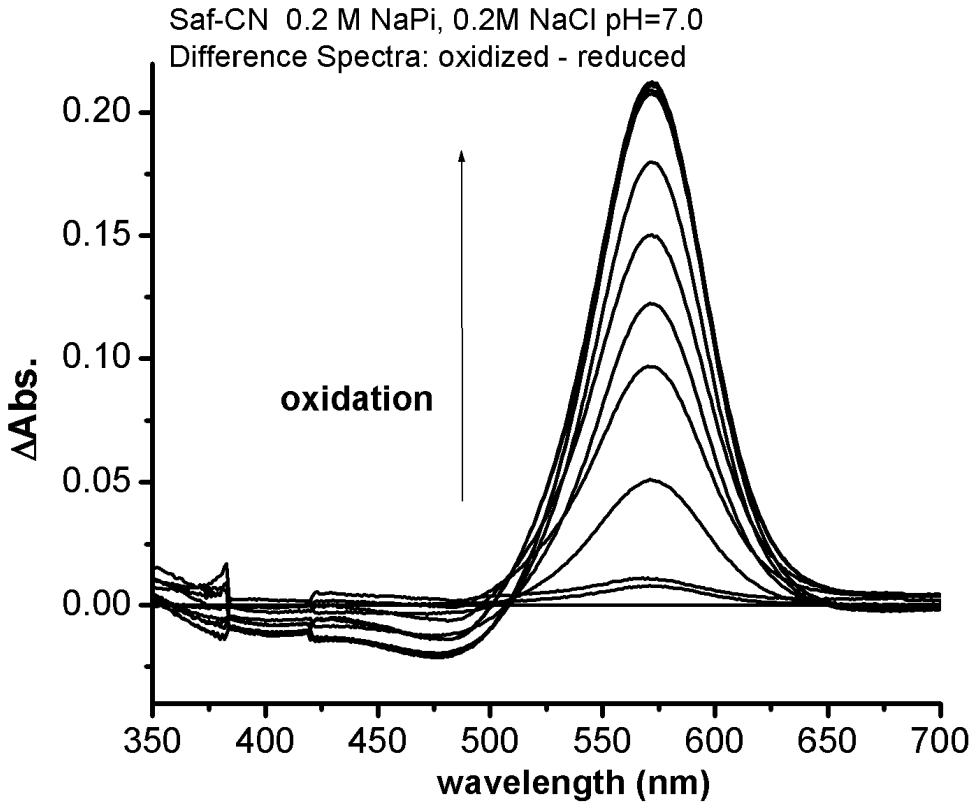

Figure 4.6. Difference spectra (oxidized –reduced) of p-cyanosafranine.

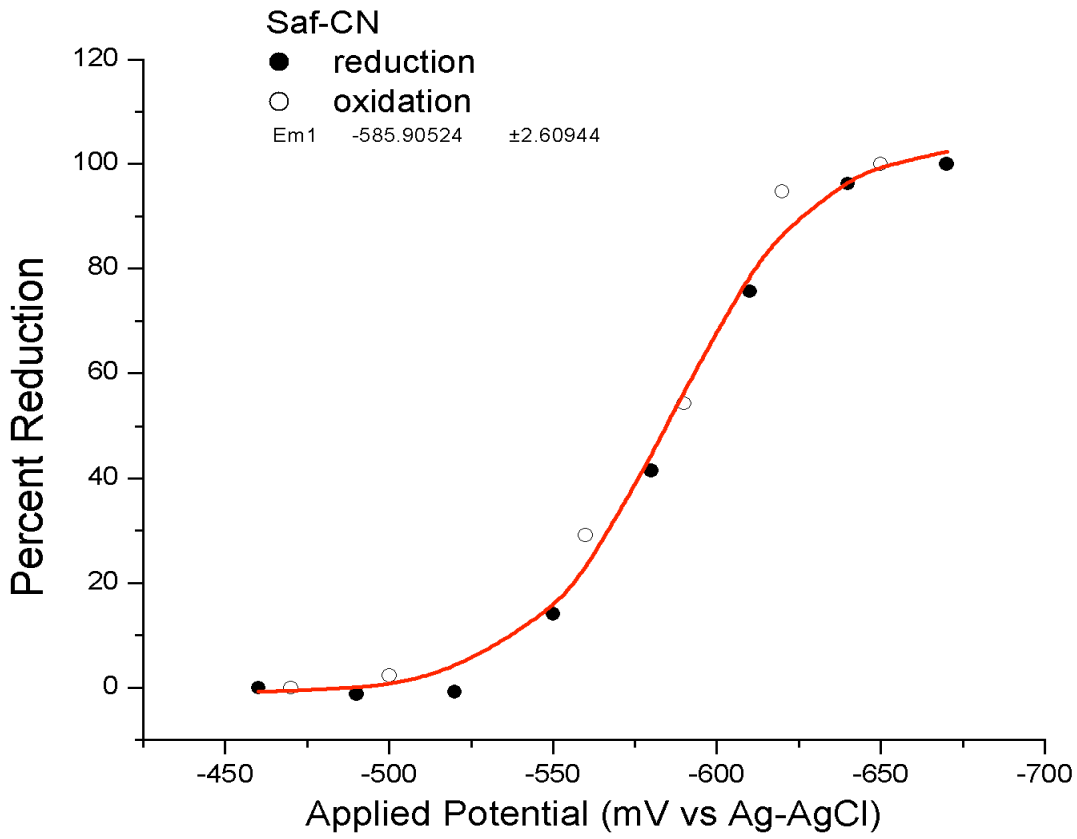

Figure.4.7. Spectroelectrochemical data of p-cyanosafranine. The applied potentials are referenced against Ag-AgCl which is +210 mV (NHE). The data were fit with the Nernst equation.

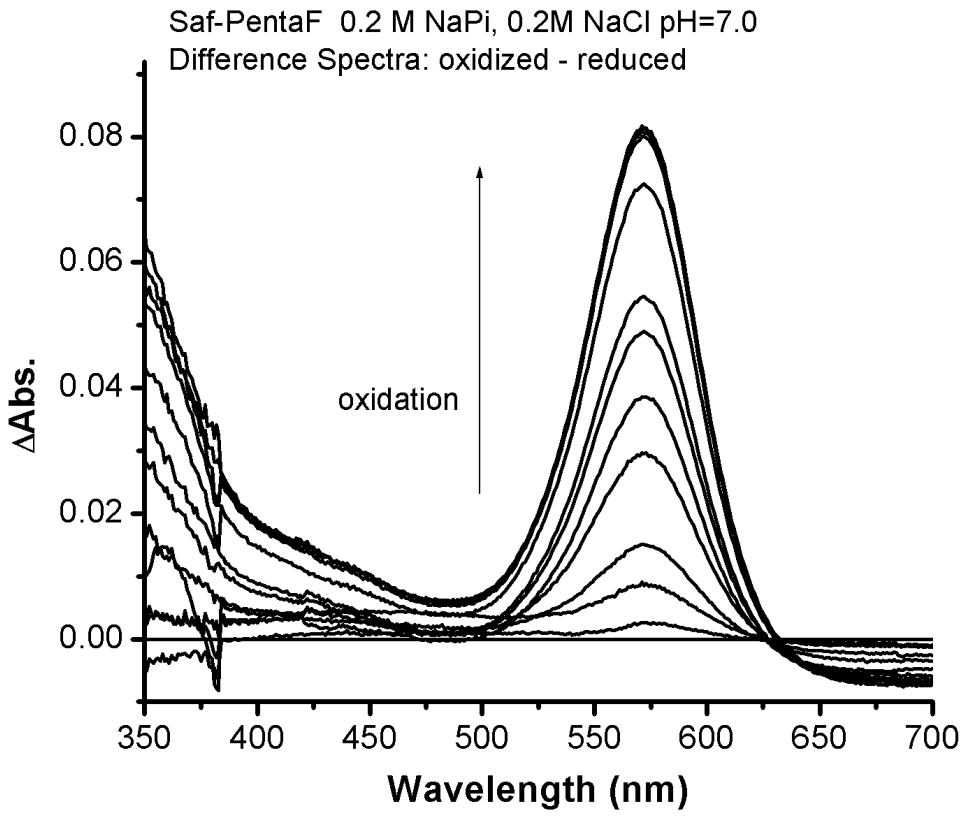

Figure 4.8. Difference spectra (oxidized –reduced) of pentafluorosafranine.

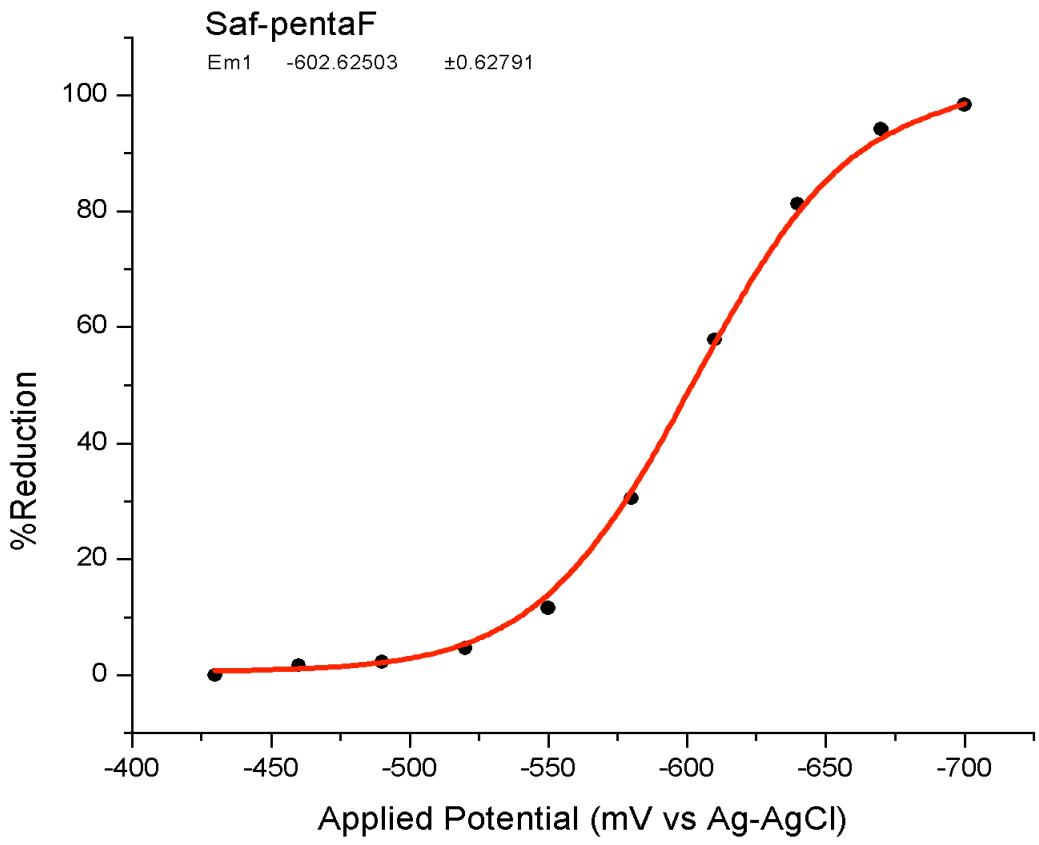

Figure.4.9. Spectroelectrochemical data of pentafluorosafranine. The applied potentials are referenced against Ag-AgCl which is +210 mV (NHE). The data were fit with the Nernst equation.

Safranine analogue	Ag-AgCl / Sat. NaCl (mV)	SHE (+197mV) at 25°C (mV)	Number of electrons	ΔE difference with safranine O (mV)	ΔG difference with safranine O (kcal/mol)
Safranine O	-479	-282	2	0	0
p-Methoxysafranine	-353	-156	2	+126	-5.75
Cyanosafranine	-585.9	-388.9	2	-106.9 +	4.93
p-Methylsafranine	-588.35	-391.35	2	-109.35 +	5.04
Pentafluorosafranine	-602.6	-405.6	2	-123 +	5.67

Table. 4.4. Reduction potential and free energy comparison between safranine O and other safranine derivatives.

4.4. Spectra analysis data.

N,N-diallyl-5-iodo-2-methylaniline (2). Yield = 75.5%. R_f = 0.7 (3:1, hexane/ethylacetate); λ_{abs}max ($CDCl_3$): 276 nm; ESIMS: *m/z* 314.0 (M^++1), 352.1(M^++K). ^{1}H-NMR ($CDCl_3$,500MHz): δ 2.12 [3H, s, C(C*H*$_3$)], 4.02 [2H, d, *J* = 2.1 Hz, C*H*$_2$-CH), 5.19 [2H, d, *J* = 2.1 Hz, CH-C*H*$_2$], 5.22 [2H, dd, *J* = 4.8, 2.1 Hz, CH-C*H*$_2$], 5.87 [2H, qd, *J* = 8.0, 6.2 Hz, CH_2-C*H*-CH_2], 6.82 [3H, qd, Ph-*H*]. ^{13}C-NMR ($CDCl_3$, 125MHz): δ 17.67 [*C*H_3], 52.6 [N(*C*H_2)-CH], 92.2 [*C*(3)], 117.88 [CH=*C*H_2], 123.0 [*C*(2)], 127.10 [*C*(4)], 131.41 [*C*(5)], 132.56 [*C*(6)], 137.83 [CH_2-*C*H- CH_2], 152.73 [*C*(1)].

N3,N3-diallyl-N1-(3-(diallylamino)-4-methylphenyl)-4-methyl-N1-(p-tolyl)benzene-1,3diamine (4). Yield = 69.6%. R_f = 0.27 (4:1, hexane/ethylacetate, 1% triethylamine); λ_{abs}max ($CDCl_3$): 310 nm, ESIMS: *m/z* 478.3 (M^++1), 500.2(M^++Na). ^{1}H-NMR ($CDCl_3$,500MHz): δ 2.12 [3H, s, C(C*H*$_3$)], 2.34 [3H, s, methylPh-C*H*$_3$], 4.02 [2H, d, *J* = 2.0 Hz, C*H*$_2$-CH), 5.19 [2H, d, *J* = 2.3 Hz CH-C*H*$_2$], 5.22 [2H, dd, *J* = 4.8, 2.4 Hz, CH-C*H*$_2$], 5.78 [1H, d, *J* = 1.5 Hz, Ph-*H*], 5.85 [1H, dd, *J* = 7.8, 1.4 Hz, Ph-*H*], 5.87 [2H, qd, *J* = 8.2, 6.2 Hz, CH_2-C*H*-CH_2], 6.51 [1H, d, *J* = 7.3 Hz, **o**-methylPh-*H*], 6.82 [1H, d, *J* = 7.0 Hz, Ph-*H*], 6.98 [1H, d, *J* = 2.44 Hz, **m**-methylPh-*H*]. ^{13}C-NMR ($CDCl_3$, 125MHz): δ 17.9 [*C*H_3], 21.3 [metPh-*C*H_3], 52.6 [N(*C*H_2)-CH], 107 [Ph-*C*], 117.4 [CH=*C*H_2], 117.8 [Ph-*C*], 120.8 [Ph-*C*], 129.9 [metPh-*C*(3)], 130.7 [metPh-*C*(2)], 131.86 [Ph-*C*], 134.2 [CH_2-*C*H- CH_2], 135.73 [metPh-*C*(4)], 142.8 [metPh-*C*(1)] , 152.18 [Ph-*C*].

N3,N3-diallyl-N1-(3-(diallylamino)-4-methylphenyl)-4-methyl-N1-(perfluorophenyl)benzene-1,3diamine (4). Yield = 70.0%. R_f = 0.45 (4:1,

hexane/ethylacetate, 1% triethylamine); λ_{abs}max (CDCl$_3$): 350 nm, ESIMS: *m/z* 554.2 (M^++1), 576.2(M^++Na). ^{1}H-NMR (CDCl$_3$,500MHz): δ 2.12 [3H, s, C(C*H*$_3$)], 4.02 [2H, d, *J* = 6.2 Hz, C*H*$_2$-CH), 5.19 [2H, d, *J* = 2.19 Hz CH-C*H*$_2$], 5.22 [2H, dd, *J* = 4.5, 2.19 Hz, CH-C*H*$_2$], 5.78 [1H, d, *J* = 1.5 Hz, Ph-*H*], 5.85 [1H, dd, *J* = 7.5, 1.5 Hz, Ph-*H*], 5.87 [2H, qd, *J* = 8.5, 6.2 Hz, CH$_2$-C*H*-CH$_2$], 6.80 [1H, d, *J* = 7.5 Hz, Ph-*H*]. ^{13}C-NMR (CDCl$_3$, 125MHz): δ 17.9 [*C*H$_3$], 21.3 [*C*H$_3$], 52.6 [N(*C*H$_2$)-CH], 107 [Ph-*C*], 114.8 [perfluoroPh-*C*(1)], 117.4 [CH=*C*H$_2$], 117.6 [Ph-*C*], 127.8 [Ph-*C*], 130.9 [Ph-*C*], 134.2 [CH$_2$-*C*H-CH$_2$], 137.73 [perfluoroPh-*C*(4)], 138.8 [Ph-*C*],140.8 [perfluoroPh-*C*(3)] , 148.2 [Ph-*C*], 152.2 [perfluoroPh*C*(2)].

4-(bis(3-(diallylamino)-4-methylphenyl)amino)benzonitrile (4). Yield = 60.0%. R_f = 0.3 (4:1, hexane/ethylacetate, 1% triethylamine); λ_{abs}max (CDCl$_3$): 310 nm, ESIMS: *m/z* 489.3 (M^++1), 511.4(M^++Na). ^{1}H-NMR (CDCl$_3$,500MHz): δ 2.12 [3H, s, C(C*H*$_3$)], 4.02 [2H, d, *J* = 6.8 Hz, C*H*$_2$-CH), 5.19 [2H, d, *J* = 2.19 Hz CH-C*H*$_2$], 5.22 [2H, dd, *J* = 5.1, 2.4 Hz, CH-C*H*$_2$], 5.78 [1H, d, *J* = 1.5 Hz, Ph-*H*], 5.85 [1H, dd, *J* = 7.5, 1.5 Hz, Ph-*H*], 5.87 [2H, qd, *J* = 7.8, 4.2 Hz, CH$_2$-C*H*-CH$_2$], 6.80 [1H, d, *J* = 7.5 Hz, Ph-*H*], 6.81 [1H, d, *J* = 2.44 Hz, **o**-benzonitrilePh-*H*], 7.39 [1H, d, *J* = 2.6 Hz, **m**-benzonitrilePh-*H*]. ^{13}C-NMR (CDCl$_3$, 125MHz): δ 17.9 [*C*H$_3$], 52.6 [N(*C*H$_2$)-CH], 107.1 [Ph-*C*], 110.2 [benzonitrilePh-*C*(4)], 117.4 [CH=*C*H$_2$], 117.6 [Ph-*C*], 118.6 [benzonitrilePh-*C*N], 123.4 [benzonitrilePh-*C*(2)], 127.8 [Ph-*C*], 130.8 [Ph-*C*], 133.3 [benzonitrilePh-*C*(3)], 134.4 [CH$_2$-*C*H- CH$_2$], 138.8 [Ph-*C*], 150.2 [benzonitrilePh-*C*(1)].

2,8-bis(diallylamino)-3,7dimethyl-10-(p-tolyl)phenazine-10-ium-5-oxide (5). Yield = 49.0%. R_f 0.7 (1:1, hexane/ethylacetate, 1% triethylamine); λ_{abs}max (CDCl3): 302 nm; ESIMS : m/z 507.3 (M^++1), 529.2 (M^++Na); ^{1}H-NMR (CDCl3 ,500MHz): δ 2.12 [3H, s,

C(CH_3)], 2.34 [3H, s, methylPh-CH_3], 4.02 [2H, d, J = 2.0 Hz, CH_2-CH), 5.19 [2H, d, J = 2.3 Hz CH-CH_2], 5.22 [2H, dd, J = 8.8, 2.1 Hz, CH-CH_2], 5.87 [2H, qd, J = 8.1, 6.2 Hz, CH_2-CH-CH_2], 6.47 [1H, s, Ph-H], 6.88 [1H, s, Ph-H], 7.23 [1H, d, J = 2.3 Hz, **m**-methylPh-H], 7.72 [1H, d, J = 2.44 Hz, **o**-methylPh-H]. ^{13}C-NMR (CDCl3, 125MHz): δ 17.9 [CH$_3$], 21.3 [metPh-CH$_3$], 52.6 [N(CH$_2$)-CH], 113.1 [Ph-C], 117.4 [CH=CH$_2$], 118.9 [Ph-C], 125.6 [metPh-C(2)], 126.4 [Ph-C], 130.86 [Ph-C], 132.7 [metPh-C(3)], 134.2 [CH_2-CH- CH_2], 140.78 [metPh-C(1)], 143.8 [metPh-C(4)] , 147.2 [Ph-C].

2,8-bis(diallylamino)-3,7dimethyl-10-(perfluorophenyl)phenazine-10-ium-5-oxide (5). Yield = 62.0%. R_f = 0.9 (1:1, hexane/ethylacetate, 1% triethylamine); λ_{abs}max (CDCl$_3$): 360 nm, ESIMS: *m/z* 583.2 (M^++1), 606.2(M^++Na). ^{1}H-NMR (CDCl$_3$,500MHz): δ 2.12 [3H, s, C(CH_3)], 4.02 [2H, d, J = 6.2 Hz, CH_2-CH), 5.19 [2H, d, J = 2.1 Hz CH-CH_2], 5.22 [2H, dd, J = 6.8, 2.1 Hz, CH-CH_2], 5.87 [2H, qd, J = 8.5, 6.2 Hz, CH_2-CH-CH_2], 6.47 [1H, s, Ph-H], 6.88 [1H, s, Ph-H]. ^{13}C-NMR (CDCl$_3$, 125MHz): δ 17.9 [CH$_3$], 52.6 [N(CH$_2$)-CH], 111.5 [perfluoroPh-C(1)], 113.1 [Ph-C], 117.4 [CH=CH$_2$], 117.9 [Ph-C], 126.4 [Ph-C], 127.8 [Ph-C], 130.1 [Ph-C], 134.2 [CH_2-CH-CH_2], 137.73 [perfluoroPh-C(3)], 143.3 [perfluoroPh-C(4)] , 147.5 [Ph-C], 148.6 [perfluoroPhC(2)].

10-(4-cyanophenyl)-2,8-bis(diallylamino)-3,7-dimethylphenazine-10-ium-5-oxide (5). Yield = 57.0%. R_f = 0.4 (1:1, hexane/ethylacetate, 1% triethylamine); λ_{abs}max (CDCl$_3$): 360 nm, ESIMS: *m/z* 518.2 (M^++1), 540.1(M^++Na). ^{1}H-NMR (CDCl$_3$,500MHz): δ 2.12 [3H, s, C(CH_3)], 4.02 [2H, d, J = 6.8 Hz, CH_2-CH), 5.19 [2H, d, J = 2.19 Hz CH-CH_2], 5.22 [2H, dd, J = 5.1, 2.1 Hz, CH-CH_2], 5.87 [2H, qd, J = 7.8, 4.2 Hz, CH_2-CH-CH_2], 6.47 [1H, s, Ph-H], 6.88 [1H, s, Ph-H],7.64 [1H, d, J = 2.44 Hz, **m**-benzonitrilePh-H], 8.2 [1H, d, J = 2.6 Hz, **m**-benzonitrilePh-H]. ^{13}C-NMR (CDCl$_3$, 125MHz): δ 17.9 [CH$_3$], 52.6

[N(CH_2)-CH], 112.6 [benzonitrilePh-*C*(4)],113.1 [Ph-*C*], 117.4 [CH=CH_2], 117.9 [Ph-*C*], 118.6 [benzonitrilePh-*C*N], 126.1 [benzonitrilePh-*C*(2)], 126.8 [Ph-*C*], 127.2 [Ph-*C*], 130.8 [Ph-*C*], 132.3 [benzonitrilePh-*C*(3)], 134.4 [CH_2-*C*H- CH_2], 147.3 [Ph-*C*], 148.2 [benzonitrilePh-*C*(1)].

3,7-diamino-2,8-dimethyl-5-(p-tolyl)phenazin-5-ium (6). Yield = 35.0%. Rf = 0.3 (6:3:1 isopropanol/ethylacetate /5% aqueous acetic acid). λ_{abs}max (20 µM KH_2PO_4, 100 µM KCl, pH=8) 570nm; λ_{em}max (20 µM KH_2PO_4, 100 µM KCl, pH=8) 535nm; ESIMS: m/z 331.2 (M^++1); ^{1}H-NMR ($CDCl_3$,500MHz): δ 2.23[3H, s, C*H*3], 2.64 [3H, s, methylPh-CH_3], 6.36[2H, bs, phenazin-NH_2], 6.8 [1H, s, phenazin-*H*], 7.32 [1H, d, , *J* = 2.44 Hz, **m**-methylPh-*H*], 7.43[1H, s, phenazin-*H*], 7.8[1H, d, *J* = 2.44 Hz, **o**-methylPh-*H*];^{15}N-NMR (CD_3OD 50 MHz): δ 414.84.

3,7-diamino-2,8-dimethyl-5-(perfluorophenyl)phenazin-5-ium (6). Yield = 45.0%. Rf = 0.5 (6:3:1 isopropanol/ethylacetate /5% aqueous acetic acid). λ_{abs}max (20 µM KH_2PO_4, 100 µM KCl, pH=8) 570nm; λ_{em}max (20 µM KH_2PO_4, 100 µM KCl, pH=8) 511nm; ESIMS: m/z 407.2 (M^++1); ^{1}H-NMR ($CDCl_3$,500MHz): δ 2.13[3H, s, C*H*3], 6.5[2H, bs, phenazin-NH_2], 6.86 [1H, s, phenazin-*H*], 7.82[1H, s, phenazin-*H*];^{15}N-NMR (CD_3OD 50 MHz): δ 523.57.

3,7-diamino-5-(4-cyanophenyl)-2,8-dimethylphenazin-5-ium (6). Yield = 30.0%. Rf = 0.4 (6:3:1 isopropanol/ethylacetate /5% aqueous acetic acid). λ_{abs}max (20 µM KH_2PO_4, 100 µM KCl, pH=8) 570nm; λ_{em}max (20 µM KH_2PO_4, 100 µM KCl, pH=8) 559 nm; ESIMS: m/z 342.2 (M^++1); ^{1}H-NMR ($CDCl_3$,500MHz): δ 2.13[3H, s, C*H*3], 6.4[2H, bs, phenazin-NH_2], 6.86 [1H, s, phenazin-*H*], 7.36[1H, s, phenazin-*H*], 7.6 [1H, d, , *J* = 2.44

Hz, **m**-benzonitrilePh-*H*], 8.2[1H, d, *J* = 2.44 Hz, **o**-benzonitrilePh-*H*];^{15}N-NMR (CD_3OD 50 MHz): δ 401.87.

4.5. Conclusions.

We have developed a novel synthetic route leading to a wide variety of safranine analogues. The overall number of synthesis steps was reduced from our previous synthesis efforts, and the yields were increased considerably. This simple synthesis includes an inexpensive way to incorporate an isotope at the reduction site, giving insight to the chemical reactivity of the cofactor in the enzyme, and enabling us to the compare the behavior of various analogues during the enzymatic activity [8,12]. We have shown that these flavin-like cofactors exhibit a variety of photophysical and electrochemical properties, and the spectral diversity could prove advantageous in creating biochemical sensor arrays. All of our safranine analogues have higher reduction potentials than safranine O that means more driving force for oxidative reactions in the enzyme, like the oxidation of nicotinamide cofactors such as NADH and NADPH.

4.6. Future developments.

Exploring the photophysical and electrochemical properties, and the isotopic shifts inside our artificial enzyme bundles, are the next steps in characterizing these artificial flavin-like cofactors. An investigation of pH-dependent oxidation-reduction potentials of both one- and two-electron transfers is underway.

4.7. Bibliography.

1. J. F. Corbett, *Journal of the Society of Dyers and Colourists*. **1972**.88, 438–443.

2. George Albert Swan, Desmond Geoffrey Ivins Felton. *Phenazines*. **1957**. Interscience publishers INC., New York, Interscience publishers LTD., London, pages 118-148.

3. A.W. Hofmann and A. Geyger, *Ber*. **1872**. 5,526.

4. Jocelyn Field Thorpe, Martha Annie Whiteley, Sir Thomas Edward Thorpe. *Thorpe's Dictionary of Applied Chemistry*, 4th ed. Longmans, Green, London. **1937**.1, 576.

5. Nanda, V., and Koder, R. L. *Nature Chemistry.* **2010**. 2, 15-24.

*6. Ronald L. Koder, P. Leslie Dutton. Dalton Trans., **2006**, 3045-3051.*

7. Koder, R. L., Anderson, J. L. R., Solomon, L. A., Reddy, K. S., Moser, C. C., and Dutton, P. L. *Nature.* . **2009**. 458, 305-309.

8. Raju, G., Capo, J., Lichtenstein, B.R., Cerda, J.F., Koder, R.L. *Tetrahedron Letters.* **2012**. 53, 1201–1203.

9. *V. Massey. Biochemical Society Transactions.**2000**. 28, (4), 283-296.*

*10. Benfang Lei, Shiao-Chun Tu. Biochemistry. **1998**. 37, (41), 14623-14629.*

11. Clarke, W.M. *Oxidation Reduction Potentials of Organic Systems*. ed. **1960**. The Williams and Wilkins Co., Baltimore.

12. Koder, R. L., Walsh, J. D., Pometun, M. S., Dutton, P. L., Wittebort, R. J., Miller, A.-F. *J. Amer. Chem. Soc.* **2006**.128,15200-15208.

13. Muchowski, J. M. and M. C. Venuti. *The Journal of Organic Chemistry.***1980**. 45, 4798-4801.

14. Altman, R. A. and S. L. Buchwald. *Nat. Protocols.* **2007**. **2**, 2474-2479.

15. Kelkar, A. A., N. M. Patil, et al. *Tetrahedron Letters.* **2002.** 43, 7143–7146

16. Ley, S. V. and A. W. Thomas. *Angewandte Chemie International Edition.* **2003**. 42, 5400-5449.

17. Goodbrand, H. B. and N.-X. Hu. *The Journal of Organic Chemistry.* **1998**. **64**, 670-674.

18. Manifer, T, Rohani, S, Bender, T. P., Goodbrand, H. B., Gaynor, R and Saban, M. *Industrial and Engineering Chemistry Research.* **2005**. 44, 789-798.

19. M. Kaik and J. Gawronski. *Tetrahedron: Asymmetry*. **2003**. 14, 1559–1563.

20. James G Speight. *Lange's Hand Book of Chemistry.* **2005**. Sixteenth Ed. McGraw-Hill.

21. Ralph N. Salvatore, Cheol Hwan Yoon, Kyung Woon Jung. *Tetrahedron.* 2001. 57, 7785-7811.

22. Yoneda, F., Y. Sakuma, M. Ichiba, K. Shinomura. *Journal of the American Chemical Society*. **1976.** 98, 830-835.

23. S. Chandrasekhar, R. Reddy, R. J. Rao, *Tetrahedron.* **2001**. *57*, 3435-3438.

24. Richard C. Stewart and Vincent Massey. *The Journal of Biological Chemistry*.**1985.** 260, 13639-13647.

25. Lichtenstein, B.R., Cerda, J.F., Koder, R.L. and Dutton, P.L. *Chemical Communications.* **2009**.2, 168-170.

26. Cerda, J.F., Koder, R.L., Lichtenstein, B.R., Moser, C.M., Miller, A.-F., Dutton, P.L. *Organic & Biomolecular Chemistry*. **2008**. 6, 2204-2212.

27. Klemba, M., Gardner, K.H., Marino, S.,Clarke, N.D., and Regan, L. *Nature Struct. Biol.* **1995**.2, 368-373.

28. Hellinga, H.W., and Richards, F.M. *J.Mol. Biol.* **1991**. 222,763-785.

29. Telmer, P.G and Shilton, B.H. *J.Mol. Biol.* **2005**. 354,829-840.

30. Benson, D. E., Wisz, M.S., and Hellinga, H. W. *Proc. Natl Acad. Sci. USA.* **2000**.97,6292-6297.